Nanomechanical Testing of Diatoms

Marius Juelsrud Vebner

THE NORWEGIAN UNIVERSITY
OF SCIENCE AND TECHNOLOGY
DEPARTMENT OF ENGINEERING DESIGN
AND MATERIALS

MASTER THESIS SPRING 2013
FOR
STUD.TECHN. MARIUS JUELSRUD VEBNER

NANOMECHANICAL TESTING OF DIATOMS
Nanomekanisk testing av kiselalger

A worldwide effort is focused on finding cost-effective renewable energy sources, while CO_2-emissions from conventional energy continue to increase. As a possible solution to this problem, one of nature's most efficient light harvesting organisms is investigated. Diatoms, a type of algae, are protected by nanostructured shells, termed frustules, with a design that exceeds the capabilities of human engineering in many ways. However, before diatoms can be used in industrial applications, reliable mechanical measurements of diatoms are needed, revealing their properties both at a local and global scale.

In this master thesis, nanomechanical testing of diatoms shall be performed based on the experience gained from the candidate's project thesis. The candidate shall further explore the test methods developed in the project thesis with the aim to obtain test schemes giving reproducible results describing the mechanical properties of diatoms. Next, calculation methods shall be developed to analyze the mechanical responses from the different methods.

Nanoindentation
The internal dome should be investigated in the frustule shell. If this is more size-consistent than the whole frustule, this should be used as a more reproducible method of testing global properties for different sized frustules with the nanoindenter. As it was observed in the project thesis, the frustule layers appear to be connected through the polypeptides and polyamines. If this is true, the proposed nanoindentation should be a good method to show a clear difference in the mechanical strength due to different amount of organic content left in the frustule.

The tip chosen for the experiments should be carefully chosen. One alternative is to use a circular tip with a large enough radius to avoid penetrations and crack propagations. A second alternative is to perform nanoindentations with a sharper tip to further investigate the correlation between response and distance from frustule center. A sharper tip will induce penetrations in the foramen, and crack propagation can be investigated in an AFM. With this

method, local properties will be extracted giving valuable information on both geometry and the biosilica itself. Dynamic nanoindentation with an oscillating tip should also be evaluated as a third alternative. This provides continuous measurements of the elastic modulus, also known as continuous stiffness measurement as described by Oliver and Pharr.

Cantilever bending test
Even though no successful tests were performed during the candidate's project thesis, the cantilever bending test is still assumed to be a promising method to test local properties. Therefore, the cantilever bending test shall be further developed and explored. Micro-cantilever beams have been reported as successful in literature on other materials and these tests should be studied to apply same techniques on diatom frustules.
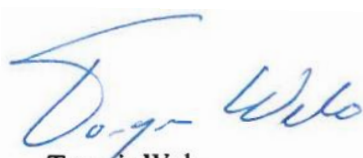
FEM-analysis
When the cantilever beam is produced, a triangular cross-section from the areola will be left on the foreman structure. This will have minor contributions to the moment of area. To investigate this contribution, a FEM-analysis should be performed. The results from the FEM-analysis should also be used to compare the results obtained in from the cantilever bending test.

The thesis should include the signed problem text, and be written as a research report with summary both in English and Norwegian, conclusion, literature references, table of contents, etc. During preparation of the text, the candidate should make efforts to create a well arranged and well written report. To ease the evaluation of the thesis, it is important to cross-reference text, tables and figures. For evaluation of the work a thorough discussion of results is appreciated.

Three weeks after start of the thesis work, an A3 sheet illustrating the work is to be handed in. A template for this presentation is available on the IPM's web site under the menu "Masteroppgave" (http://www.ntnu.no/ipm/masteroppgave). This sheet should be updated one week before the Master's thesis is submitted.

The thesis shall be submitted electronically via DAIM, NTNU's system for Digital Archiving and Submission of Master's thesis.

The contact person is (navn på veileder i utlandet, bedrift eller lignende)

Torgeir Welo
Head of Division

Christian Thaulow
Professor/Supervisor

NTNU
Norges teknisk-
naturvitenskapelige universitet
Institutt for produktutvikling
og materialer

"What has fins like a whale, skin like a lizard, and eyes like a moth? The future of engineering. "

-Tom Mueller, National Geographic (2008)

Preface

Much the same way that a musician must practice his or her instrument, scientists must be doers in order to be proficient in novel fields of research. Therefore, a learning-by-doing approach was thought to give the best results in the work of this master thesis. Theoretical knowledge was constantly improved while first-hand experience with diatoms and different equipment was gained.

Together with project supervisor, Prof. Christian Thaulow, an experimental approach have been chosen in this thesis. The focus have been to further develop the two most promising test methods: the nanoindentation and the cantilever bending test. The theoretical and analytical part of this study have therefore been reduced to a minimum, this includes both finite element analysis and development of theoretical calculations. This decision was made to give more room for testing and practical work.

I would like to thank Post Doc. Julien Romann, my contact person towards the SOLBIOPTA research group and the Department of Biotechnology at NTNU. Our discussions linking the mechanical properties to biological and optical properties of the diatoms have been highly valued. The research group in the nanomechanical department have also been a great support with their experience on nano- and microscaled mechanical testing. A special thanks is directed to Bjørn Rune Sørås Rogne and Håkon Gundersen for training and advise for the equipment and instruments used. Further I would like to acknowledge my fellow students in room 212 at Verkstedteknisk. In particular Øyvind Våland, nanolab partner and fellow student, for encouraging conversations and a helping hand on different LaTex-related problems. Finally, a large thanks is directed to project supervisor, Prof. Christian Thaulow, for introducing me to the diatoms and giving me this chance to learn directly from nature.

Marius Juelsrud Vebner

Sammendrag

Nanomekanisk testing av kiselalger

av Marius Juelsrud Vebner

Norges teknisk-naturvitenskapelige universitet
Fakultet for produktutvikling og materialer

Diatomer, en stor algegruppe, er beskyttet av et nanoporøst skall som er bygget med et design som overgår dagens ingeniørers kunnskap og ferdigheter. Disse skallene består av biologisk silisiumdioksid og gir organismen mer enn et fysisk skjold. Deres lysfangende egenskaper kombinert med høy grad av mekanisk og bakteriell beskyttelse gjør at diatomer er interesante i vitenskapelig forskning.

Denne oppgaven presenterer diatomene og deres eksepsjonelle egenskaper. En diatom utkragerbjelketest er innledet og kan potensielt være den første testmetoden som kan fastslå de virkelige materialegenskapene i diatomenes biosilica. Utkragerbjelker er isolert fra det interne laget i diatomskallet med størrelser ned til $0{,}35 \times 1{,}5 \times 4\,\mu$m. En strukturert karakterisering er igangsatt for å identifisere den interne geometrien i *Coscinodiscus Centralis*. De innledende målingene av skallene indikerer at den interne hevelsen i *C. Centralis* ikke er en størrelseskonsistent komponent. Likevel er klare trender sett i deres mekaniske respons når frustuler med ulike forbehandlinger er tested med nanoindentering. Observasjoner etter indenteringer utført i en picoindenter indikerer at porene i det interne laget er viktige for å hindre sprekkvekst i diatomenes skall.

Abstract

Nanomechanical Testing of Diatoms

by Marius Juelsrud Vebner

Norwegian University of Science and Technology
Department of Engineering Design and Materials

Diatoms, a major group of algea, are protected by a nanostructured shell, built with a design that exceeds the capabilities of human engineering. These shells, termed frustules, consist of biosilica and give the organism more than just a physical armor. Light-harvesting properties combined with great mechanical and bacterial protection makes diatoms interesting in scientific research.

This thesis presents the diatoms and their exceptional properties. A diatom cantilever bending test is initiated and could potentially be the first test method to determine the true material properties of biosilica in diatoms. Cantilever beams are isolated from the internal layers of the diatom frustules with sizes down to $0{,}35 \times 1{,}5 \times 4\,\mu\text{m}$. A structural characterisation is initiated to identify internal geometries in the frustules of the *Coscinodiscus Centralis*. The initial measurements indicates that the internal elevation in the *C. Centralis* is not a size-consistent component. Still, clear trends are seen in their mechanical response when frustules with different pretreatments are tested by nanoindentation. Observations after indentations performed in a picoindenter are indicating that the pores in the internal layer are important to hinder crack propagation in diatom frustules.

Contents

Chapter 1

Introduction

More than 3,5 billion years have gone since the first living cells were moving randomly on earth [1]. From then, evolution has made each organism adapt to survive in its natural environment. The result of Darwins famous theory is what we today can see around us in nature. Due to technological equipment, humans are now capable of studying the essential building blocks in these organisms. The result is a constant growing field of science called biomimetics. By learning from nature, structures and functions in biological systems can be used as models for designers and engineers [2].
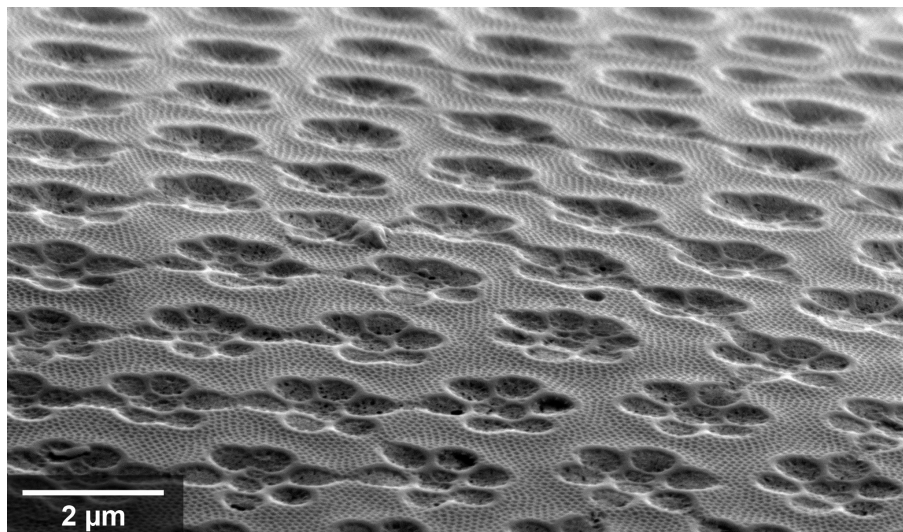

FIGURE 1.1: SEM-image of the cribrium, one of the outermost layers in the *Coscinodiscus Centralis*, the most studied diatom species in this work.

Fig. 1.1 shows the external layer of the nanoporous structure in a diatom frustule. These shells are built with a design that exceeds the capabilities of human engineering today. Their frustules are the main reason why diatoms have been the subject of numerous studies. This master thesis will focus on the development of reliable test methods to determine the mechanical properties of diatom shells.

Compared to bulk silica, which is one of the most brittle materials known [3], the diatom shells are surprisingly tough. Scientists have revealed that the frustules consist of organic materials [4] and not only biosilica. Understanding the combination of their composite structure and their complex geometry could inspire the way we build light-weight materials today. Within the field of optics, scientists are trying to understand how these shells captures the sunlight, a potential which makes the diatoms interesting for various applications in the solar cell industry.

Before diatoms can be used in industrial applications, mechanical measurements are needed to fully understand their mechanical strength. This is also important if diatoms are to be used as models in material science. Therefore, reliable and reproducible testing methods will be important to identify their properties. Not only to reveal the true properties of their biosilica, but also to understand the effects of different chemical treatments or implantation of other metals in the diatom shells.

This study is a continuation of the work done in the master thesis of S. H. Bjørnøy, "Nanomechanical Testing of Diatoms" [5] and the authors project work "Nanocomposites from Diatoms" [6]. This thesis begins by introducing valuable background theory both on the diatoms and the equipment used. Then, a review of previous mechanical testing on diatoms is given. The practical work in this thesis is divided in three: First, a characterisation of the diatom shell is presented. The focus is then shifted towards nanoindentation on an internal area to detect the mechanical importance of the organic components. The third part presents a further development of the diatom bending tests, initiated spring 2012 at NTNU by S. H. Bjørnøy. The mechanical testing performed is focused on the internal layer of the diatom shell, the foramen. The outer layers are believed to have other functions and does not contribute to the mechanical strength [7].

Chapter 2

Theory

This chapter presents background theory relevant for the experiments performed in this master thesis. As the diatom biology and hierarchical composition are important factors when developing a test scheme, a prestudy of the diatoms is presented. This is followed by an introduction to the most used instruments. In the end of this chapter, elementary beam theory is given, used in the initial estimations of the mechanical properties in diatoms.

2.1   Prestudy of Diatoms

Diatoms are one of the largest algae groups and a common type of what we refer to as phytoplankton [8]. They are unicellular, photosynthetic organisms and have been on this planet for more than 180 million years [9]. They are found in waters all over the world, wherever there is enough light and nutrients. Diatoms contribute significantly to global primary production with their photosynthesis [10]. Despite their small contribution to the worlds biomass [11], their carbon fixation is equivalent to the fixation of all the tropical rainforests in the world [12]. In 1977, 12 000 diatom species where identified and known by scientists [10]. Today, the number of living diatom species is estimated to be above 200 000 [13]. In common for them all is their unusual properties that are subject to diverse scientific research. What first started as a fascination among amateur scientists of the diatoms ornate, silica shells, has become more than just a source of interest

3

with modern technology. The diatoms are today involved in various novel fields of research, both as a inspiration and for direct applications.

This section will give a brief introduction to the diatoms in general. When a more detailed description is needed the diatom *Coscinodiscus centralis* will be used as an example. This is because the *C. centralis* is the species treated in the practical part of this study. They are one of the biggest diatom species, easy accessible in Trondheimsfjorden and feature several interesting aspects.

2.1.1   Cell Structure and Hierarchical Design

There is nothing special with the diatom protoplast compared to other single-celled algae [8]. They contain organelles such as nucleus, mitochondria and plastids. What makes diatoms particular is their intricate cell wall with its complex hierarchical design. These outer shells are termed *frustules* and are mostly made of silica (SiO_2). They are highly differentiated with their specie-specific pore structure, but do all consist of several layers. The variation of shape and size of diatoms, is used in taxonomy. The system of F. Hustedt from 1930 [14] is still used to divide the different diatom families, generea and species where the main division is between the centric diatoms and pennate diatoms.

Aulacodiscus sp.   *Amphitetras sp.*   *Didymosphenia sp.*   *Podocystis sp.*
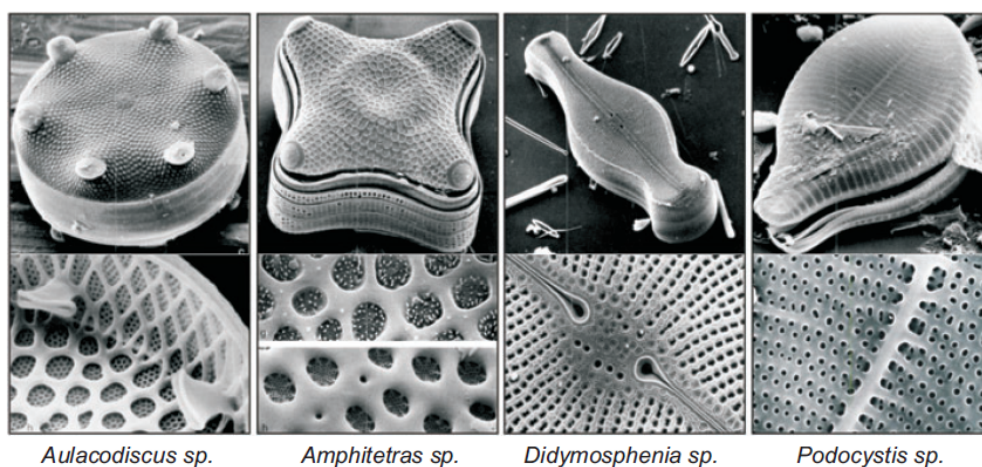
FIGURE 2.1:   SEM-images illustrating the difference between four diatom species [15]. The lower images are showing the variation in pore size and distribution in the cell wall.

The word diatom is derived from the Greek *diatomos*, which means cut in half [16]. As seen in Fig. 2.2, the diatom cell wall, their shell, consists namely of two valves. They are termed *epitheca* and *hypotheca* [8]. The epitheca is slightly larger and overlaps the other half. Together the two parts completely enclose the living organism and are held in place by several girdle bands. The metaphor of a Petri dish is frequently used to describe the shape of radial centric diatoms in literature [9, 15, 17, 18].
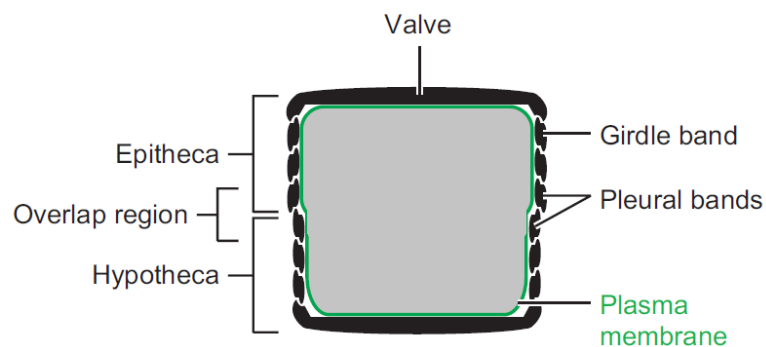

FIGURE 2.2: Schematic structure of the diatom cell [15]. The gray area represents the protoplast, the green line depicts the plasma membrane. The living organism is protected by two valves, termed epitheca and hypotheca. They are held together by several girdle bands.

In 1992, Linder et al. [19] used a Scanning Force Microscope (SFM) to start the first systematic investigation of the topography on diatoms. Fifteen years later, Losic et al. continued this work with an Atomic Force Microscope (AFM) [20]. The diatom genera they studied, was the *Coscinodiscus* sp. The term "sp." indicates that the exact species is unknown. Hence, this is not necessarily the same species as studied in this thesis, but consist of the same layers. The outer layer, in contact with the external environment, is termed the *cribellum*. This was reported to be a thin layer, less then 50 nm, containing the finest pores of around 45 nm in diameter. These pores were believed to be big enough for nutrition uptake, but too small to let bacteria and most viruses enter. The cribellum is weakly connected to the rest of the frustule and was reported to contained some organic matter [20]. The next layer is the *cribrum* and was reported to contain pores of intermediate size, 190 nm in diameter. This layer was later measured to be relatively thin, about 50 − 60 nm by A. K. Noren [21], MCs graduate from NTNU 2011.

Losic et at. could further report that the *areola* was the main structural part of the frustule with a thickness of $2000 - 2500$ nm. This layer was built up with thin walls in a honeycomb structure, around 135 nm wide [21]. This hexagonal pattern is a well known core structure in sandwich plates in composite materials due to their heigh bending stiffness-to-weight ratio [22]. The innermost layer, closest to the living organism, is the *foramen*, measured to be around 360 nm thick [20]. This layer was characterised with the hexagonally arranged pores, $1\,150$ nm in diameter. A. K. Noren illustrated the geometrical composition of the *C.* sp. available at NTNU as seen in Fig. 2.3. This species is believed to be the same species as referred to as the *C. centralis* in the practical part of this thesis.
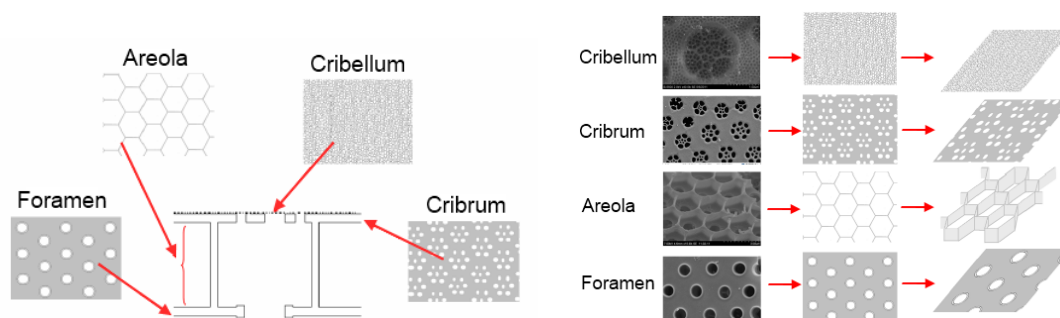

FIGURE 2.3: Illustration of the four different layers, the cribellum, cribrum, areola and foramen in the *Coscinodiscus* sp. [21].

2.1.2 Biology and Chemical Composition

As diatom grows, they expand in only one direction due to restrictions from the rigidity in the silica frustule [8]. The epitheca and the hypotheca are moved apart and new girdle bands are created inside a Silica Deposition Vesicle (SDV) to accommodate further expansion. Reproduction of diatoms occurs mainly by *mitotic* cell division. This is a vegetative reproduction where a single mother cell divides into two daughter cells. As shown in Fig. 2.4, a new hypotheca in each daughter cell is created just before the cell divides.

Because the new valve is formed within the confines of the parental cell, the mean cell size tends to decline. However despite the size change in the diatom diameter, Stefano et al. have discovered that their pore size remain constant [23]. To prevent that the diatoms converge to infinite small organisms, some species

have developed a method of restoring their size by *meiotic* division. The cell undergoes an enormous increase in volume and new silicified valves are formed.
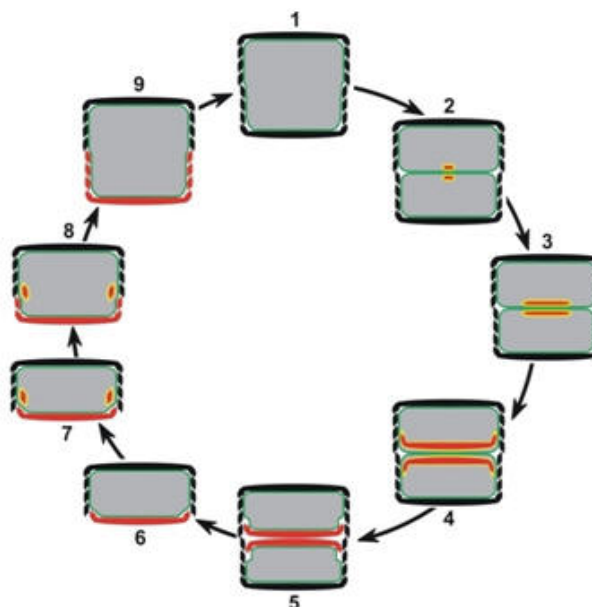

FIGURE 2.4: Cell cycle illustration [15]: (1) The cell is ready for cell division and (2) biosilica (red) is formed in each daughter cell inside an SDV (yellow). (3–5) The SDV expands as more and more silica is deposited. (6) The daughter cells separate and (7–8) new girdle bands are created in separate SDV's. (9) After the synthesis of the final girdle band, cell expansion stops and DNA replication is initiated.

Diatom reproduction is a rapid process for most species and requires little space. More than one million diatom cells per millilitre of culture can easily be obtained [20]. This offers the possibility of cheap industrial production of nanostructured silica through the culture of diatoms. Hence, knowledge about their reproduction process would be highly valued.

In 1977, Chiappino and Volcani were the first to state that the diatom biosilica is a composite material [4]. The frusutles contain organic materials and not only pure silica. These organic components were later identified and described as fundamental constituents of the diatom biosilica formation [24]. Kröger et al. dissolved the silica matrix with hydrofluoric acid, and isolated a set of polypeptides called silaffins. When added to a solution of silicic acid (SiH_4O_4), which is naturally present in water [10, 25], they started to generate networks of silica nanospheres within seconds. Pure silica nodules were also reported in the AFM-study of Losic

et al. with diameters ranging from $20 - 70$ nm in the two outer layers in the diatom valves [20].

The isolated sphere diameters observed by Kröger et al. were bigger, $50 - 700$ nm depending on the slaffin type, concentration and pH level. Further studies showed that the silaffins were covalently bound to another organic compound [24], namely long-chained polyamines. In contrast to the slaffins, the polyamine chains are believed to be species-specific [17], but they are also important in the silica formation [24, 26].

Even though scientists have identified the proteins behind the silica biomineralization, the exact pattern production and phase transformations are still unknown. However, several theories and models have been proposed to explain the mechanism behind the silica morphogenesis in diatoms [17, 25, 27–29].

2.1.3   Optical Properties

As a photosynthetic organism, diatoms appear to have evolved to become masters of sun harvesting. Their nanoporous surface might control the propagation of light to enhance the photosynthesis. This is one of their most interesting properties, thus scientists are trying to understand how light is controlled within their structure. In 2004, Fuhrmann et al. showed that the diatom shell can influence incoming light and can therefore be regarded as living photonic crystals [30]. Photonic crystals are materials with spatially ordered and periodic nanostructures which only allow certain wavelengths of light to pass through [31]. The potential for solar cell applications has therefore been studied as e.g. new dye-sensitized solar cells [32].

2.2   Equipment

2.2.1   Confocal Microscope

A confocal microscope is an optical instrument used for dimensional measurements, surface analysis and 3D-characterisation. The operational principle is based on the

limited depth of focus in optics with vertical scanning [33]. The region in focus
is shifted over the whole surface topography in combination with a vertical scan.
Various sensors detect the changes in sharpness to reproduce a 3D-representation
of the sample. The vertical- and lateral resolution are set by the user and are
normally down to 10 nm and one micrometer respectively [33].

When comparing the working principle to an atomic force microscope or a nanoin-
denter, exact topographic information can be obtained in shorter time and without
physical contact with the sample. Confocal microscopy does not require any sam-
ple preparation and will therefore reproduce images with no disturbances from
sample coatings or physical objects.

2.2.2   Scanning Electron Microscope

A Scanning Electron Microscope (SEM) is primarily used to image and view a
surface with electrons. The sample is therefore placed in a vacuum chamber. An
electron beam is normally emitted from a a sharp tungsten needle at the tip of an
electron gun [34]. The beam is then focused through 1–3 condenser lenses. Before
the beam hits the specimen, it passes through a pair of scanning coils or deflector
plates. These coils/plates deflects the beam in the x and y axis and makes the
beam scan the sample surface in a raster fashion. The size of the scan is manually
decided by the user with the magnification.

The area in the sample effected by the electron beam is called the interaction
volume. The acceleration voltage decides the depth of this volume. The electrons
are usually accelerated to an energy between 1 keV and 30 keV. A higher accel-
eration voltage, allows the electrons to penetrate deeper into the sample surface.
Independent of the acceleration, different signals are produced when the electrons
from the beam, i.e. the primary electrons, interacts with the sample surface:

Secondary electrons (SE) are ejected electrons from the specimen atoms. They
   have low energy, below 50 eV [34], and originate from the top nanometers of
   the sample surface.

Backscattered electrons are electrons from the primary beam with high energy
and are reflected out of the interaction volume.

X-rays are produced when electrons are knocked out of the atoms in the surface.
When the empty space is filled, excess energy can be when the atom is
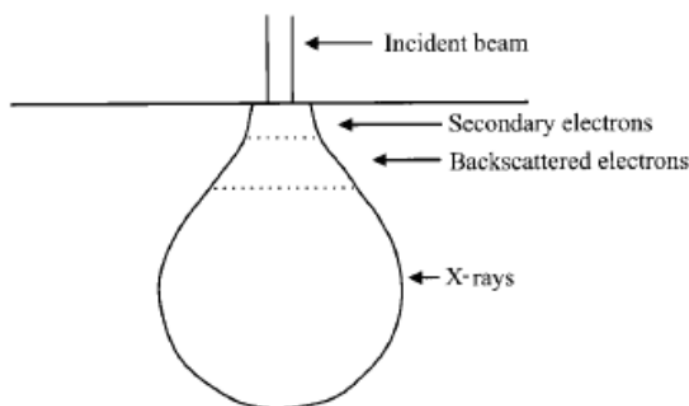brought to a relaxed state.

FIGURE 2.5: The interaction volume and the regions from which secondary
electrons, backscattered electrons and X-rays may be detected [34].

By varying the type of detector, detector parameters, beam current or voltage,
information from distinct regions of the interaction volume can be detected as
illustrated in Fig. 2.5. The most common detector when imaging a surface, is the
Everhart-Thornley Detector(ETD) which captures the secondary electrons.

Samples used in SEM must be electrically conductive. Non-conductive samples
are charged when exposed to the electron beam, creating image errors. This can
be avoided with a thin conductive coating and is specially important for biological
samples.

2.2.3   DualBeam FIB

The DualBeam Focused Ion Beam (FIB) is an instrument that combines an elec-
tron beam, as described in section 2.2.2, with an ion beam. The instrument allows
the user to view, image and perform *in situ* machining of a sample at nanoscale.
The treated sample is mounted on a stage with three-axis translation, rotation
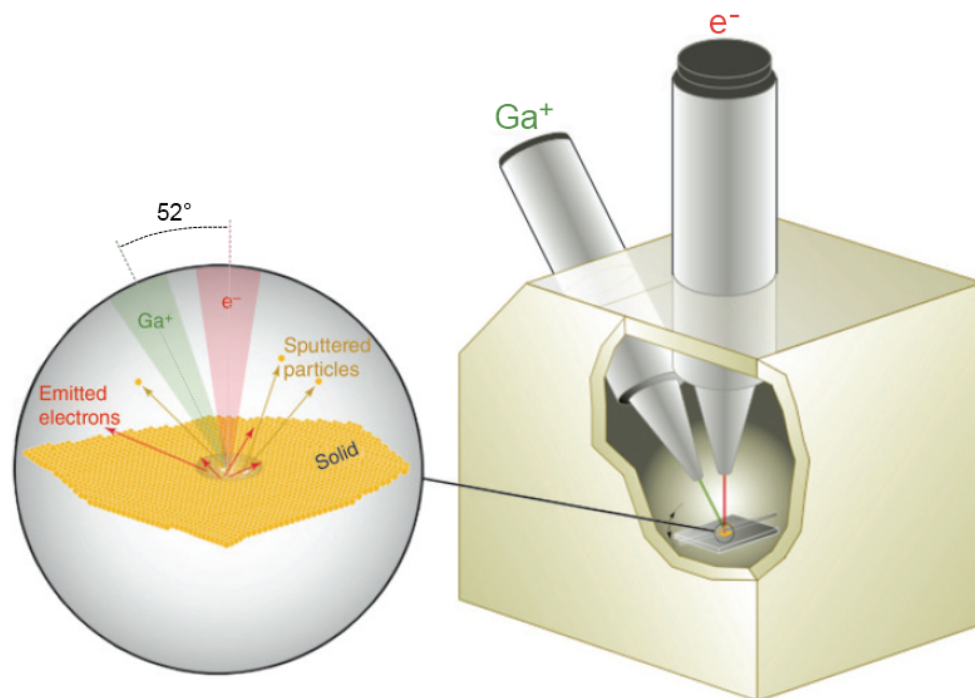and tilt capabilities [35].

FIGURE 2.6:   Illustration of a DualBeam FIB. Expanded view shows the electron- and ion beam sample interaction [35]. The angle between the two beams is 52°.

The ion beam is similar to the electron beam, except that ions, typically Ga^+, are rastered over the surface [35]. When the sample is exposed to ion beam, a small amount of the sample is sputtered away, either as electrons, ions or neutral atoms. These particles are captured by detectors and used to image the sample.

As seen in Fig. 2.7, the FIB is substantially destructive to the sample surface. In addition to the sputtering action, ions will also be implanted at the surface. By milling a sample in a controlled way, the instrument is used to machine structures and is frequently used as a tool for both characterisation and sample fabrication.

A gas injection system is installed in the DualBeam FIB and gives the instrument important additional functionalities. The delivery of local gases can be used to enhance the etching rate, deposit material on the sample or prevent re-depositioning of sputtered particles [35]. In addition, the instrument features an OmniProbe navigation system with a tungsten needle for nanomanipulation and sample navigation.
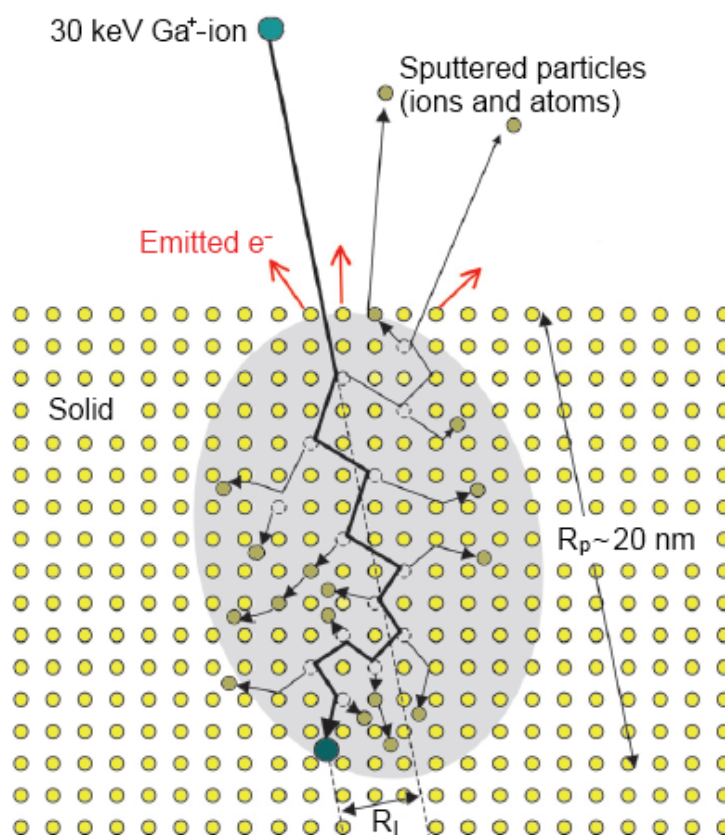
FIGURE 2.7: Schematic illustration adapted from Volkert et al. of a collision cascade generated by a 30 keV Ga^+-ion, showing damaged volume in grey, the projected- (R_p) and lateral range (R_l) of the implanted ion [35].

As for a normal scanning electron microscopy, a layer of conductive coating should be sputtered on organic samples like diatoms to avoid charging effects from the electrons when used in a DualBeam FIB.

2.2.4   Nanoindenter

A nanoindenter is an instrument built to measure and test mechanical properties of small volumes. The most frequent application, is to determine the modulus of elasticity and hardness, but it can also be used to estimate yield strength, fracture toughness, scratch hardness and wear properties [36]. The instrument itself consists mainly of an active vibration isolation system, a sample stage, a digital microscope, a tip connected to a transducer and a piezo-scanner. It is based on the same principles as traditional hardness tests, e.g. Vickers and Brinell [37]: by indenting an object into a specimen surface for a defined interval of time,

material properties can be revealed by measuring the size of the plastic impression, i.e. the area of contact, for a given indenter load [38].
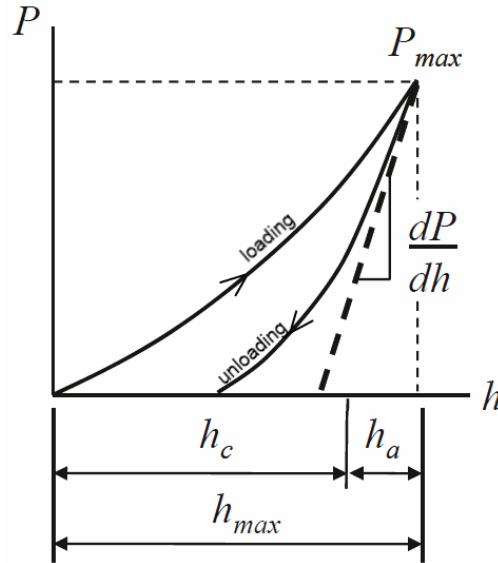

FIGURE 2.8: Compliance curves of the loading and unloading adapted from Oliver and Parr. $\dfrac{dP}{dH}$ is referred to as the contact stiffness and is the slope of the elastic unloading from maximum load. H_{max} is the total depth of penetration, while h_c is the contact depth and h_a is the depth of the circle of contact to the specimen free surface. [36].

While impressions caused by traditional indenters can be measured by optical inspection, indents performed with a nanoindenter are normally in a size-range below a few micrometers. This makes optical techniques very difficult. Only after Oliver and Pharr developed their analytical method in 1992 [36], the nanoindentation has been possible to use in a scientific context.
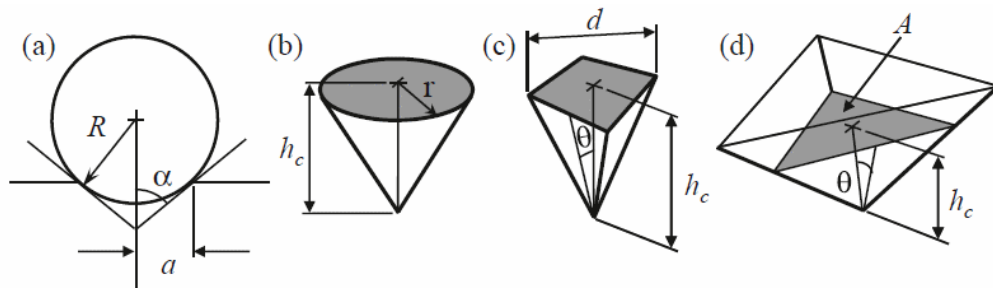

FIGURE 2.9: Indentation parameters for (a) spherical, (b) conical, (c) Vickers, and (d) Berkovich indenter tips (not to scale) [38].

The method developed by Oliver and Parr, is related to the specific indenter tip being used. There are two main groups of indenter tips, spherical and pyramidal tips. The last group can be found in various shapes, sizes and geometries as illustrated in Fig. 2.9. With known geometry of the indenter tip, the area of contact can be determined from experimental readings of indenter load and displacement [36]. For a Berkovich- or a cube corner indenter tip, the formula is:

$$A = 3\sqrt{3}h_c^2 tan^2\theta \qquad (2.1)$$

where, A is the area of contact, h_c the contact depth and θ the tip radius. Another way of determining the area is with an experimental approach on a substrate with known hardness and elastic modulus. A set of at least 20 indentations are done in the substrate with different loads and a polynomial function is fitted to the curve as an alternative area function [39]. The same technique could be applied if the indenter tip is used over a larger time so the geometry has slightly changed as a result of wear and tear. A normal polynomial expression is:

$$A = C_1 h_c^2 + C_2 h_c + C_3 h_c^{1/2} + C_4 h_c^{1/4} + C_5 h_c^{1/8}... \qquad (2.2)$$

where $C_1 - C_5$ are constants and h_c measured as seen in Fig. 2.8. With known area function, the hardness can be calculated with maximum load:

$$H = \frac{F_{max}}{A} \qquad (2.3)$$

The area function is further used to calculate the "elastic modulus" with the contact stiffness $\frac{dP}{dh}$, i.e. the slope of the elastic unloading from maximum load:

$$E^* = \frac{1}{2}\frac{dP}{dh}\frac{\sqrt{\pi}}{\sqrt{A}} \qquad (2.4)$$

The "elastic modulus", E*, obtained from these calculations, is often referred to as the reduced modulus or the combined modulus of the system. E* is a value representing a combination of the modulus from both the indenter and the sample.

Since the hardness of the tip normally is much higher than for the substrate, corrections are seldom applied.

In addition to indentations, a nanoindenter can be used to image a surface with a physical scan. This is a function used to both localize correct test areas and to image a surface after testing. The working principle is based on the forces between the tip and the sample during a raster movement of the tip on a determined scan-area. This force is defined by the user and is registered by the transducer in the same way as applied load during an indent. The quality of the image is dependent on the setpoint, scanning speed and the tip geometry. A sharper tip will naturally improve the quality. Two different images are created after each scan.. These images are based on the force gradient error (GF) and topology (TF) in both directions of the scan. The indenter tip can also be used as a concentrated micro-load in e.g. mechanical bending tests.

2.2.5   Picoindenter

A picoindenter is a scaled-down nanoindenter, built to fit inside a regular SEM-chamber. Both the instrument itself and the samples used need therefore to be vacuum compatible and conductive. The operation principles are the same as for a nanoindenter, but the picoindenter set-up allows the user to see the mechanical experiments in situ with high magnification. This makes the picoindenter ideal in the development of new test schemes. Both test methods and parameters can be optimized based on the actual response of the sample tested and not only assumptions after load-displacement analysis.

The small scale results in restrictions in terms of sample size, load- and displacement range. However, the load and displacement resolutions are in the same range as for the nanoindenter, typically 3 nm and 0,02 nm respectively [40].

Chapter 3

Previous Mechanical Testing of Diatoms

Diatoms are exposed to various mechanical challenges in their natural environment. Not only are they a target for predators, but they are also exposed to abrasive particles in the water [41]. Their surprising mechanical properties have therefore been the subject in numerous scientific studies. In this section, a historical overview from literature with the main results of previous mechanical testing methods will briefly be given. Then, previous nanomechanical testing at NTNU will be presented.

3.1   Literature Review

The first published mechanical study of diatoms was done by Almqvist et al. [42] with AFM nanoindentation in 2001. The test was performed on the diatom species *Navicula pelliculosa* as a microscopic Vickers hardness test. Measured hardness and elastic modulus varied from $1-12\,\text{GPa}$ and 7 to hundreds of GPa respectively, depending on the location of the indents. Almvist et al. stated that further AFM testing was necessary to serve as a complementary tool in the study of silica biomineralization and pattern formation in diatoms.

In 2003, Hamm and Merkel [43] explored the defence potential of whole diatom frustules. Using calibrated glass microneedles, loading tests were performed on centric and pennate diatoms. In general they observed that remarkably high forces, equivalent to $100 - 700$ tons $\times \, \mathrm{m}^{-2}$, were needed to break the frustules. Surprisingly, the highest forces were measured in the smallest diatom frustules. It was shown that the frustule size and the mechanical strength had an inverse relationship. Hamm and Markel also observed cracks following a path *around* the silica spheres and pores. Hence, the fracture area almost doubles compared to a crack propagating along a straight line. If this is a general behaviour of crack propagation in diatom frustules, this significantly increases the energy necessary to break the frustule.
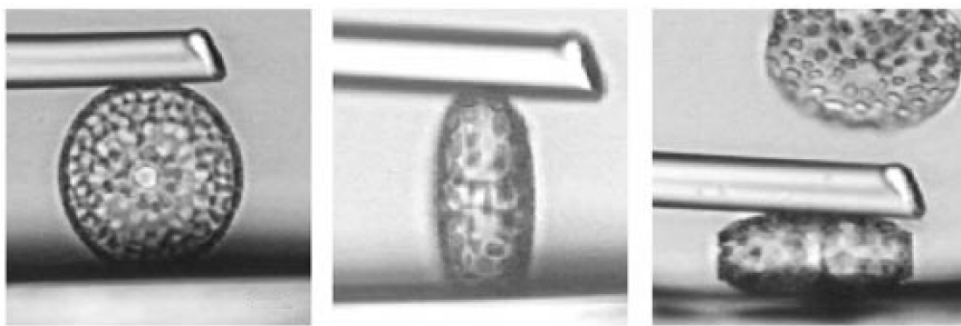

FIGURE 3.1: Mechanical testing of whole diatom frustules, adapted from Hamm and Merkel [43]. A glass needle was used to crush fully assembled diatom frustules

Losic et al. did not only carry out topological experiments as described in section 2.1.1. In 2007 they performed nanomechanical testing of diatom biosilica surfaces with an AFM nanoindenter [7]. The previous work by Almqvist et al. had been executed without precise location of the actual indents. Thus, with technologically advanced equipment, Losic et al. could reveal the regional variation of the mechanical properties on the valves. The lowest values for the hardness and elastic modulus were found in the cribellum, the outermost layer. They also observed that the hardness decreased slightly from the center to the edge of the frustule. An opposite trend was observed for the elastic modulus which increased slightly with distance from the center. The variation was assumed to be caused by difference in the pore size, pore distribution and also the biomineralization process it self.

The calculations used, were based on the general method of Oliver and Pharr [36] as described in section 2.2.4. Even though Losic et al. used low loads in the range between $1-12\,\mu N$, penetrations of the indented layers were observed. This observation indicates that the nanoporous layers were deflecting during testing. In other words, the measured depth of deformation was really a parameter describing a deflection of a larger area in combination with the indentation of the actual layer tested. This deflection was not corrected in the calculations. The contact area was therefore measured to be larger than what it was in reality as it included the deflection of the whole layer. A too large contact area effects the results with a lower hardness (Eq. 2.3) and a lower elastic modulus (Eq. 2.4). The values obtained by Losic et al. could still be suitable for comparisons between regions and layers, but does not present the real properties that the diatom biosilica exhibit.
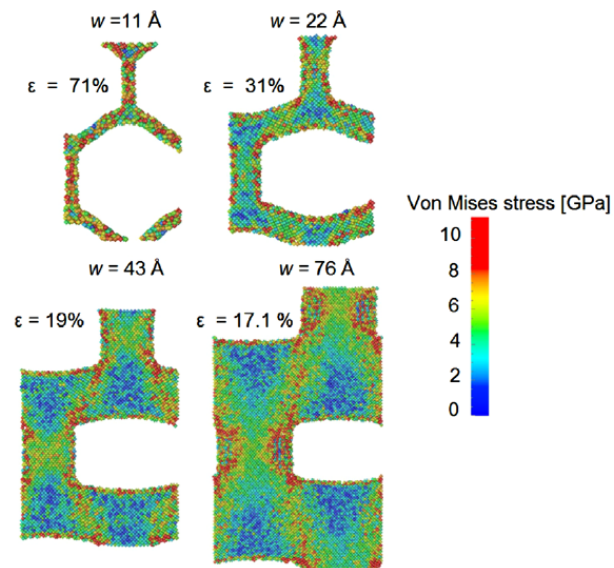

FIGURE 3.2: Von Mises stess field at the maximum stress, for different wall widths [3] of a silicon structure. The goal of the study was to simulate the brittle-to-ductile transition due to small geometries.

In 2010, Buehler et al. hypothesized that the nanoporous geometry was the key to the mechanical properties of the diatom frustules [3]. One of their arguments was that the hexagonal pattern of the areola gives a high moment of inertia which increases the capacity to withstand deformations. With a molecular simulation tool, a three-dimensional silicon structure was exposed to uni-axial, tensile load. By adjusting the model-wall width, the plastic regime was greatly influenced. For smaller wall widths, the maximum stress and the modulus were reduced. When

the wall width was reduced to a size of $11\,\text{Å}$, the structure deformed into a hexagonal shape during loading (Fig. 3.2). The result was a more homogeneous stress distribution compared to the original rectangular shape. The behaviour of the originally brittle silicon changed towards a more ductile fashion, allowing deformations up to $80\,\%$ without breaking. These results are showing how geometric variations at nanoscale can effect the global mechanical properties. However, since the tests were based on a pure silicon model, they are not directly comparable to the diatom frustules, but rather pointing out the importance of the geometry of the complex nanostructure. It should be mentioned that the scale modelled by Buehler et al. was four times smaller than the smallest diatom pores of $45\,\text{nm}$.

3.2 Testing at NTNU

In 2011, S. H. Bjørnøy initiated nanomechanical testing of diatom frustules at NTNU with a different approach [5]. Samples of the *Coscinodiscus centralis* were treated with three different methods. Chemical cleaning of the frustules, i.e. removal of the living organism, was followed by centrifugation and a rinse in water. The total recipe from the Department of Biotechnology is attached and found in Appendix A. The difference between the methods, was the chemical agent used: sodium dodecyl sulphate (SDS), sulphuric acid (H_2SO_4) and hydrogen peroxide (H_2O_2). These distinct methods made the samples different in terms of the quantity of remaining organic content in the frustules. The mildest treatment was the SDS-cleaning followed by the H_2SO_4-cleaning. For the harshest treatment with H_2O_2, not only was the algae inside removed, but also larger quantities of the organic material in the frustule. This was confirmed with fluorescence microscopy done by Post Doc. Romann and was expected to be seen if the frustules were tested mechanically. Paired with the interest of finding the mechanical contribution from the nanostructured geometry in the diatom frustules, this was the main motivation for the development of S. H. Bjørnøy's test scheme.

Three Point Bending Tests
The test scheme introduced, was a three point bending test for diatom beams. The

beams were prepared in the DualBeam FIB with an average size of $22 \times 4 \times 3{,}5\,\mu$m. After fabrication, they where moved with the in-situ OmniProbe navigation system to a pre-made sample holder of solid steel. The samples were then transferred to a nanoindenter where the beams were exposed to single loading from the indenter tip. The load was placed at the center of the beam and increased until fracture as illustrated with the SEM images in Fig. 3.3. Both complete beams with the entire frustule thickness and beams made from isolated layers were tested.
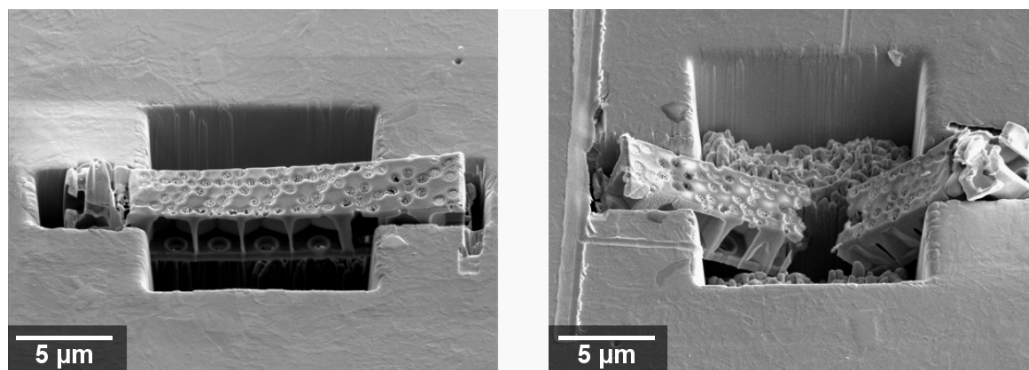

FIGURE 3.3: SEM images of the complete "H_2O_2-beam3", adapted from the master thesis of S. H. Bjørnøy [5] before and after loading in the three point bending test. The images show the beams at a 52° angle.

This test did not reveal any clear correlation between the different chemical treatments and the mechanical behaviour. However, the initial fracture stress for a complete beam was estimated to be 336 ± 73 GPa, 3 times the fracture stress for amorphous fused silica. Beams made from the entire frustule fractured at a $4-10$ times larger force than beams from a single foramen layer.

Cantilever Bending Test (CBT)

To continue the development of a diatom bending test, an analysis was done in the initial work by the author in 2012 [6]. The conclusion was clear: the three point bending test contained too many uncertainties. It was suitable to detect the mechanical contribution from the different layers. However it could not detect the material properties of pure biosilica nor the the effect of different chemical treatments. Geometric variations in the samples and artificially induced platinum depositions were some of the aspects making the test scheme inconclusive. Thus, based on S. H. Bjørnøy's suggestions for further work, the author of this thesis

initiated a diatom cantilever bending test. If the cantilever beams were made small enough, the beams could be made from single massive layers without pores and the varying geometry. Another assumed advantage, was that the cantilever could be tested while still being connected to the rest of the frustule. The foramen layer was reported to only be 369 nm thick [20]. If the beam was positioned close to a supporting areola wall, the foramen beam was assumed to be thin enough to break without deflections in the supporting frustule. This would in turn make the step of transferring the beam to a separate sample holder unnecessary and save valuable production time.

A cantilever bending test minimizes geometric variation from the different layers as well as the porous structure in the diatom valves. Secondly, the CBT might detect organic materials, dissolved around the silica nodules reported by Losic et al [20], in the biosilica matrix. In addition, one of the solar applications of diatom frustules includes metabolic insertion of other metals, e.g. titanium dioxide (TiO_2) [44]. Hence, the mechanical consequence of this doping could also be revealed with the CBT. This would be highly valued when decisions should be made based on an expected inverse relationship between mechanical properties and optical functionalities. Therefore, the CBT in theory is a suitable test scheme for investigations of pure diatom biosilica.

Nanoindentation

S. H. Bjørnøy performed a handful attempts of nanoindenations on diatom frustules. This technique was further studied and became the main focus in the previous work by the author [6]. The goal of the testing done by the author was two-sided. Firstly, the *C. centralis* have a small elevation in the central region on the foramen, i.e. the internal layer. This internal dome was assumed to be more size-consistent than the whole diatom. If this was correct, nanoindentation of this internal dome could be a good way of getting more reproducible results by deflecting a larger area with the indenter. The expected contribution from organic content, in the frustules was hoped to be detected in this experiment. Three nanoindentations were done with load-control and a set-load of 200 μN. The results from the nanoindentations in the authors project work are seen in Fig. 3.4. They show a clear difference between SDS-cleaned and H_2O_2-cleaned frustules. As

described earlier in this section, this trend was expected as the harsher cleaning method removed more of the organic material in the diatom frustules.
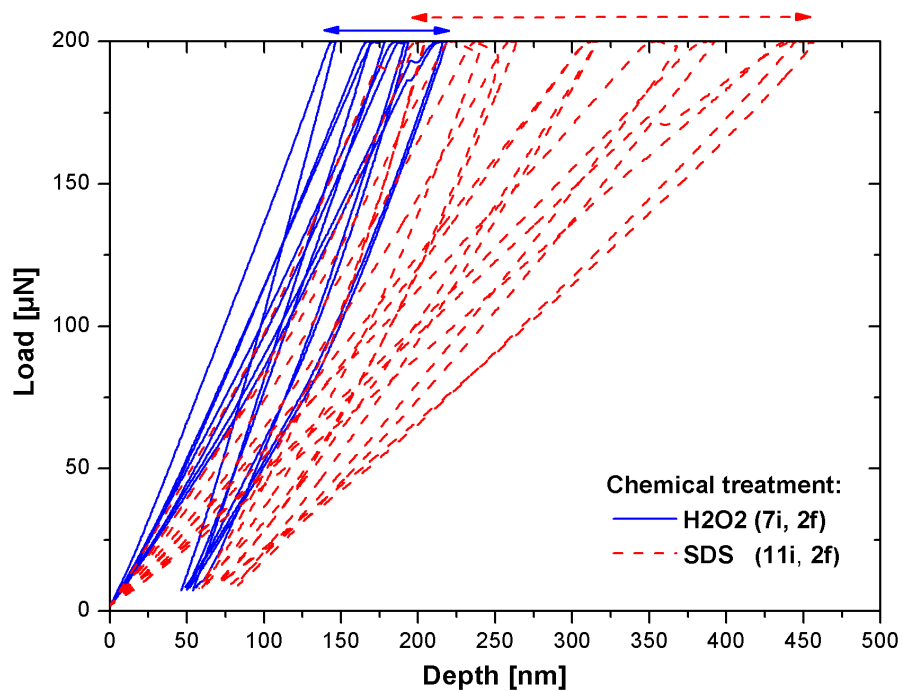

FIGURE 3.4: Graphical illustration of all the *W45-S* samples tested in the authors project work. The test was done in a nanoindenter with a maximum pop-in depth of 50 nm. The numbers indicates the amount of indents, *i*, and frustules, *f*, tested in the initial experiments.

Fig. 3.4 represents around half of the indentations performed. Only the indentations without fracture, here defined as indents where the load-depth curves had pop-ins below 50 µm, were included. This was justified with the argument that diatom biosilica is a brittle material. Crack propagation is not as predictable for brittle materials so the sudden penetrations of the frustules were therefore assumed to be irregular.

Chapter 4

Experimental Details

With a learning-by-doing approach, the test schemes have constantly been changed and improved during the work in this thesis. This chapter is written to give an understanding of the final experimental set-up for the different methods. The important progress in the test scheme development and discussions are presented in Chapter 5.3.2 and 5.6.2. Discussions are therefore kept to a minimum in this chapter, but brief descriptions are given to present the relevance of each method.

For all the experimental methods, single frustules with concave orientation, i.e. the foramen facing up, were of interest. The diatoms used were initially planned to be diatoms from culture from the laboratories in the Department of Biotechnology at NTNU. As these samples turned out to be from another diatom species, they were found unsuitable for the experiments in this thesis. As a consequence, diatoms collected from Trondheimsfjorden were quickly introduced. These were from the same species as used in the authors project work, but referred to as the *Coscinodiscus* sp. since the exact species was unknown at the time. Now they are identified as the *C. centralis*.

As described in section 3.2, the diatoms used in this study have gone through one of the three chemical treatments; SDS, H_2SO_4 and H_2O_2. To distinguish the different samples in this thesis, a name convention was introduced and maintained throughout the whole study. This can be found in Appendix B.

4.1   Characterisation

As presented in section 2.1.1, measurements of the *Coscinodiscus* sp. have already been performed and published in literature and previous master thesis. However, some important parameters are still not quantified for the species used in this study. The goal of the characterisation was therefore to get an indication of the internal topography, relevant for further development of the mechanical test methods.

Two instruments were used, a nanoindenter and a confocal microscope. For both methods, samples were prepared in the same way as for the mechanical nanoindentations. A solution of methanol and diatom frustules was moved from a container and placed on a glass slide with a pipette. The methanol evaporated in air and van der Waals forces were expected to be strong enough to prevent the frustules from moving.

4.1.1   Characterisation in the Nanoindenter

The nanoindenter Hysitron TI950 Triboindenter in the nanomechanical laboratory at NTNU was used to investigate details in the center of the internal part of the diatoms. A sharp diamond cube-cornered tip, with radius of 40 nm, was used. The scan size was set to 60 μm and located in the center of the frustule layer as seen in Fig. 4.1.

The goal of this investigation was to quantify the size of the internal dome, described in section 3.2. The hypothesis was that the internal dome is more size-consistent than the whole diatom itself and therefore a good area for global reproducible testing.

Some of the frustules were imaged after they had been tested mechanically with nanoindentations on the internal dome. Indents were therefore visible in some of the images. As the brittle silica only induces local fractures, the indents were believed not to effect the topographic measurements.
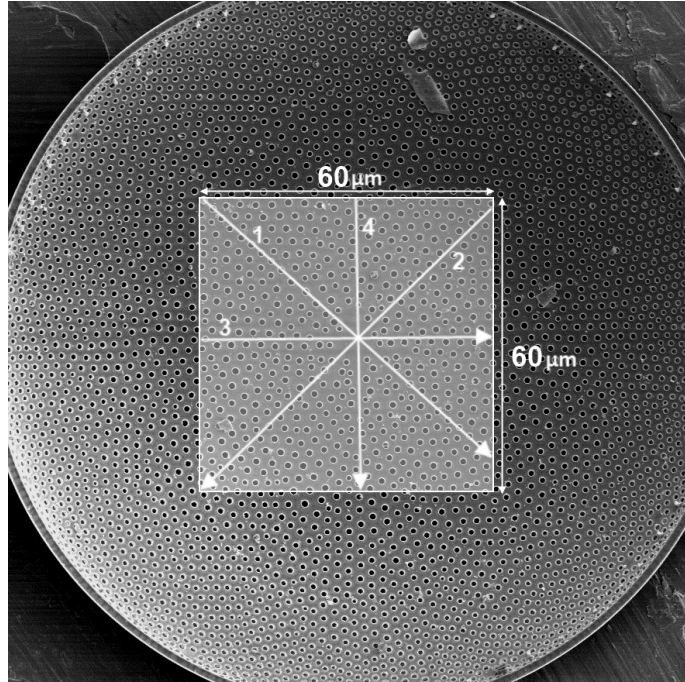
FIGURE 4.1: Illustration of the imaged section on an SEM-image. The arrows indicates the positive direction of the profile curves extracted.

Before imaging, both the tip and the optical system were calibrated with the Hysitron TriboScan software. A tip velocity of $12\,\mu ms^{-1}$ with a setpoint of 1–$2\,\mu N$ was used to obtain good quality images. With these scanning parameters, the scanning time was around 45 minutes for each image with a scan-size of $60\,\mu m$. In total 14 frustules were imaged with the nanoindenter. After imaging, the results were analysed with the open-sources software Gwyddion. Four different profile-lines were drawn on each sample as illustrated in Fig. 4.1. X- and y-parameters, at the top and the two lowest points at the frustule, were measured. From these six values, following data was extracted:

Dome diameter (D) was measured as the average distance between L_x and R_x from all four profile curves. Knowing the distance to the frustules lowest point was an important parameter if the goal was to indent the area in direct contact with the substrate.

Tilt (T) was calculated from the profile line with the largest vertical distance between L_y and R_y. This parameter gives an indication of the contact area between the frustule and the substrate along the lowest part of the dome.
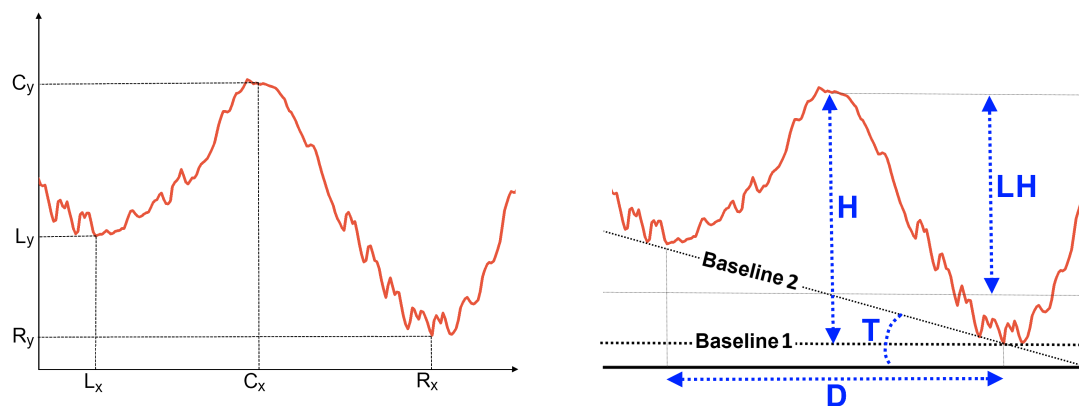
FIGURE 4.2: Illustration of how the measured parameters from the profile-lines after each scan were used to calculate the wanted geometrical information of the internal dome. Note: the x-axis and y-axis are not in scale to better illustrate the measurements done in this experiment.

Height of dome (H) was measured from the horizontal baseline 1. This line was the horizontal line from the lowest point as seen in Fig. 4.2. The height of the dome was then measured from this baseline up to the highest measured C_y from the four profile-lines. This value was important when navigating the indenter tip in the picoindenter to avoid collisions.

Levelled height of dome (LH) was measured from a baseline 2, made by the average value between point L and R. The height of the dome was then measured from this baseline up to the highest measured C_y from the four profile-lines. This value was important to investigate the size-consistency of the internal dome.

4.1.2   Characterisation in the Confocal Microscope

The Alicona Infinite Focus Microscope in NTNU's Tribology lab was used to measure the topography of the whole frustule. The vertical- and lateral resolution was set to 50 nm and 1 μm respectively. Scan time was between 1 and 2 minutes per frustule. In total, 33 frustules were examined in the confocal microscope.

The goal of the measurements in the confocal measurements, was to quickly get an indication of how the size was varying between the different frustules. In addition, these parameters would be useful in the picoindenter experiments, where the tip

was manually navigated. Knowing the geometries of the samples was therefore essential to avoid coalitions which could damage the samples or the equipment.

The images from the confocal microscopy were analysed with the Alicona software. Following information was extracted from the measurements in the confocal microscope:
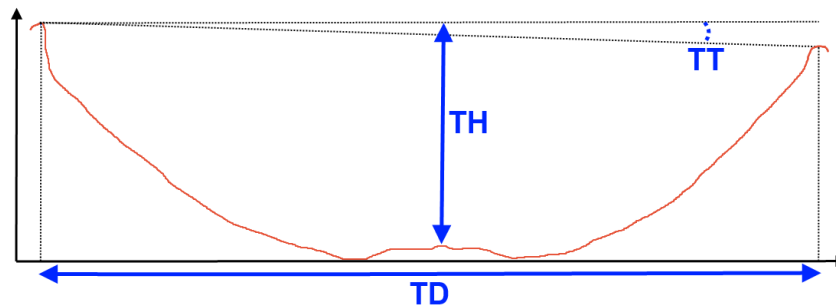

FIGURE 4.3: Illustration of how the measured parameters from the profile-lines after each scan were used to calculate the wanted geometrical information of the whole frustule. Note: the x-axis and y-axis are not in scale to better illustrate the measurements done in this experiment.

Total diameter (TD) of the diatom frustule. This was measured with four profile lines and the average value was used.

Total height (TH) was measured from the top of the internal dome to the highest value of L_y or R_y among the four profile lines.

Total tilt (TT) was calculated with simple trigonometry on the profile-line with largest vertical difference between the two measured top points.

4.2   Nanoindentation

The initial testing by the author [6], showed a clear correlation between the different pretreatments and the mechanical response. However, the initial experiments were only performed on four different diatom frustules. The goal was therefore to reproduce the same test on a large number of samples. Only then would statistically valid results be obtained and a final conclusion could be drawn. The testing at a more local scale, was planned to be more experimental by varying

indent location, force and tip geometry. Since the response from the indentation on the internal dome not went as expected, these local indentations were used to investigate the different responses seen in on the internal dome. Therefore, the same tip and set-load were used, but on smaller areas to better control position of the indents.

For all nanoindentation experiments, a standard sample preparation procedure was followed. A solution of methanol and diatom frustules was moved from a container and placed on a glass slide with a pipette. The methanol evaporated in air and van der Waals forces were expected to be strong enough to prevent the frustules from moving. The glass-slides were then moved to the nanoindenter and single frustules with concave orientation, i.e. the foramen facing up, were located in the optical camera.

Before testing, both the tip and the optical system were calibrated. A pre-scan was necessary to locate a suitable area for indentation and a scan of the surface after the indent could subsequently help to explain measured response. The scan size was $20 \, \mu m$. A tip velocity of $32 \, \mu m s^{-1}$, a setpoint of 1–$3 \, \mu N$ and an integral gain of 240 was used to obtain good quality images. The frustules were scanned with a lower tip velocity, $16 \, \mu m s^{-1}$, after the indents.

4.2.1   Indentation of the Internal Dome

One of the functions of the organic content in the diatom frustules is to keep the different layers attached to each other like a glue [20]. Observations in the previous work by the author, indicates the same. Whole areola- and cribrum layers have commonly been found detached from each other, especially among the H_2O_2-cleaned frustules. In addition, when exposing single layers to Ga^+-ions or the electron beam in the DualBeam FIB, exposed layers moved individually due to local heating. The structure in a diatom frustule could therefore be regarded as an advanced composite structure. The grip and friction between the brittle biosilica layers is assumed to be high, since the nanoporous layers have rough surfaces. With general composite theory [22], it was assumed that the global structure would behave stiffer if the organic content, i.e. the glue, was removed.

For the diatom frustules, mechanical theories of composite structures is extremely hard to apply. The mechanical properties of the biosilica and the organic content are unknown. In addition, the exact location of this organic content is unknown. Moreover, the geometry is strikingly complicated with details down to the nanoscale. Still, the SDS-cleaned frustules were expected to behave more elastic than the H_2O_2-cleaned frustules. Therefore, by testing the center area of the diatom frustules with a larger load, the mechanical contribution from the organic content was hoped to be detected.

The original strategy was to perform the indentation on diatoms cultivated at the laboratory in the Department of Biotechnology at NTNU. Five frustules were investigated, but they turned out to be from a completely different diatom species. They were therefore replaced with diatoms collected with a net in Trondheimsfjorden by scientists from the Department of Biotehnology at NTNU.

Both deflection of the whole internal dome and local penetrations were of interest. This was assumed to be dependent on the location of the indent and the geometry of the indenter tip. The tests on the lab-samples, and the first test on the net-sample, were all done with a conical tip with a radius of 0,6 µm. The conical tip induced the same amount of cracks and pop-ins as the cube-cornered tip used in the initial testing [6]. The conical tip was thus changed to a cube-cornered tip as used in the initial testing. In this way, the results could be compared with previous testing and the images would have better quality since a cube-cornered tip is sharper. The cube-cornered tip had 90° edges and was given to be 40 nm by the manufacturer.

The indents were performed in the center of the foramen. All indents where located systematically, one in the center and four indents in four different directions, $3 - 5$ µm from the center. Additional $4 - 5$ indents were normally performed $8 - 12$ µm from the center. All indents were performed with load-control. The maximum load (set-load) was set to 200 µN with a trapezoidal load function. The loading sequence started with 5 seconds of loading, a 2 second holding-segment followed by 5 seconds of unloading. In total, 275 indents were performed on 35 different frustules.

4.2.2   Local Indentations

As reported in literature, $60 - 70\,\%$ of the diatom's frustule is essentially void space. Still, only $50\,\%$ of the indentations were penetrating the foramen layer. For the local indentation, the goal was to investigate how the geometry of the frustule effects the mechanical response of the indentation. By performing a smaller series of indents on a smaller scan-size, the indents could be performed under more control. The relation between the location of the indentations and their mechanical response was therefore studied at smaller areas. It appeared to be two extreme cases in terms of stress distribution which occurred during the indentation on the internal part of the frustule.

Case A: Indentations Between the Foramen Pores

By indenting the center between three foramen pores, the underlying areola would be exactly beneath if the pores are of the same size. This was observed in the SEM images from the DualBeam FIB as seen in Fig. D.1 in Appendix D. The foramen would therefore be supported directly by the areola cross, i.e. the intersection between three of the areola walls. An illustration of the indents location is seen in Fig. 4.4. The dotted lines on the left image are drawn to represent the areola walls seen in the right image.
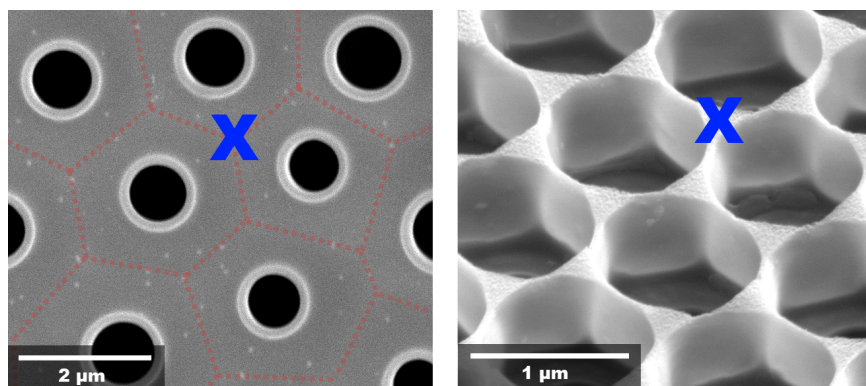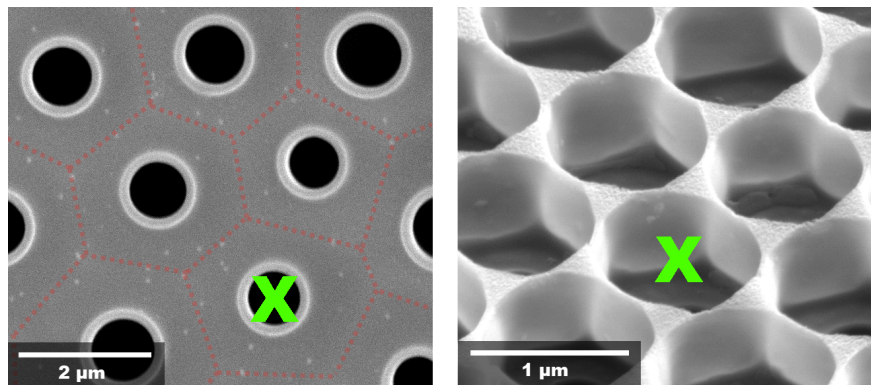

FIGURE 4.4: Schematic illustration of the planned location of the indentation between the foramen pores. When the indent was located at the cross, the indents was assumed to be supported by the underlying areola structure. The two images are not from the same frustule, but used to illustrate the two inner layers of two different frustules.

Indentations between the foramen pores was also performed in the picoindenter. As the actual indent and the frustules response could be observed *in situ*, the force was increased stepwise from 50–1000 μN.

Case B: Indentations in the Foramen Pores

By indenting inside the foramen pores (Fig 4.5), the deflection of the free-standing foramen layer will be detected. At low loading, the foramen layer could be viewed as fixed to the areola walls. At higher loads, the force from the indenter tip would be distributed through the foramen-areola connection and down the areola walls. If the set-load of 200 μN could be defined as high or low in these conditions, was one of the questions of interest. The fact that only 50 % of the indents on the internal dome fractured the foramen layer seen as ductile pop-ins, is indicating that the foramen layer is tougher than first assumed.

FIGURE 4.5: Schematic illustration of the planned location of the indentation in the foramen pores. When the indent was located in the center of a foramen pore, the indent was assumed fracture more easily as it was as far as possible from the supporting areola structure. The two images are not from the same frustule, but used to illustrate the two inner layers of two different frustules.

4.3   Cantilever Bending Test

Knowing the material properties of pure biosilica would benefit the future work of finite element analysis and atomistic modelling of diatoms. This would further make realistic mechanical simulations possible, an important step towards

the use of diatom frustules in industrial applications. Therefore, revealing these parameters was one of the main areas of focus in this study.

4.3.1   Preparation in DualBeam FIB

The sample preparation for the cantilever bending test (CBT) in this study was based on the same principles as S. H. Bjørnøy [5]. Diatom frustules were moved from a solution of diatoms and methanol and placed on a SEM-stub with a pipette. The sample was then dried with nitrogen and coated in the Cressington 208 HR B sputter-coater with a 10 nm coating of platinum-palladium, 80 % and 20 % respectively. This layer would conduct the electrons away to avoid charge-up effects from the electron beam. After the sputter coater, the sample was again exposed for the nitrogen gun so frustules with week van der Waals bondings were blown away. The samples were then moved to the FEI Helios NanoLab DualBeam FIB. Frustules with concave orientation, i.e. the foramen facing up, were located with the electron beam before the cantilever beams were prepared with the ion beam.

The stage was tilted from -7° to 52° to isolate the foramen layers as solid cantilever beams. All beams were milled out between the foramen pores as seen in Fig. 4.6 in the DualBeam FIB. The pore-distribution in the foramen was the limiting factor for the beam-size. In general, beams of $1,5 \times 5\text{–}8\,\mu\text{m}$ were produced. The thicknes of the beams, i.e. the foramen layer, was between 450 nm and 620 nm. The "cleaning cross section"-tool was used for the milling with a milling depth of $z = 0,30\,\mu\text{m}$. The material treated was sat to Si (silicium) in the software. To make enough space for the indenter tip during the actual bending tests, structures within $5\,\mu\text{m}$ from the beams were milled away. As the beams would be lost when they fracture in the bending test, measurements according to Eq. C.2 was done prior to testing on the SEM-images.

For imaging, best results were obtained with the electron beam set at a voltage of 10 000 keV and a beam current of $0,69\,\text{pA} - 1,4\,\text{nA}$. For the Ga-source, a voltage of 30 000 keV and a beam current of 28 pA created the best images with minimal destruction from the ions. The beam current was increased during the milling to $93\text{pA} - 0,92\,\text{nA}$, with the lowest current closest to the beam. The current should
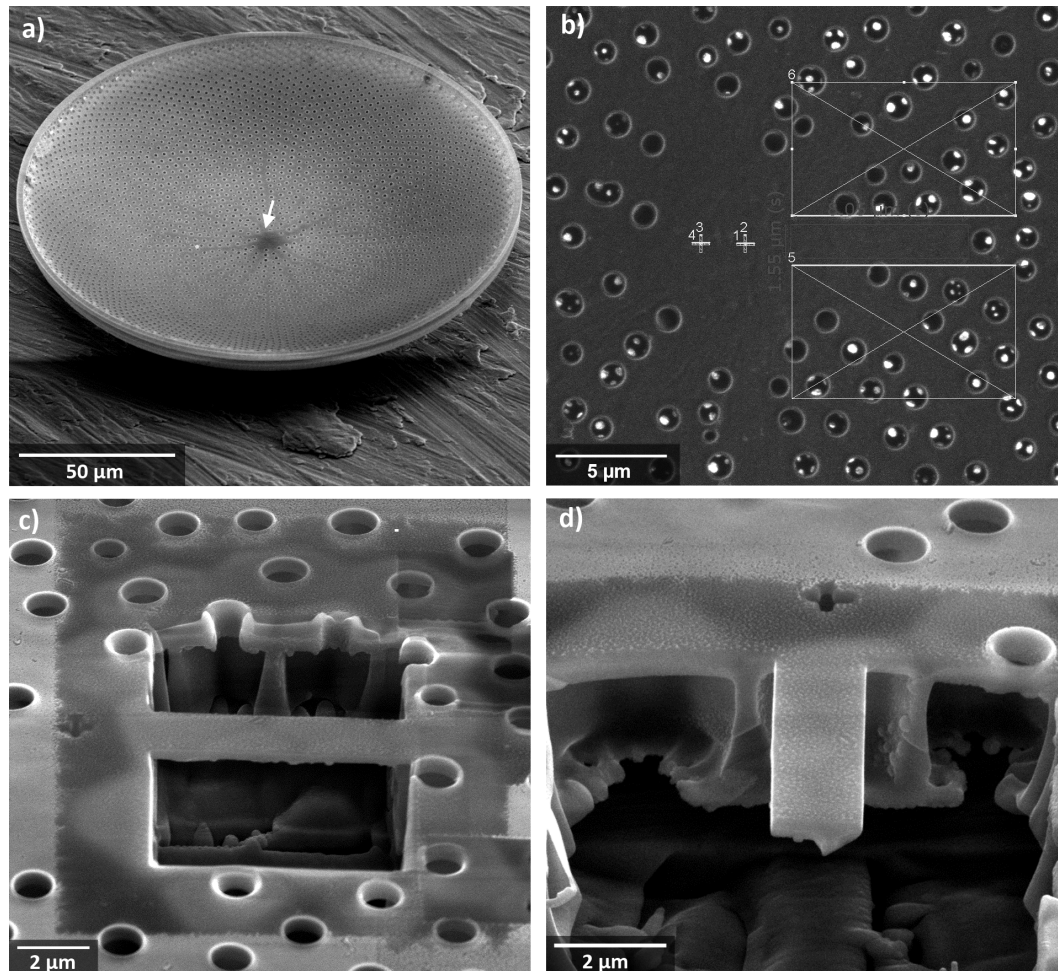
FIGURE 4.6: Stepwise illustration of the beam preparation: a) A frustule with concave orientation was located and the stage was tilted to 52°. The arrow marks an area in a center region of the foramen layer where the pores were aligned with a distance large enough to mill out a beam. b)With the rectangular measurement tool, outlines of a beam was created with desired dimensions. The areas of the two first mills, above and below the beam, were then drawn. c) The foramen was isolated from the structure below by milling with the stage tilted to 10° and then -7°. Stage was then rotated 180° and milled at a tilt of -7°. d) The stage was rotated 90° and tilted back to 52° to mill away the right area as seen in c.

be further reduced when beams are prepared for actual testing. The mentioned values were found suitable during the development of the test-scheme, but causes too much destruction from the ion-beam for reproducible and trustworthy testing. The Everhart-Thornley Detector (ETD) was used for both columns.

An effort was made to position the indenter tip with as less contact with the beam as possible, both in the nano- and the picoindenter. Before the beams were moved to the indenter for testing, $1-2$ position marks, i.e. crosses with lines of

800×100 nm, were therefore milled out. They were positioned 2 µm apart and 2 µm from the beam as seen in Fig. 4.6 d. To practice the positioning of indenter tip in both instruments, aluminium mock-ups were produced and used before the methods were applied on the diatoms. These mock-ups would had the same geometries as the diatom beams, but were completely stable as they were massive and attached to the substrate.

4.3.2   CBT in the Nanoindenter

A conical tip with a radius of 0,6 µm was used, based on the results of S. H. Bjørnøy [5] and other reported micro-cantilever tests [45]. Because the beams were only some hundred nanometers thick, the first beams broke during the initial scanning. To avoid this, the setpoint was reduced from 2 µm to 0,1 µm during the scanning when locating the beams in the nanoindenter. In addition, more time was spent locating the beams by imaging the area with the position marks. By finding the global position of the two crosses, the exact position of the coming indent was calculated and measured.

4.3.3   CBT in the Picoindenter

The importance of seeing the mechanical response *in situ* when developing a test method is imperative. For testing at micro- and nanoscale, size is therefore one of the main challenges as illustrated in Fig D.7 in Appendix D. The picoindenter was introduced as an essential instrument for further development of the test scheme. Beam geometries, load parameters and regulation of the load/displacement during loading was some of the parameters studied with the picoindenter.

The Hysitron PI 85 SEM PicoIndenter was used. The instrument was installed inside the SEM Zeiss Supra 55 VP at the Electron Microscope Laboratory at NTNU. As seen in Fig. 4.7, the picoindenter was mounted on the SEM-stage and tilted 30°. After the sample and the tip was in focus with the electron beam, all movements were controlled by the stage in the picoindenter. The angled view of the SEM made the vertical navigation of the indenter tip difficult and should also
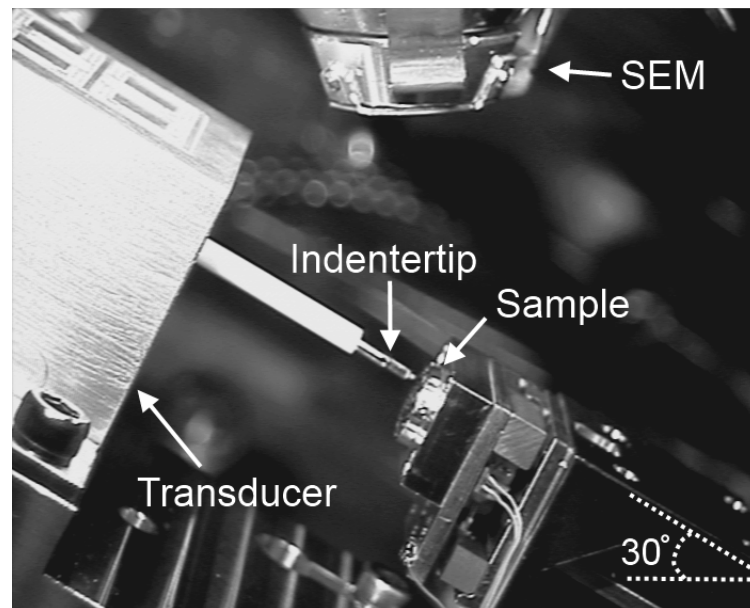
FIGURE 4.7: Image from the optical camera in the SEM-chamber. The whole picoindenter is mounted on the stage and then tilted to a 30° angle.

be remembered when studying the images from the cantilever bending test from the picoindenter. The tip always was perpendicular to the sample, also after when the stage was tilted as seen in Fig. 4.7.

After some sessions in the picoindenter, dust and other particles had been seen on the indenter tip if it was not carefully cleaned with a swab drenched in ethanol. This was therefore done, since particles could make the frustules get stuck easier on the indenter tip.

4.3.4 Cantilever Test Analysis

The initial plan was to analyse the cantilever beams with basic fracture mechanics and beam theory. Based on previous micro-cantilever tests reported in the work of Matoy et al. in 2009 [45], a simple model was made to use this theory on the diatom cantilever beams. Elastic modulus, fracture stress and even fracture toughness were some of the values of interest. Due to time limitations in this work, the analysis was discontinued. The initial strategy for the analysis can be found in Appendix. C.

Chapter 5

Results

The results from the characterisation, nanoindentation and the cantilever bending tests (CBT) of diatom frustules are presented in this chapter. Brief descriptions and explanations are given, but discussions are kept in a minimum. The word "results" might be misleading for some of the test methods as the goal was to gain experience with the equipment and try out different parameters.

Extensive results for can be found in the appendices when specified.

5.1   Characterisation

A summary of the results from the characterisation with the nanoindenter and the confocal micoscope are presented in Table 5.1 and 5.2 respectively. The raw data and formulas for the statistical calculations can be found in Appendix B.1.

5.1.1 Characterisation in the Nanoindenter

Fig. 5.1 shows a typical result from the caracterisation in the nanoindenter.
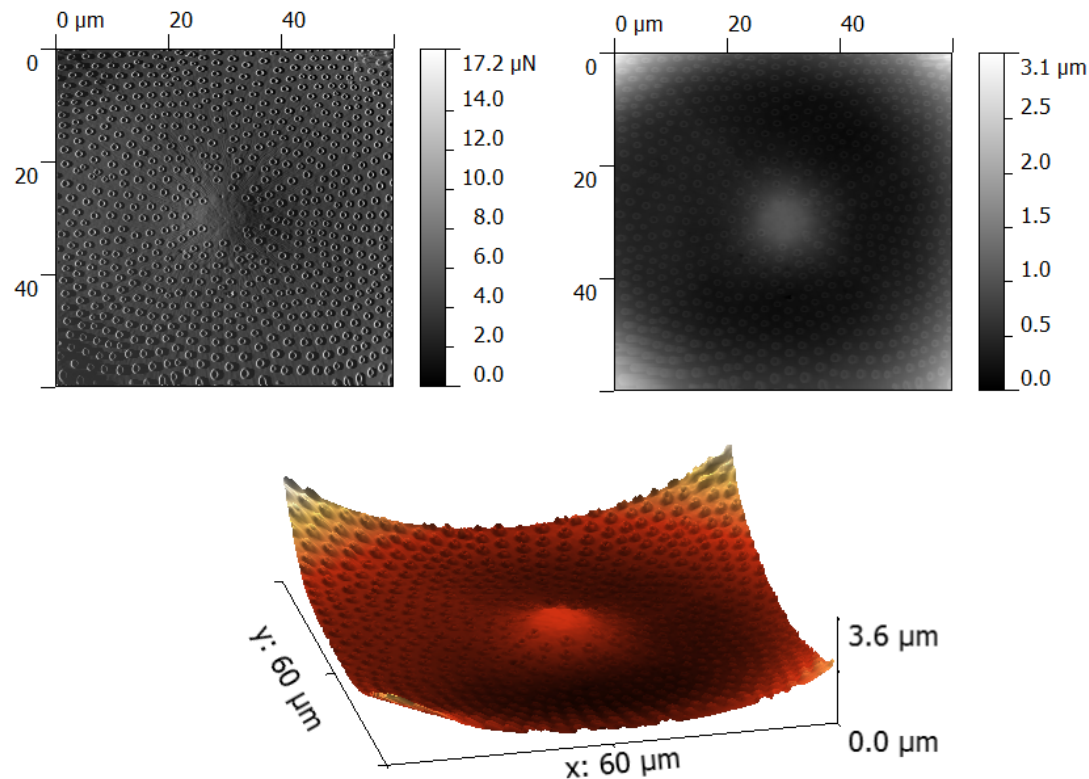
FIGURE 5.1: Images of the gradient error (top left), topography (top right) and a 3D-representation (bottom) of the surface topography. Note: the z-axis is not in the same scale as the x- and y-axis in the 3D-representation.

Ten frustules were successfully imaged. Four images were regarded as unsuccessful due to particles (parts of girlebands and layers from other frustules) on the sample or because movement of the frustules were detected.

TABLE 5.1: Summary of the characterisation in the nanoindenter (n=10), where H is the height of the internal dome, LH is the levelled height of the dome, L is the length of the dome and T is the tilt as defined in Fig. 4.2

	H	LH	L	D
Max	977 nm	942 nm	29,3 µm	2,3°
Min	330 nm	615 nm	22,6 µm	0,5°
Mean	592 nm	734 nm	34,0 µm	1,22°
SD	242 nm	100 nm	10,7 µm	0,70°

5.1.2 Characterisation in the Confocal Microscope

In total, 33 frustules were successfully imaged in the confocal microscope. Fig. 5.2 presents two images from the Alicona software from the topography analysis.
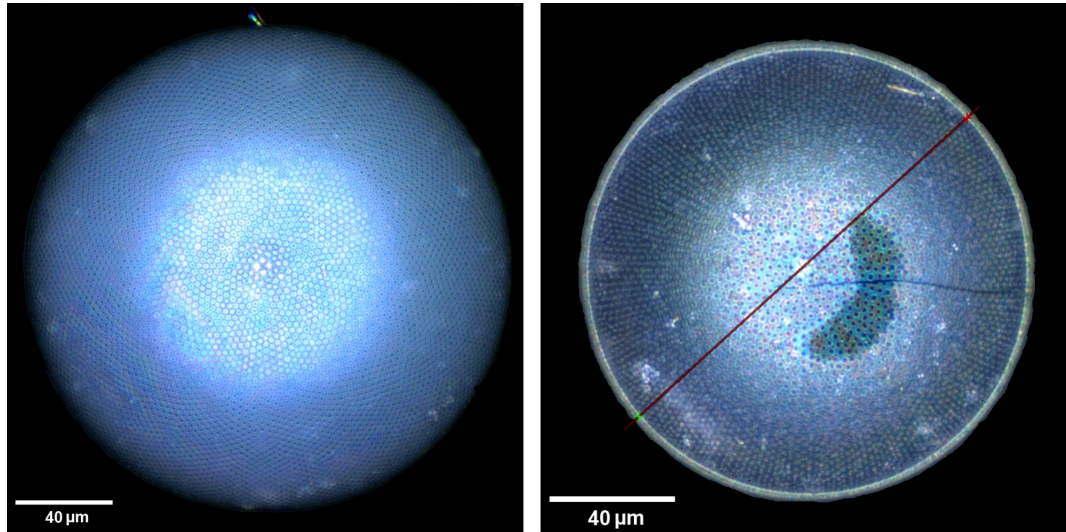
FIGURE 5.2: Images from the Alicona software of the external side, cribrum (left) and the interenal side, foramen (rigth). For frustules with a convex orientation, i.e. the external side facing up, only measurements of the diameter were performed.

Both frustules with a concave and a convex orientation were used for diametric measurements. For the tilt and internal height, only the frustules with a concave orientation were used. A summery of all the results in the confocal microscope are presented in Table 5.2.

TABLE 5.2: Summary of the characterisation in the confocal microscope, where TD is the total frustule diameter, TH is the total height from the internal dome to the highest edge and TT is the tilt of the whole frustule as defined in Fig. 4.3.

	TD (n=33)	TH (n=20)	TT (n=20)
Max	231,16 µm	36,3 µm	6,9°
Min	140,3 µm	17,4 µm	0,4°
Mean	173,4 µm	25,1 µm	2,8°
SD	22,9 µm	5,1 µm	2,0°

5.2   Nanoindentation

5.2.1   Indentation of the Internal Dome

After eliminating frustules with cracks or other defects, 233 successful indents on 30 different frustules were ready to be analysed after testing. Table 5.3 presents all the different tests done on the internal dome in chronological order. A name convention for the different samples can be found in Appendix B together with the extensive results.

TABLE 5.3: Summary of all nanoindentations performed on the internal dome, i.e. the elevation in the center of the foramen layer, in the diatom valves. A series of $5-10$ indents were performed on each frustule. Pop-ins larger then $50\,nm$ were counted to quantify the indents which fractured the indented foramen layer.

Sample	Tip used	Frustules tested	Indents performed	Pop-ins
C1-H_2O_2	Conical	5	25	0 (0%)
S1-H_2O_2	Conical	1	9	5 (56%)
S1-H_2O_2	Cube-cornered	5	45	28 (52%)
S1-H_2SO_4	Cube-cornered	4	29	16 (42%)
S1-SDS	Cube-cornered	5	50	22 (37%)
S2-H_2O_2	Cube-cornered	5	39	19 (40%)
S2-SDS	Cube-cornered	5	36	26 (72%)
TOTAL		30	233	116 (50%)

Fig. 5.3 presents representative indent-series from each of the samples in Table 5.3. The first indent-series done on the diatoms from culture, is seen in Fig. 5.3 a. The diatoms from sample C1-H_2O_2 were grown in the laboratories at the Department of Biotechnology at NTNU. The results after indentation were very different compared to the results in the initial work (Fig 3.4). The depth of the deflection reached $3\,000-3\,500$ nm before the load reached the set-load of $200\,\mu m$. It was assumed that something was elementary different. The frustules were therefore studied in the DualBeam FIB where cross-sections were made to investigate the structure of the sample. SEM-images of different parts were taken and compared with the "net haul"-samples from Trondheimsfjorden.
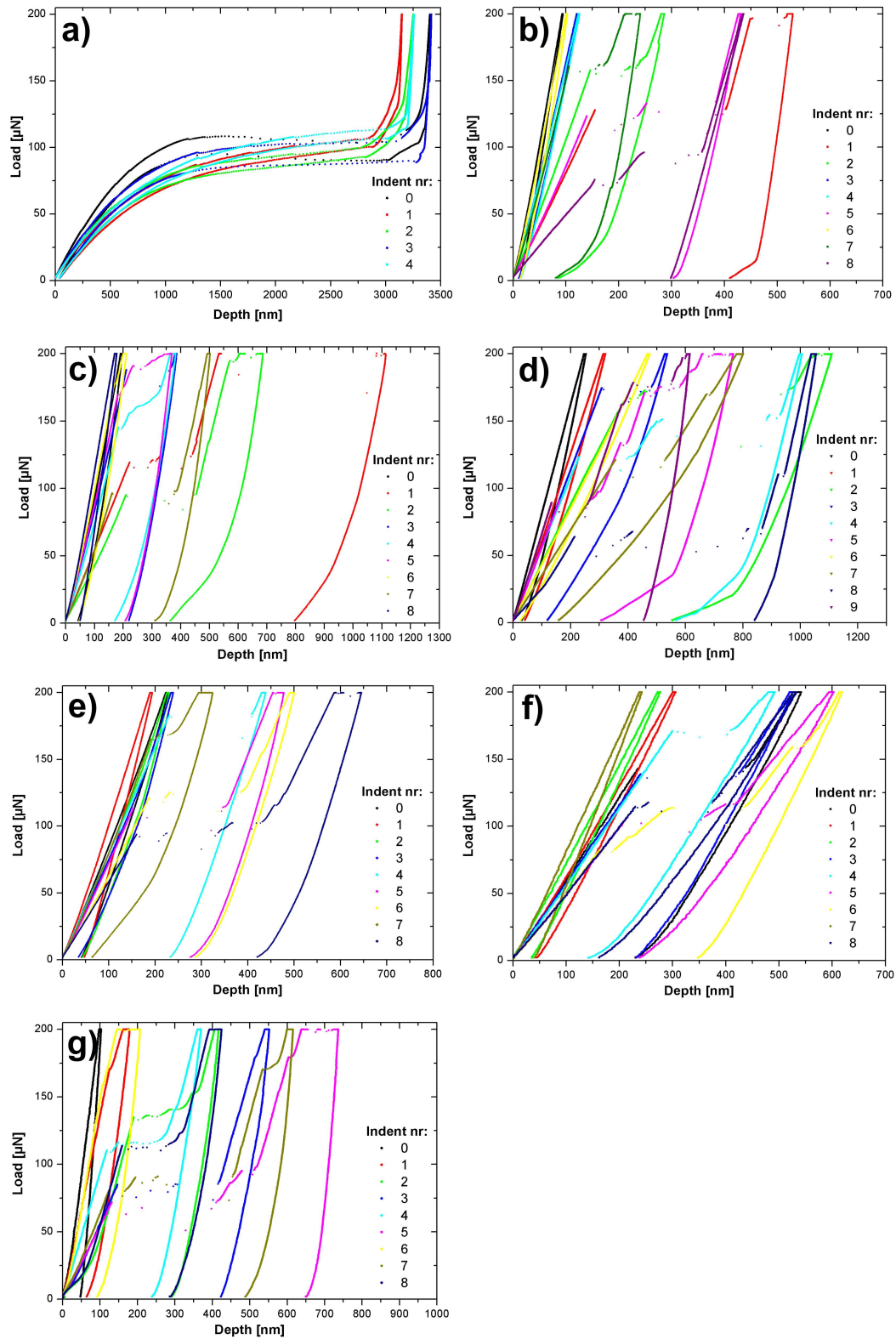
FIGURE 5.3: Typical load-displacement curves representing the indents done on the internal dome. Larger graphs are found in Appendix B.2. a) C1-H_2O_2-A: "net-haul"-sample, conical tip. b) S1-H_2O_2-C: "net-haul"-sample, conical tip. c)S1-H_2O_2-F: "net-haul"-sample, cube-cornered tip. d)S1-H_2SO_4-C: "net-haul"-sample, cube-c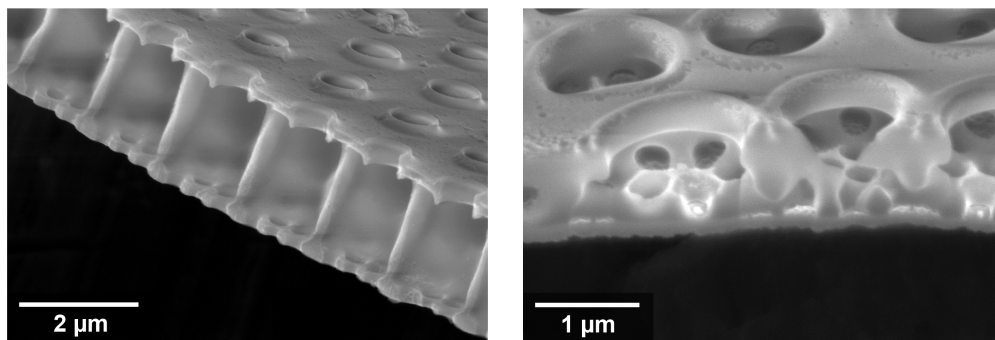ornered tip. e)S1-SDS-G:"net-haul"-sample, cube-cornered tip. f)S2-H_2O_2-G: "net-haul"-sample, cube-cornered tip. g) S2-SDS-B: "net-haul"-sample, cube-cornered tip

FIGURE 5.4: Comparison between a cross-section from a diatom frustule collected in Trondheimsfjorden (left) and a frustule from culture (right). The diatoms from culture got pores aligned with less space between them, both in the foramen layer and the cribrum layer. The biggest difference is the absence of the carrying areola structure in the frustule from culture.

The results from the nanoindentation on diatoms from culture, will be further discussed in section 5.5.1. As they were not regarded as interesting at this point, the samples were replaced with diatoms from Trondheimsfjorden. Nanoindentation on the internal dome was again performed as earlier and this time the mechanical response did remind of the initial testing. The results where analysed in two different ways. The first analysis was based on the chemical pretreatment as done in the initial testing by the author [6]. The second analysis was based on the pop-ins created, i.e. the fractures of the foramen layer.

Chemical Treatment

The different chemical treatment, i.e. removal of the organic content, was expected to be visible in the mechanical response of the frustules. Fig. 5.5 compares the new results with the initial ones. All the indents without fractures, i.e. pop-ins larger than 50 nm, were included. The samples were at this point 4 months old. In the initial experiments, the frustules were fresh when tested. A fresh batch of diatom frustules was therefore ordered for further testing.

The results from batch S2 (Fig. {fig:ind-dome-S2) show an opposite trend of what was seen in the initial testing. As earlier when the results not were as expected, the samples were brought to the Nanolab for observation. Frustules from the same sample were placed on a SEM-stub, coated in the sputter coater and investigated with the DualBeam FIB.
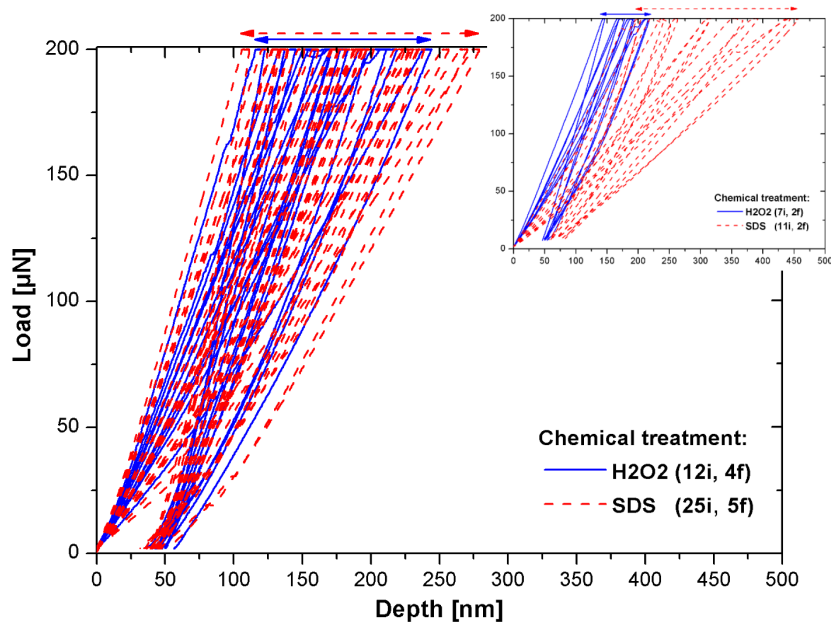
FIGURE 5.5: Load-displacement curves from batch S1 done to compare the response from the pretreatment with H_2O_2 and SDS. Top right is the graph from Fig. 3.4 with the initial results for comparison. Both cleaning-methods results in an average deflection of 175 nm at 200 μN load.
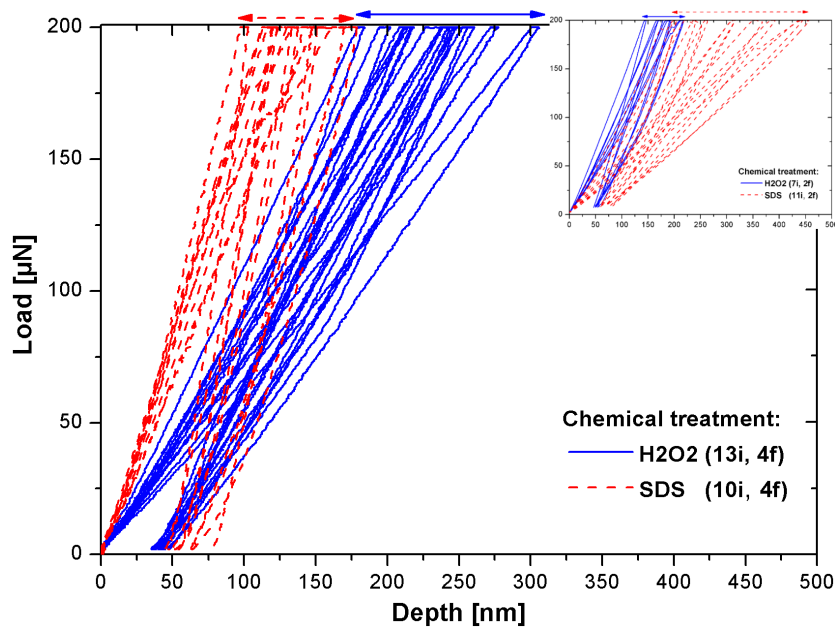

FIGURE 5.6: Load-displacement curves from batch S1 done to compare the response from the pretreatment with H_2O_2 and SDS. Top right is the graph from Fig. 3.4 with the initial results for comparison. The response have shifted compared to the initial results. The H_2O_2-cleaned frustules got an average deflection of 225 nm while the SDS-cleaned frustules now behaves stiffer with a deflection of 125 nm at 200 μN load.
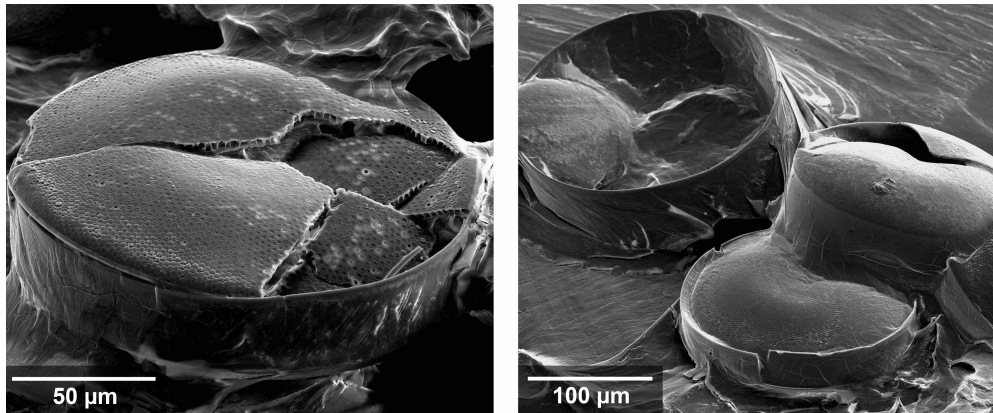
FIGURE 5.7: SEM-images from the DualBeam FIB of SDS-cleaned frustules from batch S2. The frustules were only coated with conductive coating (10 nm) and placed on a SEM-stub. They were then imaging with the electron beam. The valves were still partly attached to the girdle bands. The frustules were covered in some kind of film, much thicker than the conductive coating.

The results from the H_2SO_4-cleaned frustules (Fig. 5.3 d), was supposed to be visible in the graphs with a response between the harshest treated samples with H_2O_2 and the softest ones with SDS. However, they behaved like the frustules cleaned with SDS and H_2O_2, i.e. the results were very scattered. Thus, indentations on the batch cleaned with H_2SO_4 was discontinued.

Location and Pop-ins
The analyses after the nanoindentations were not only sorted and analysed based on the chemical pretreatment. In addition, pop-in depths and pop-in speeds were examined. Further was the relations between the mechanical response and distance from the frustule center investigated. No clear results were seen, although some of the indent-series showed that more indents in the center region went to fracture. Some of the graphs can be found in Appendix B.2.

5.2.2   Local Indentations

Case A: Indentations Between the Foramen Pores
Fig. 5.8 shows indent-series CaseA1 performed with support from the areola walls, on a 7 μm area. Indent 0 and indent 1 are performed on the determined location while indent 2 has moved slightly. Indent 2 appears also to have penetrated deeper than the two first indentationts (Fig. 5.8). The curve representing indent 2 in Fig. 5.9 confirms that the last indent penetrates slightly deeper.
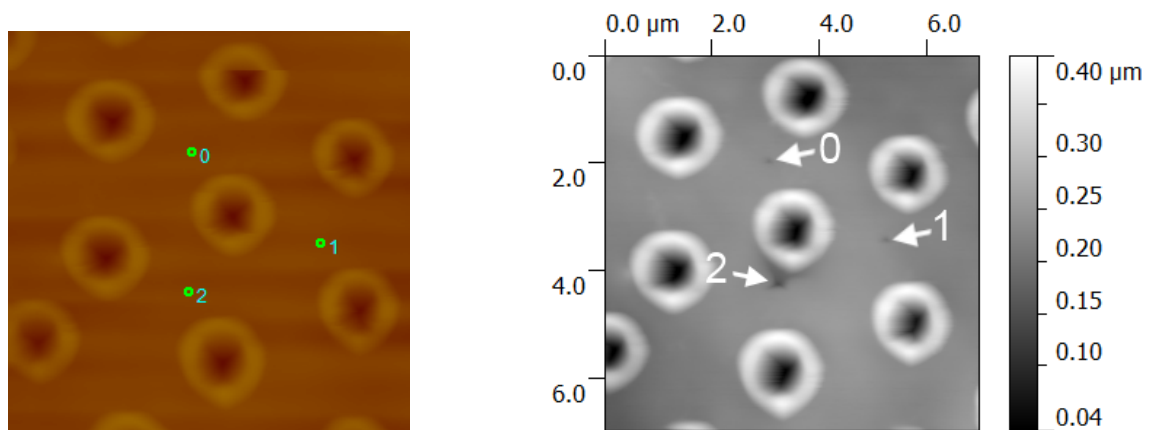
FIGURE 5.8: Images showing defined location of indents prior to testing (left) and a topographic image after indentation (right) from indent-series CaseA1. The arrows marks position of the indents seen as darker areas, i.e. local deflections of the foramen. Indent 2 moved approximately 0,5 μm from the defined location.
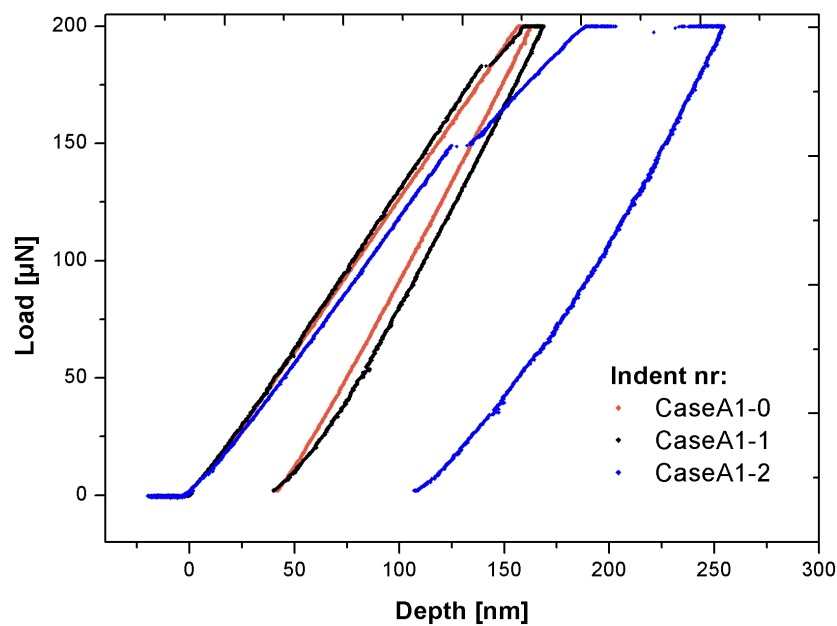

FIGURE 5.9: Load displacement curve of indent-series CaseA1. Both indent 1 and indent 2 have tiny pop-ins at a load of 185 μN and 145 μN respectively.

In total were 7 indents performed with high precision between equally shaped foramen pores, i.e. above the areola cross. All of these had a linear-elastic response as seen on indent 0 and 1 from indent-series CaseA1 (Fig 5.9).

The same method was applied in the picoindenter and the response could be seen with through the electron beam *in situ*. Fig. 5.10 shows a SEM-image after one of the indents between the foramen pores with a set-load off 200 μN. Also here was a cube-cornered tip applied.
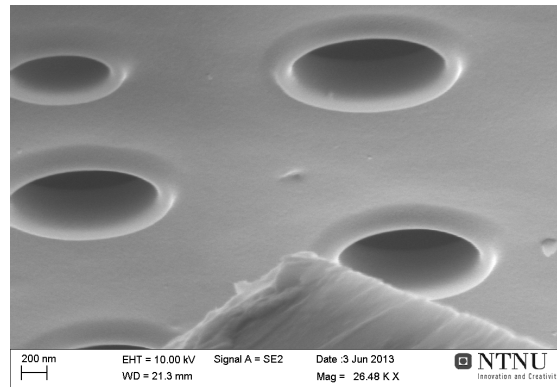
FIGURE 5.10: SEM-image after indent with a set load of 200 μN in the picoindenter.

Fig. 5.11 shows two SEM-images from the picoindenter where three indents were performed on the same location between two foramen pores. A stepwise increase of the load was done until fracture. As seen in the load-displacement curves in Fig. 5.12, the foramen fractured at a load of 555 μN after 656 nm displacement on the third indent.
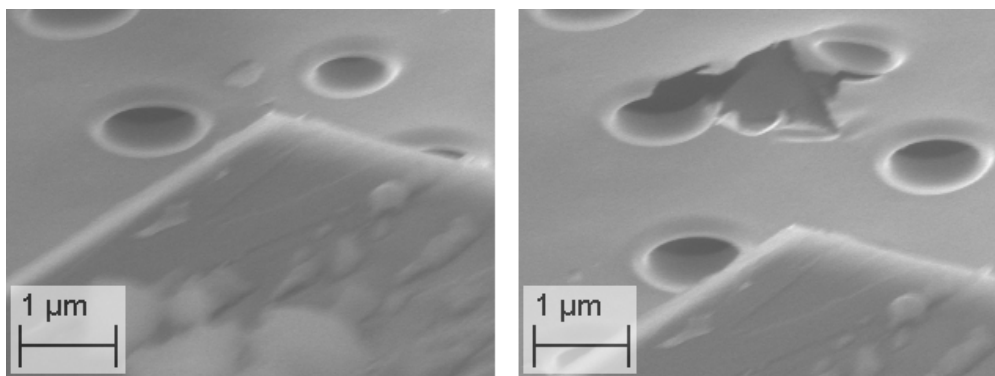
FIGURE 5.11: SEM-images after the first load of 50 μN (left) and 1000 μN (right) in the picoindenter.
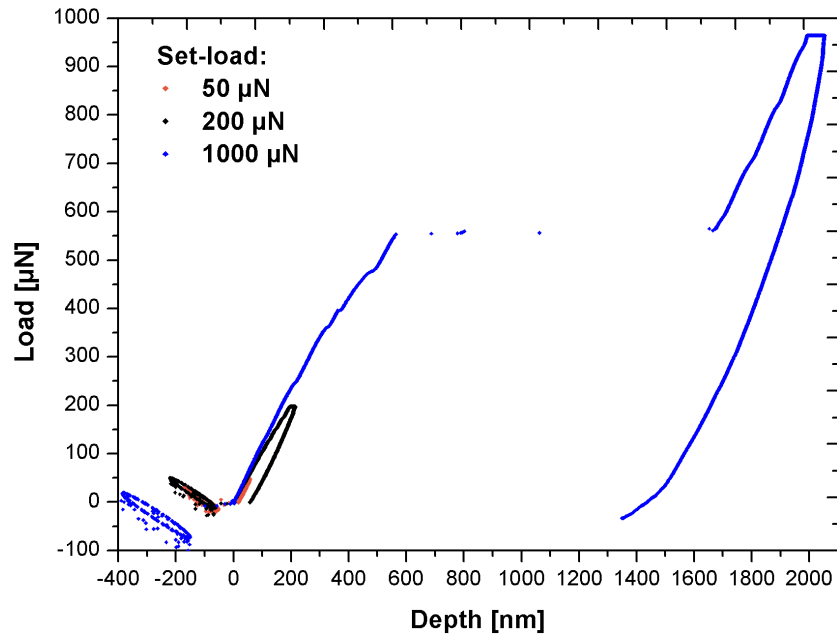
FIGURE 5.12: Load-displacement curve with set-loads of $50\,\mu\mathrm{N}$, $200\,\mu\mathrm{N}$ and $1000\,\mu\mathrm{N}$ in the picoindenter. The foramen fractured at a load of $555\,\mu\mathrm{N}$.

Case B: Indentations in the Foramen Pores

Fig. 5.13 shows SEM-images before and after two indents performed in a foramen pore with the picoindenter. As seen in the load-displacement curves in Fig. 5.14, the foramen fractured in the second indent at a load of $360\,\mu\mathrm{N}$ after a $697\,\mathrm{nm}$ displacement.
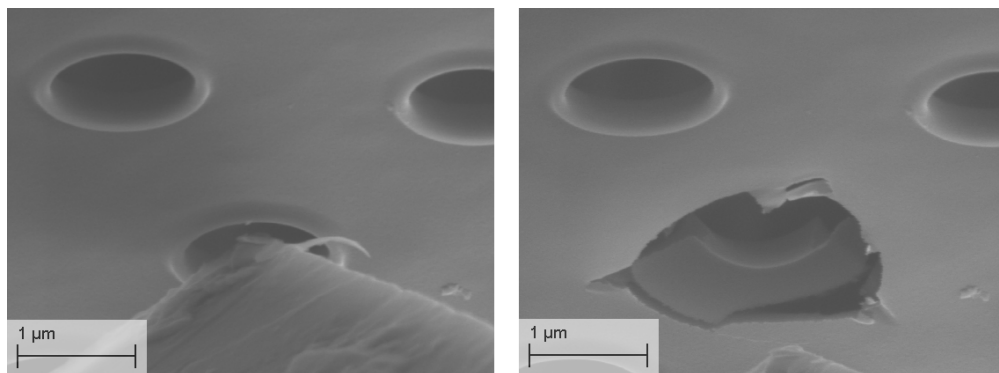
FIGURE 5.13: SEM-images before (left) and after (right) two indents of $200\,\mu\mathrm{N}$ and $500\,\mu\mathrm{N}$ in a foramen pore. The foramen fractured at a load of $360\,\mu\mathrm{N}$.

In the nanoindenter, 5 indents were done inside foramen pores in 4 different series. Set load was 200 µN and all of the indents fractured the foramen layer before they reached set-load as seen in Fig. 5.15.
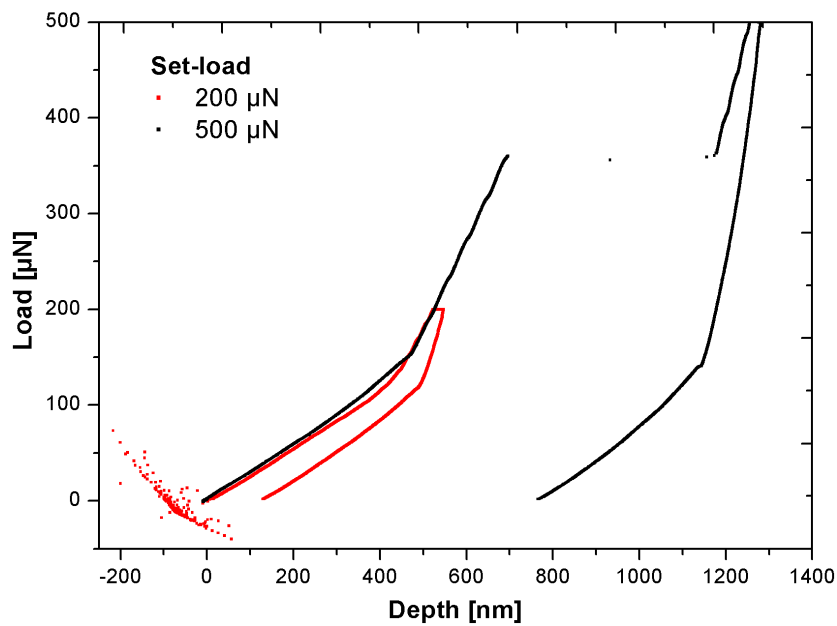
FIGURE 5.14: Load-displacement curves after from indent-series CaseB-4 with two indents of $200\,\mu N$ and $500\,\mu N$ in a foramen pore. The foramen fractured at a load of $360\,\mu N$. Both curves consist of a two-phased behaviour.
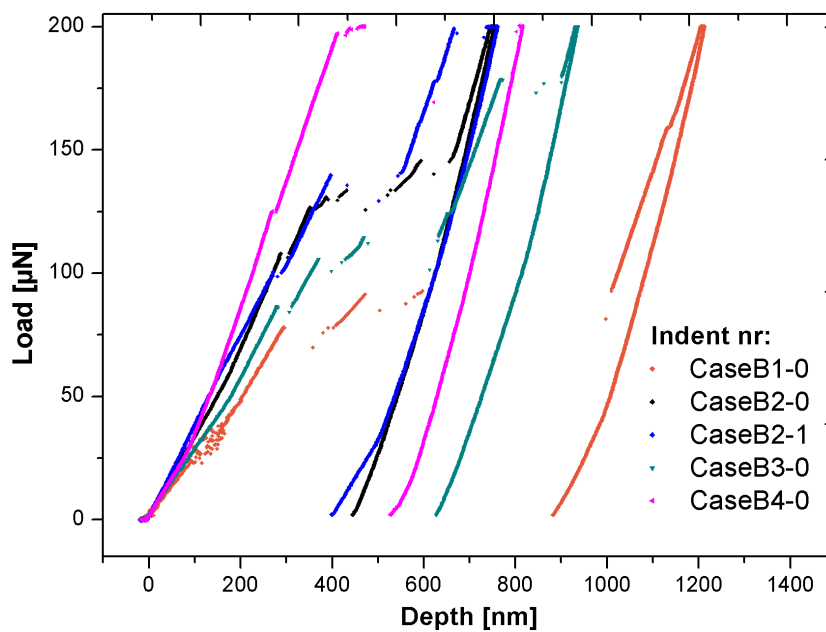

FIGURE 5.15: Load-displacement curves of all the indents with the cube-cornered tip and a set-load of 200 μN. All the indents were done inside foramen pores and all of them fractured before they reached set-load.

5.3   Cantilever Bending Test

21 diatoms cantilever beams were successfully produced in the DualBeam FIB. Additionally 10 beams were almost successfully produced, but due to drift of the ion beam, or moment in the sample during milling, they were not usable. The beams were isolated from the compact foramen structure with sizes from $2 \times 9 \times 0{,}6\,\mu$m down to $1{,}3 \times 4 \times 0{,}35\,\mu$m. However, no successful bending tests were performed during this study. The results in this section are therefore a presentation of both successful and unsuccessful parameters applied. This will reveal the progress of the testing and hopefully function as a framework for further attempts on CBT's.

5.3.1   CBT in the Nanoindenter

In total 10 beams were brought to the nanoindenter for cantilever bending tests. In addition, aluminium mock-ups were tested in order to try out new techniques and methods. Unfortunately, all the first diatom beams broke before the actual bending test was started. This happened during the physical scan, when a too high set-point made the indenter tip fracture the cantilever beam. A parameter study was initiated. A set-point of 0,1 µwas sufficiently low to avoid fracture of the cantilever during imaging.
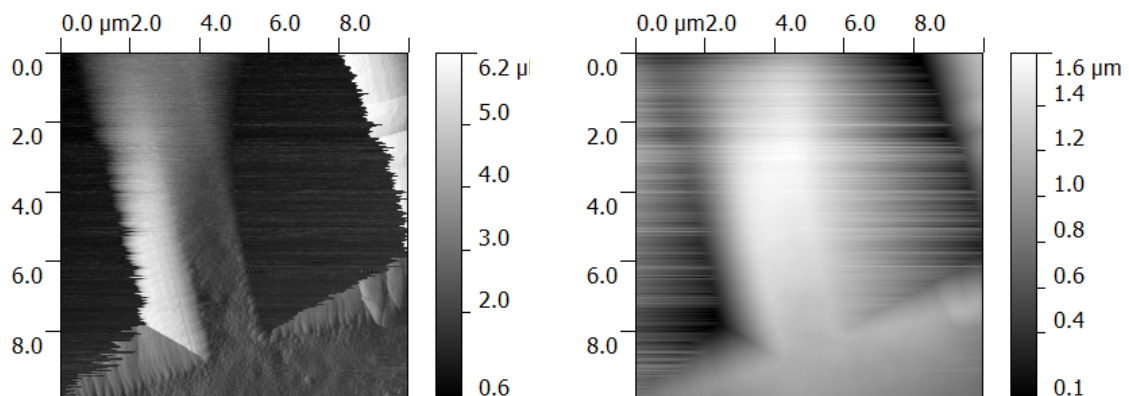

FIGURE 5.16: Gradient image (left) and topographic image (right) of beam N5 in the nanoindenter. The set-point used was 0,1 µN.

Beam N5 was image with a setpoint of 0,1 µN and is seen in Fig. 5.16. This sample was the first exposed to the loading by the indenter tip. The set-load was sat at 50 µN based on the results of S. H. Bjørnøy's testing of isolated foramen beams in the three point bending test. The load-displacement curve is seen in Fig. 5.17.
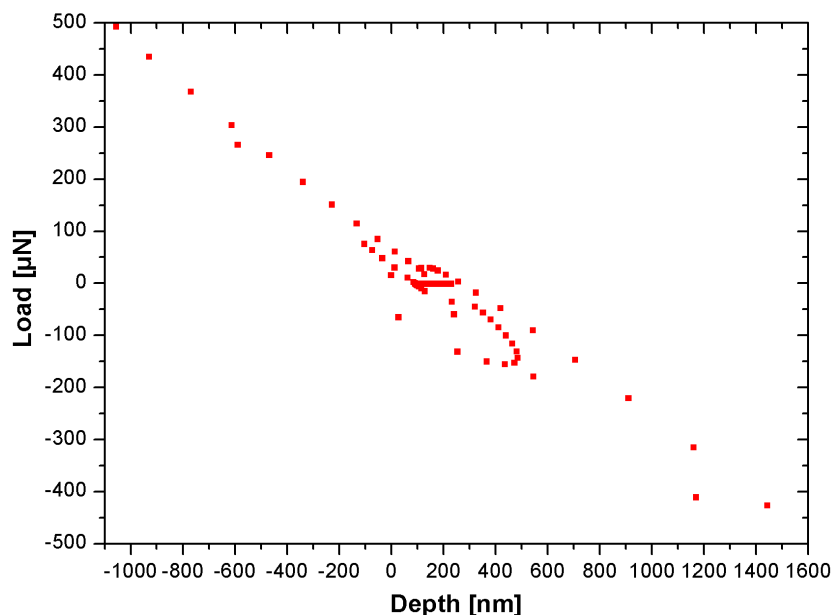
FIGURE 5.17: Load-displacement curve after an attempt of loading beam N5.
The tip did not register the counter-force from the beam and the result is a
"graph" with scattered datapoints.

As the load-displacement curve from beam N5 is illustrating (Fig. 5.17), the transducer was registering random datapoints. When plotted by the software, they were registered as if the tip was oscillating with a higher and higher magnitude. The expected curve would have been similar to the curves from the nanoindentations: A linear-elastic deflection, but with a larger deflection at lower loads. Although the force and deflection information not was captured, the beam broke. Fig. 5.18 shows the cross-section of the fracture-surface when studied and measured with the electron beam in the DualBeam FIB. The black arrows marks circular areas that appears to be inside the biosilica matrix.

The loading of beam N5 was done in the same way as during the nanoindentation. A prescan was needed before the positions of the indents were distributed as in Fig. 5.8. Although beam N5 was imaged, it was assumed that the scan made the beam weaker. The interaction between the tip and the beam was therefore reduced by creating position marks in front of the beam. The area with the position mark was imaged followed by a calculated movement with the off-set to the wanted area of the loading. The indent was then done as quick as possible. This significantly reduced the time from the last movement of the tip and the actual loading. This was assumed to reduce the chance of drift in the system. The result is seen in Fig. 5.19 and Fig. 5.20 on beam N7. The first loading was done in a distance $5\,\mu m$ from the edge of the frustule with a set-load of $20\,\mu N$. The load-displacement curve
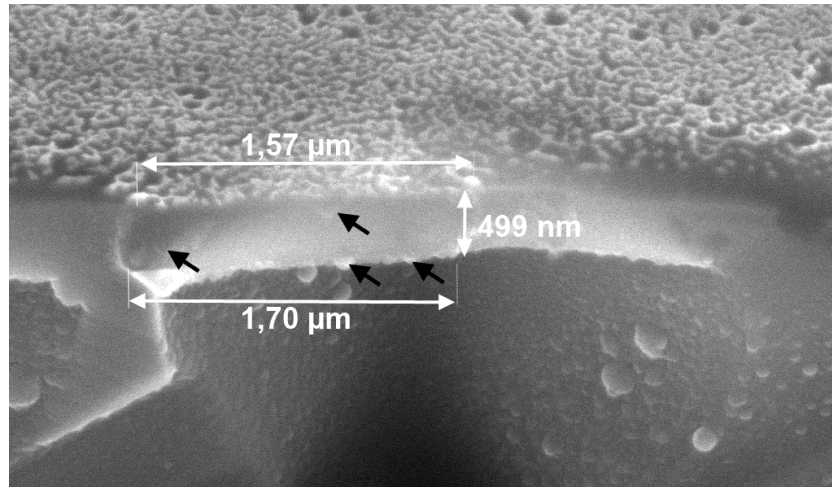
FIGURE 5.18: Cross-section with the average measurements on beam N5. The black arrows marks circular areas inside the biosilica matrix.

from this loading was more as expected. A large deflection was present on a low load, but the beam went elastically back to the original position after the loading. A new load was performed with a higher set-load, $75\,\mu N$. The loading stopped at $38\,\mu N$ with a deflection of $1600\,nm$. The set-load of $75\,\mu N$ was reached when the system registered a random datapoint.
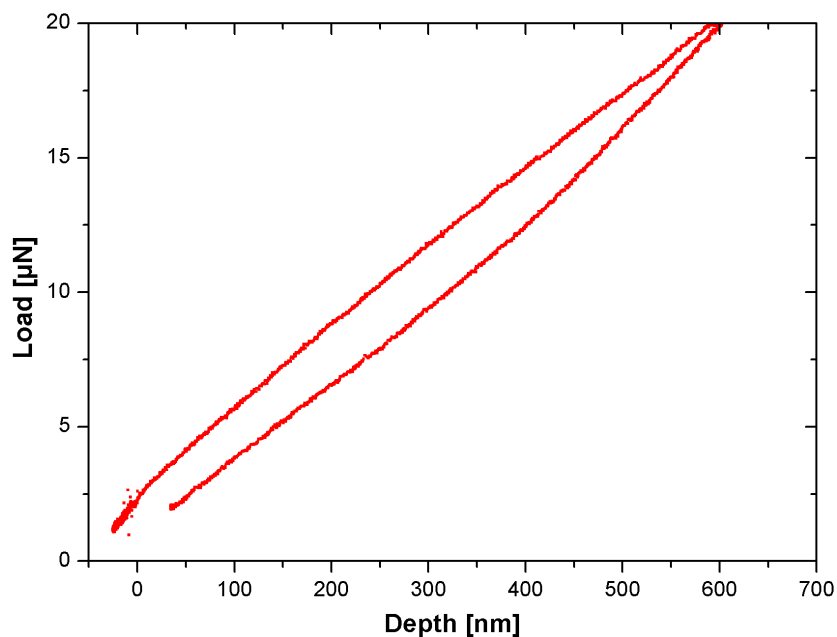
FIGURE 5.19: Load-displacement curve after first loading of beam N7. The rate of the displacement is more as expected in this loading.
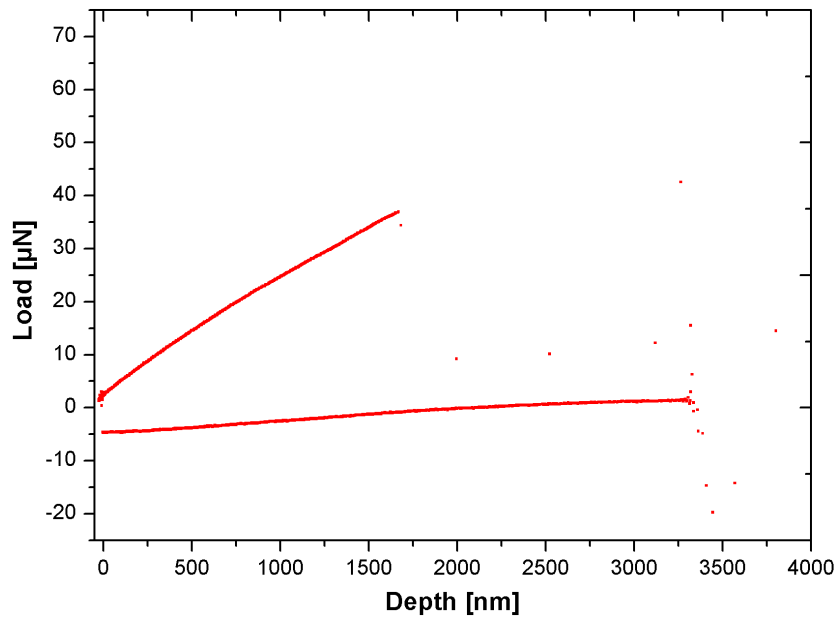
FIGURE 5.20: Load-displacement curve after second loading of beam N7.

The loading of beam N7 was the most successful attempt in the nanoindenter. Beam N1–N3 did all brake during imaging and beam N10 got stuck on the indenter tip. Beam N4, N6, N8 and N9 were loaded, but no results were obtained.

5.3.2   CBT in the Picoindenter

The picoindenter at NTNU had barely been used before this study. The first result from this instrument was therefore to get the equipment running and to be able to navigate manually on the sample surface. This was first practised on aluminium mock-ups with the same geometry as the diatom beams.
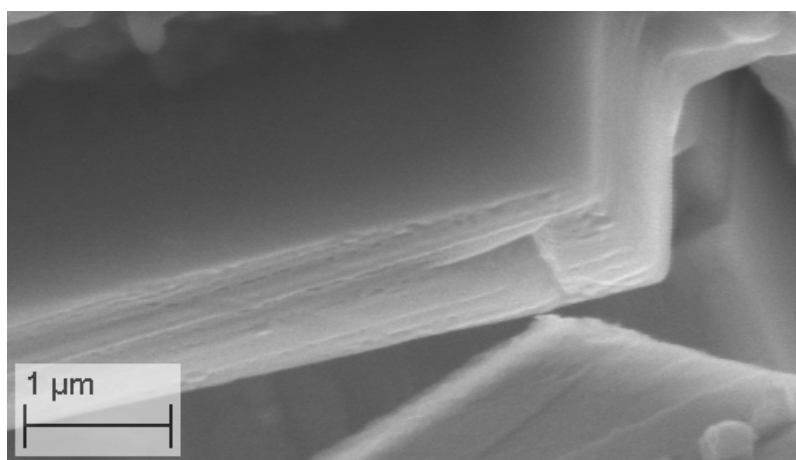

FIGURE 5.21: SEM image of the aluminium mock-up after an indentation. From the triangular indent in the beam, it is clear that the indenter tip was perfectly positioned.

When the sample navigation was under control, next was finding suitable parameters. In total, 5 beams were brought to the picoindenter, but all of them broke without getting a proper response of the pure biosilia. The best attempt of a bending test is shown in the image-series in Fig. 5.22 with the following load-displacement curve of the second indent in Fig. 5.23. The beam was first loaded at 1,5 μm from the beam end with 50 μN. However, the beam was more flexible than assumed, and bent all the way down to the substrate. This happened during an uncontrolled oscillating movement of the tip and did first stop when the beam was bent all the way down to the substrate. After unloading, the beam was still complete and returned to initial position. The load was moved to the middle of the beam, 4 μm from the fixed point in the frustule. Fig. 5.23 shows the load-displacement curve from the second loading.
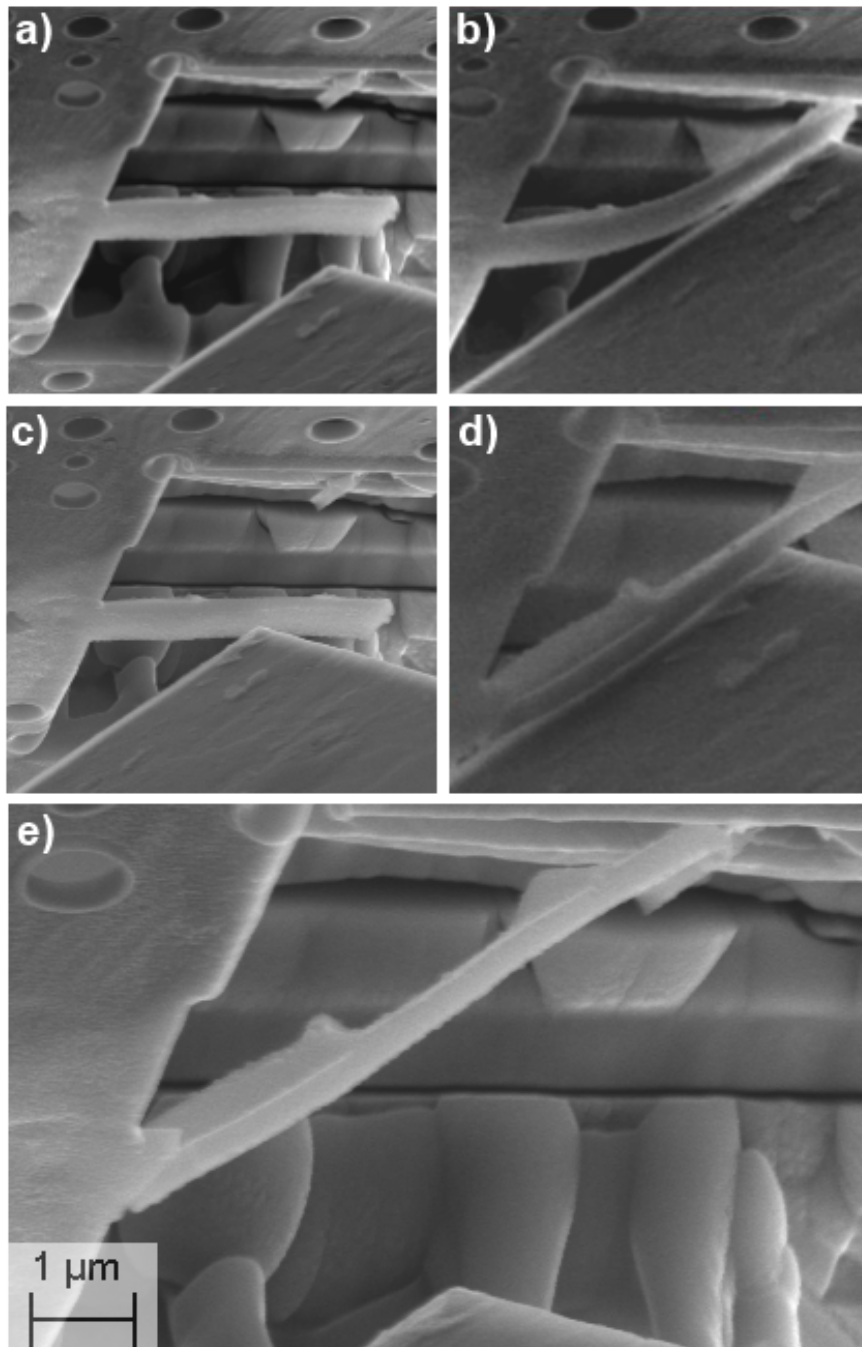
FIGURE 5.22: SEM-images of beam P4 from CBT in the picoindenter. a) The beam was ready for the first loading, set-load 50 μN. b) A a screen-shot was captured during the loading. c) The indenter tip was moved closer to the "fixed" end, set-load was reduced to 20 μN. d) A screen-shot was captured during the second loading. The indenter tip appears to be in contact with the rest of the frustule on the left side. e) Image of the fractured beam after loading.
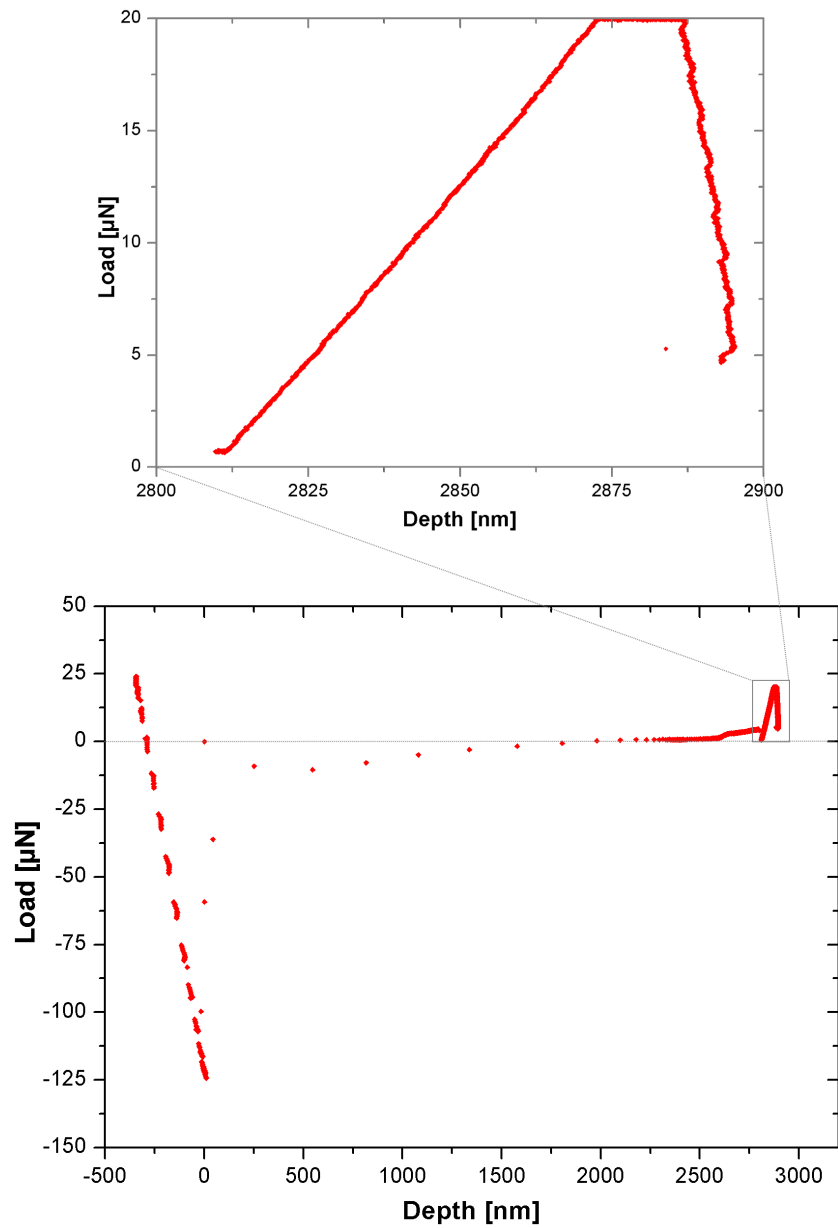
FIGURE 5.23: Load-displacement curve after the second indentation on beam P4. By adjusting the scale of the graph, a proper load-displacement curve is visible in the upper section. The depth of the displacement is around 60 nm with a load of 20 μN.

Discussion

When developing a test method for mechanical measurements, reproducibility is the first goal. A test is worthless if it is not representative and equal for all specimen and samples. In this chapter, analysis of the test validity is presented together with a thorough discussion of the results.

5.4   Characterisation

The characterisation was performed to get a first indication of relevant geometrical information not found in literature. These values were regarded as essential for further development of the mechanical test scheme. It should be mentioned that the results only represent the species *C. centralis*, i.e. one out of 200 000 diatom species. Still, the frustule topography should be known and quantified. The quality of the results from the characterisation, is based on the amount of samples tested and the different sources of error. These errors could be caused by the experimental set-up, measurements, calculations or the statistical analysis. Their impact on the results are discussed below for both of the two characterisation methods.

The measurements from both instruments were based on manually drawn profile curves and points of interest have been found by graphical readings.

5.4.1   Characterisation in the Nanoindenter

When studying the extensive results in App. B.1, almost 90 % of the frustules were tilted in the same direction. A percentage this high could indicate a systematic error. Therefore, an investigation and a control of the tip movement in both forward and reversed directions was done as seen in Fig 5.24.
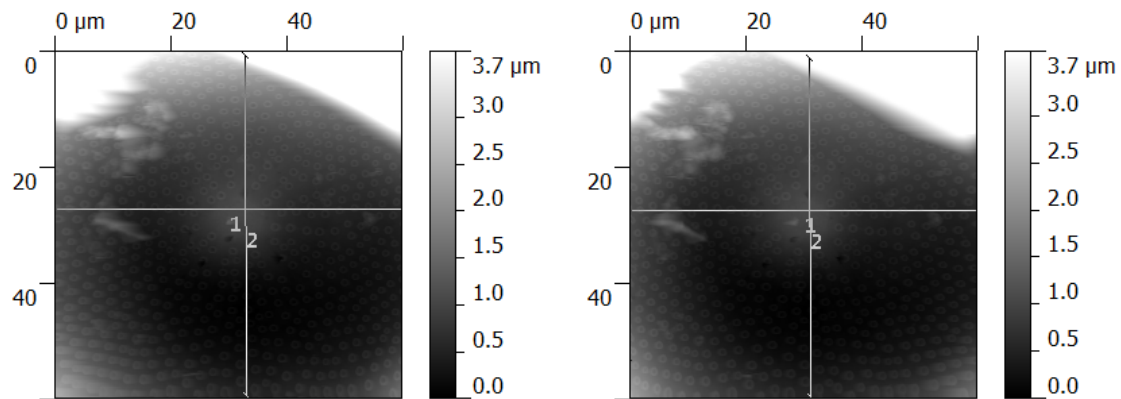
FIGURE 5.24: Forward (left) and reversed (right) scan of a frustule from sample S1-H$_2$SO$_4$. Only two of the four profile lines are here drawn, to control that the indenter tip is registrating the same topological features in both directions.
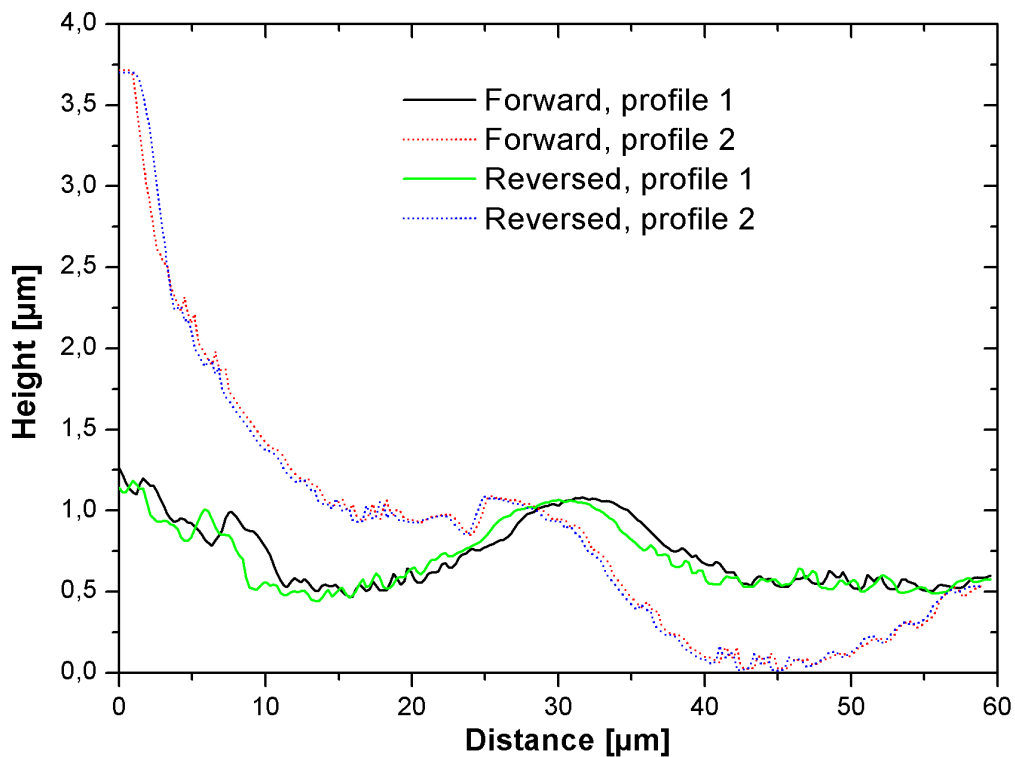

FIGURE 5.25: Control to check that the scan parameters are correct. The profile curves from the scan in forward direction are following the reversed scans for both profile 1 (straight lines) and 2 (dottet lines).

Since the profile lines were drawn manually in the computer software, the vertical shift seen on the curves in Fig 5.25 was considered to be acceptable. As the curves were following each other in both directions, it was concluded that the tilt was not caused by the indenter tip. A larger shift would indicate that some of the parameters, i.e. the scanning speed or the setpoint, were wrong. If the two curves not followed the same paths, the tip could be damaged and not be equal in all directions. This does instead point out that the number of tests (n=10) is way to low to get a good representation of the general shape of the diatom frustule. The results are therefore only an indication of the geometry of the internal dome.

Even though the results only were indications, they provide valuable information for the mechanical testing. The standard deviations reveal a wide scatter in the results and the hypothesis of a size-consistent internal dome is in danger of being rejected. The results are less scattered when the tilt is levelled, but the standard deviation is still large. This means that the internal dome not apears to be a suitable area for reproducible tests, based on size-consistency. As stated earlier, the number of tested frustules is too low so no final conclusion can be drawn. Although the results from the measurements were scattered, clear trends were observed during the nanoindentations on the internal dome. This was done in the search for a correlation between organic content and mechanical response as seen in section 5.2. This could mean that the organic content plays a more important role than the geometrical differences which appears to be present in the internal dome. This will be further discussed in section 5.5.1.

5.5   Nanoindentation

The precision of the indents was a problem for the all the tests in the nanoindenter. A drift up to 0,5 µm was seen from the determined location of indents. In an indent-series, the first indent was normally the best and thenthe position is shifted little by little. This could be caused by movements of the frustule, drift in the transducer or the piezo system. The drift is clearly seen on Fig. 5.8 were only three indents were performed. When comparing the image of the defined positions (left image) with the location of the actual indents (right image), indent 2 have moved closer to the pore. The same tendency was seen even clearer on the indentations on the internal dome where 8 − 9 indents was performed in each series. For accurate nanointentation, only a few indents should be performed in the same indent-series if accurate positioning of the indents is important.

5.5.1   Indentation of the Internal Dome

Nanoindentation was regarded as the best testing method in advance to reveal the assumed correlation between quantity of organic content left in the frustules and mechanical response. A lot of time was therefore spent on locating frustules with correct orientation without visible damages to obtain reliable and trustworthy results. The sample preparation was also an important step, to avoid agglomerations of frustules and girdle bands as seen in Fig. 5.26.
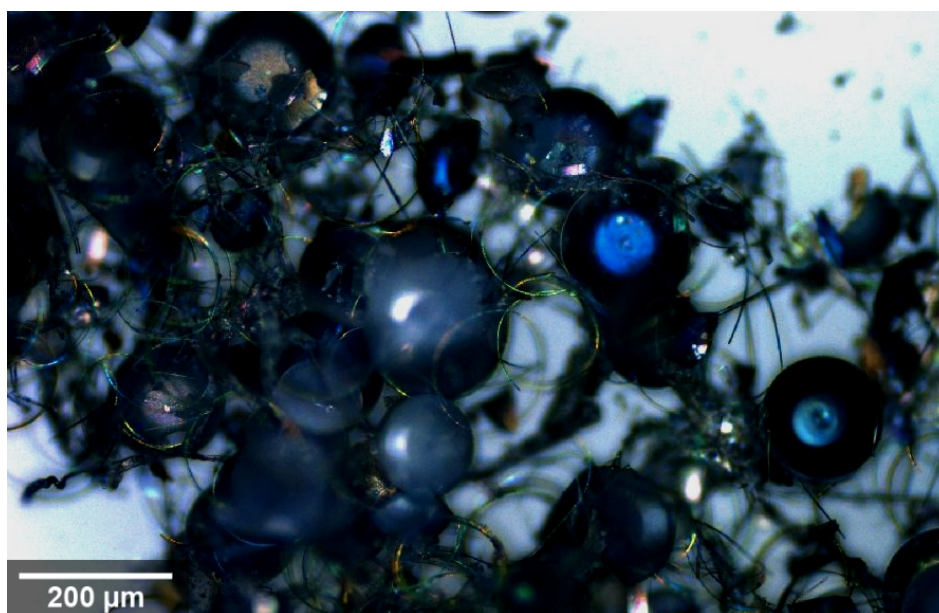

FIGURE 5.26: An agglomarate of diatom frustules and girdle bands, clearly visible in the confocal microscope. Since all experiments in this study are done on single valves, the samples must be prepared in a way that enhance separation of single valves.

As presented in section 5.2.1, the testing of the internal dome had an unexpected start when the diatoms from NTNU's laboratory turned out to be from a different species compared to the authors previous work. When consulting the biologists after the first nanoindentation, they could quickly tell that the tested diatom frustules were from the species *C. wailesii*. This was well known among the biologists, and bad communication between the different researchers led to this misunderstanding. However, the difference in the mechanical response was clearly seen when comparing the behaviour of *C. wailesii* (Fig. 5.3 a) with the *C. centralis* from the initial work by the author (Fig. 3.4). From the graphs, the response in the *C. wailesii* reminds of a visco-elastic behaviour rather than linear-elastic as the brittle biosilica previously have shown. When studying the images from the DualBeam FIB (Fig. 5.4), the biggest difference between the two samples was that

the hexagonal areola structure was absent in the *C. wailesii*. However, the diatom diversity is enormous. In literature, the difference between some of the species is reported to be as big as the difference between fish and mammals [46]. Since the nanoindentation was used as a method to reveal differences in geometrically equal structures, the testing on *C. wailesii* was ended. As a conclusion, a closer cooperation is crucial among the research groups involved for future work on diatoms at NTNU.

In the study of the *C. wailesii*, a conical tip was used. Since the results deviated as much as they did from the initial testing, the tip had to be examined as well. However, the further testing on *C. centralis* showed that the conical tip and the cube-cornered tip created similar responses. The same relation between linear-elastic behaviour and fracture was observed. This can be seen when comparing the samples in Table. 5.3 and their typical load-displacement curves(Fig. 5.3 a and Fig. 5.3 b − g). The cube cornered tip was therefore chosen for the rest of the nanoindentation. This was done to get better quality on the profile scans with the sharpest tip.

Chemical Treatment

The results from the first batch S1 (Fig. 5.5), did unexpectedly not show the same trends as in the initial work (Fig. 3.4). Both the samples treated with H_2O_2 and SDS did reach deflection depths between $100\,\mu m − 280\,\mu m$ at the set-load of $200\,\mu N$. In the initial work, the SDS-cleaned frustules behaved clearly stiffer. The SDS-cleaned frustules were believed to be more elastic due to the organic content as described in section 4.2.1. After a discussion with Post Doc. Romann, a possible explanation was believed to be the long storage time in methanol. The diatoms in the initial work were fresh at the time of testing. When the new tests from batch S1 were performed, the frustules had been stored in methanol for almost 4 months. A reaction between silica and methanol was unlikely, but the methanol could have dehydrated the organic material with a change in their properties as a consequence. This might explain why only the SDS-frustules behaved differently and had a stiffer response to the indentation. This would support the original theory that a the organic material increases ductility in the diatoms.

With this in mind, a new batch (S2) was ordered with frustules cleaned with H_2O_2 and SDS. The new results (Fig. 5.6) were even stranger than for the aged frustules from batch S1 (Fig. 5.5). The results from nanoindentation on frustules from S2 showed a clear trend when sorted on the two chemical pretreatments as in the initial work (Fig. 3.4). However, the two cleaning methods had changed their behaviour - the SDS-cleaned frustules were now the stiffest. The frustules

in sample S2 were stored in a container with ethanol, not with methanol. Still, this change was only believed to cause a slightly longer evaporation time during sample preparation without any influence on the mechanical response.

The SEM-images of the SDS-cleaned sample (Fig 5.7) show frustules covered by a thin film, yet much thicker than the conductive coating (10 nm). In addition, a lot of the frustules were broken. The first assumed explanation, was that the conductive coating had sputtered the sample with wrong parameters, resulting a thicker layer. However, both the SDS-cleaned frustules and the H_2O_2-cleaned frustules were coated simultaneously in the same chamber. As the H_2O_2-cleaned frustules were clean and without this film, the coating could not be the answer. This assumption would not explain the broken frustules either.

Another more reasonable answer, was a change in the chemical pretreatment. Post Doc. Chauton from the Department of Biotechnology at NTNU could tell that the general recipe (Appendix A) for the pretreatment had been slightly changed towards a more time-efficient cleaning process. In addition, the treatment could vary between the different operators. For the SDS-cleaned frustules from batch S2, a milder chemical wash combined with a tougher physical centrifugation was assumed to have made the sample different. The reason why the SDS-cleaned frustules behaved stiffer than the H_2O_2-cleaned frustules remains unknown. More research is needed, but it appears as if the physical stress caused in the pretreatment got a stronger impact on the mechanical properties then the quantity of organic material. A systematic investigation in cooperation with the Department of Biotechnology is needed to investigate this further.

5.5.2 Local Indentations

With a smaller scan size, the indents where believed to be located more precisely. In Case A, the goal was to hit the center between the foramen pores, supported by the underlying areola cross. The topographic image of the indented area from Fig. 5.8 is reproduced as seen in Fig. 5.27. The dotted lines were drawn to represent the areola walls. Both indent 0 and 1 were supported by the areola while indent 2 missed with almost 0,5 µm. The load-displacement curves (Fig. 5.9) reveals that indent 2 had a pop-in 200 µN and reached a displacement of 250 nm, 50 nm more than indent 0 and 1. Since movement of the frustule it self not was detected after indentation, the error in the positioning is most likely caused by drift in the piezo system.
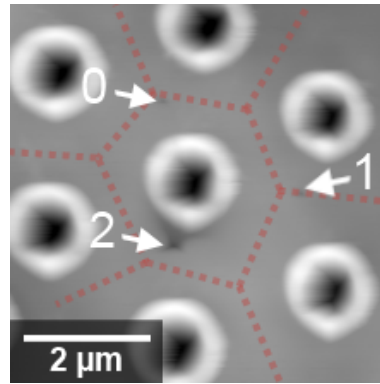
FIGURE 5.27: Image showing the position of the indents in relation the assumed position of the areola walls, here drawn with the dotted lines.

When studying the results from Case A, a clear tendency was seen: the further away an indent was from the the areola cross, the bigger was the chance off a pop-in. This observation was expected and also confirmed by the indents done in Case B with the nanoindenter. With indents positioned as far as possible from the areola structure, i.e. inside the foremen pores, deflection depths of minimum 600 nm were reached at the set-load of 200 μN. However, for the indentations in the picoindenter, the same results were not seen. If the indent was performed perfectly in the center of the pore, a remarkably high force was needed to fracture the foramen as seen in Fig. 5.14. This indicates that the load in the foramen pores is well distributed and supported by the areola walls.

Another interesting observation from the picoindenter, was the fractured areas after indentations. With high-resolution SEM-images, the deformations could be studied in detail in situ and also after the experiments. For all the indents, crack initiations were always stopped in the foramen pores as seen in the right image in Fig. 5.11. The pores appear to have a function to stop crack propagation. This have also been seen *in situ* in the initial work of the author when natural cracks in the diatom frustules propagated further due to local heating from the electron beams [6]. Also here did the crack arrest in the pores.

Crack propagation in diatom frustules has also been reported in literature. When Hamm and Merkel crushed full-sized frustules with glass needles [43], they observed that cracks propagated *around* the frustule pores. In this way the area of the fracture almost doubled with a proportional increase in the amount of energy necessary to break the valves. This was never seen during this study. All cracks propagated through the foramen pores, even cracks that were naturally present as seen in Fig. 5.28. The conditions of loading, thus also the stress-distribution in the frustules, were completely different in this work and the study of Hamm

and Merkel. Which elements contributing to which behaviour would also be an interesting topic for further work. However, in the study of Losic et al. they observed that small lips surrounds the foramen pores [20]. The function of these lips was at that time not understood, but the observations done after the local indentations can indicate that they got mechanical importance.
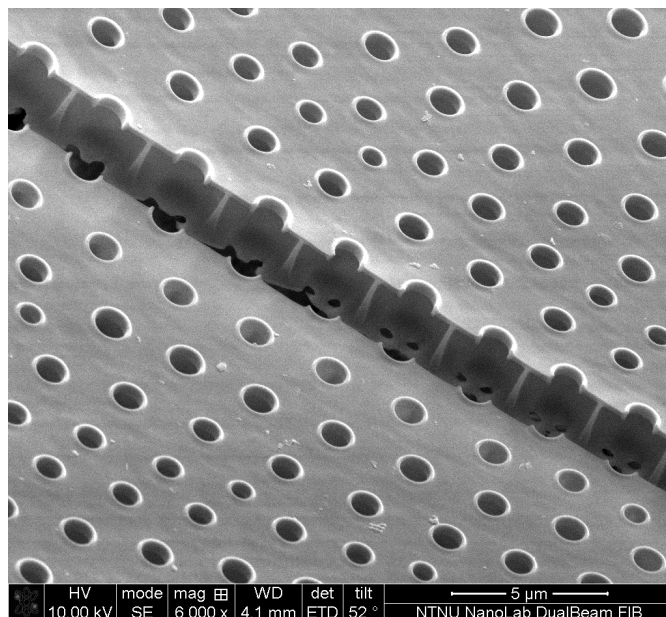

FIGURE 5.28: SEM-image of a crack in one of the diatom frustules. This crack was naturally present in the sample and could have been created during the pretreatment or even from an event before the net-haul.

The last observation done in the picoindenter, was the two-phased response on indent-series CaseB-4 (Fig. 5.14). A two-phased behaviour was present as reported both by S. H. Bjørnøy [5] and Losic et al. [7]. They concluded that the change of the contact stiffness, i.e. slope of the curves, was caused by tilting and penetration of different different layers in the diatom frustule. When the video captured from the experiment was studied, it appeared as though the whole frustule was tilting during the first part of the indent. The position of the tip was for this indent placed further away from the center as seen in Fig. 5.29.

5.6   Cantilever Bending Test

Diatom cantilevers have been produced in the DualBeam FIB in various sizes, but all made out from the foramen layer. This was done to isolate the pure biosilica so accurate material properties could be determined. To the authors knowledge, mechanical measurements without geometric variation from the different layers or the
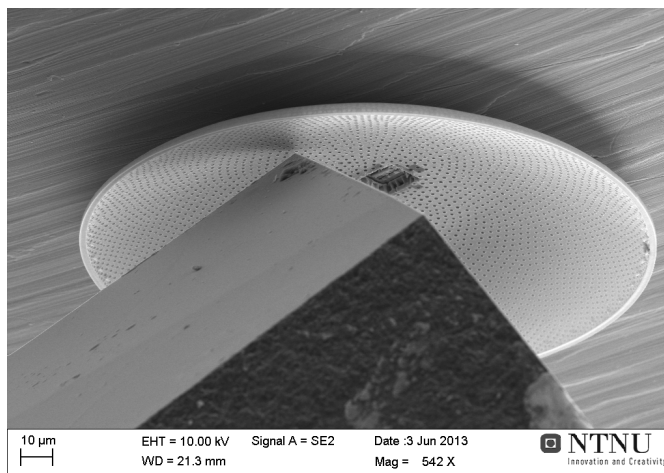
FIGURE 5.29: SEM-image of the location of the indent performed on indent-series CaseB-4 in the picoindenter.

porous nanostrucures, have never been done before on diatom valves. However, no successful cantilever bending tests were performed were material properties could be calculated. Still, the CBT is believed to be a good method for quantification of the material properties of the pure biosilica in diatom frustules. As no final results were produced during the cantilever bending experiments, this section will discuss some of the parameters used and experiences gained throughout the experimental work.

When comparing the results from the pico- and the nanoindenter, their operational principles should be kept in mind. The picoindenter is placed inside vacuum chamber in a SEM while the experiments with the nanoindenter are done in ambient pressure. For the sample, the vacuum could effect the water content in the organic material in the diatom frustules. For the system, the vacuum will reduce the damping caused by the particles in the air. This can again make the regulation process more difficult for the picoindenter.

5.6.1 Sample Preparation

The sample preparation was a comprehensive study itself. With a thickness of only some hundreds of nanometers, the beams were very fragile. This was seen mechanically in the attempts of the cantilever tests, but also during the sample preparation. The biggest problems were the tools for the machining, namely the electron beam and the ion beam. As Fig. 2.7 shows, some of the Ga^+-ions were implanted in the sample during milling. When almost all the kinetic energy from the implanted ions is converted to heat [35], thermal expansions was naturally

seen *in situ* during preparation. Movements of whole frustules and beams were seen caused by the ion beam as well as the electron beam. This made the final process of the beam production difficult and the beams had to be exposed as little as possible both beams.

Finding a general recipe for cantilever beam production was started in the initial work of the author [6]. However, optimization was needed, both to increase the quality of the beams, but also to make the preparation process faster. When aiming for a reproducible test scheme, time cannot be neglected. After 97 hours in the DualBeam FIB, the average production time per beam was in the end reduced from four to one hour.

5.6.2   The Bending Test

To locate the beam, a pre-scan was needed. This scan was initially done with a setpoint of $2\,\mu N$. When the two first beams broke during the scanning, something had to be changed. Two parameters were considered reduced to lower the moment at the beams fixed point: the beam length or the setpoint. Alternative number two was chosen and a parameter study was done on the frustule surface. The lowest usable setpoint when the tip was engaging the sample was $0{,}5\,\mu N$. However, after contact between the tip and the sample was obtained, the setpoint could be further reduced until $0{,}05\,\mu N$. This required a too low tip velocity. In the end, a tip velocity below $8\,\mu Ns^{-1}$ was combined with a setpoint of $0{,}1\,\mu N$ was low enough to image the surface without braking the beam.

The load-displacement curve for the response from beam N5 (Fig. 5.17) consist of a wide scatter of data points, registered at what appear to be at random loads and displacements. With load-control, the transducer was constantly trying to reach calculated values so the load was gradually increase to the defined set-load. This increase of load is regulated with a delay from a feedback loop, giving the next data point a correction for the vibration. However, if the tip is oscillating quicker than this regulation-loop, the system becomes unstable as seen in the load-displacement curve for beam N5.

The load-displacement curve from the testing of beam P4 in the picoindenter 5.23, appeared to be another random collection of data points. However, some interesting observations was done: As seen in the total view of the curve, the indenter started with an oscillating vertical movement, registered as rapid increase and reduction of the load. Then, the load stabilized as the indenter tip moved towards the sample. Since the curve was plotted as a scatter plot, the single data points

in the center indicates that this was a quick movement. The set-load was here sat at 20 µN and since the transducer not was registering any counter force, the tip continued the vertical movement. At a depth of 2 810 nm, a counter force was finally registered. This was probably due to the support from the diatom frustule on the left or from aluminium substrate underneath.

For a better result on the testing of the nest beams, two problems were addressed. The first problem was the uncontrolled vibrations in the indenter tip. This could probably be reduced by changing the parameters for the regulation system, but this was never succeeded. The only parameter that had en effect of changing, was the back-off distance, i.e. the distance between tip and surface right before the indent. During this study, the back-off distance was reduced down to 10 nm. The second problem was related to the sensitivity of the system. The theoretical force-resolution of the instrument is given to be down to 1 nm [39] by the manufacturer. However, since a better regulation of the system not was obtained, the counter-force from the tip was experiencing had to be increased further. This was tried in beam P4, when the loading was moved from 6,5 µm to 4,5 µm from the frustule edge. As the deflection made the beam collide with the aluminium substrate, shorter beams were made in the DualBeam FIB for the following CBTs.

Beams with 5 µm lengths were made both to be tested in the picoindenter and the nanoindenter. Unfortunately, the beams in the picoindenter were not reachable because the stage had a horizontal limit in its movement, shorter than the SEM-stub. The beams in the nanoindenter were neither tested due to the time limitations of this study.

Mechanical properties were not extracted from the CBT. However, some of the fractured areas were examined and measured. During the measurement some circular areas were detected in the fracture surface (Fig. 5.18). This could be the pure silica nodules reported by Losic et al [20]. The fractured area should namely be clean and free for conductive coating or re-deposition from the milling during beam production.

Conclusion

Frustules from *Coscinodiscus centralis* have been characterised in a nanoindenter and a confocal microscope. The initial measurements of the internal dome did not indicate a size-consistency. Still, clear trends were visible in the mechanical response of this region when differently pretreated frustules were tested by nanoindentation. It was assumed that the trends were caused by the pretreatment. A systematic investigation is needed, but it appears as if the physical stress caused by the centrifugation got a greater impact on the mechanical behaviour than the quantity of organic material left in the frustule.

The areas on the foramen layer between equally shaped pores, were found to be stronger than indents performed nearby the pores due to the support from the areola walls. However, indents performed in the exact center of the pores did withstand remarkable high forces. Observations after indentations was performed in a picoindenter, indicates that the foramen pores are important to hinder crack propagation in diatom frustules.

A diatom cantilever bending test has been initiated and could potentially become the first test method to reveal the true properties of the biosilca in diatoms. Cantilever beams have been produced in the DualBeam FIB, isolated from the compact foramen layers with sizes down to $0{,}35 \times 1{,}5 \times 4\,\mu m$. Suitable parameters were found to locate the beams and position the indenter tips in both a nanoindenter and a picoindenter.

Further work

Several interesting observations have been done throughout the work of this thesis. Suggestions for further work are therefore presented in this section to motivate for future studies on diatoms.

5.7 Nanoindentation

Effect of Chemical Pretreatment

It was assumed that not only the organic content had an effect on the mechanical response of diatom frustules after the results done in the initial work by the Author [6]. As this thesis indicates, also the physical stress induced by centrifugation could have an effect on the mechanical behaviour after pretreatments. A systematic investigation should be done to find out which elements in the pretreatment causes is responsible for the change in the mechanical behaviour, organic content left in the frustule or the physical stress induced by the centrifugation of the diatoms.

Indentation Between the Foramen Pores

Some indentations were performed between the foramen pores in this thesis to investigate the response from the testing on the internal dome. However, as described in section 4.2.1, the different layers in the diatom frustule are not physically attached to each other through the silica. With a structured indentation with suitable load parameters, organic content could maybe be detected.

The indenter tip would ideally be flat with a contact area up to 1,5 μm to fit between the foramen pores. However, if the indents are performed in the nanoindenter, the tip must be sharp enough to image the foramen surface. This experiment should be done together with a finite element analysis. Good models could be obtained by using principles of symmetry and by adjusting the parameters, material properties, e.g. the elastic modulus could be extracted.
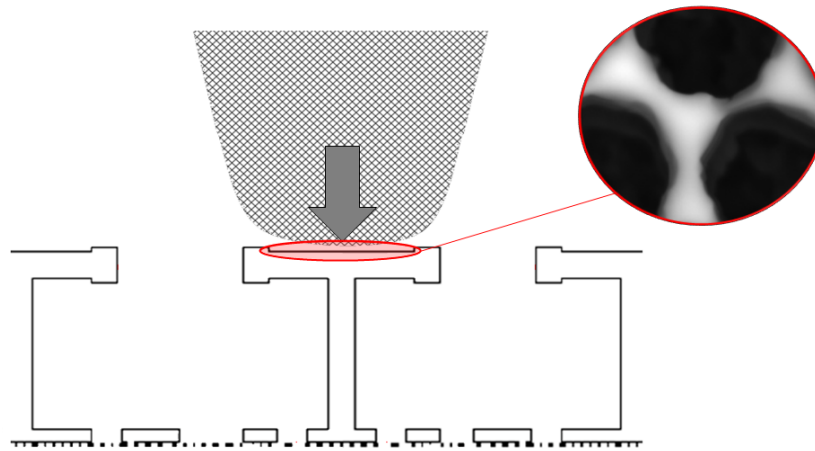
FIGURE 5.30: Schematic illustration of the planned location of the indentation between on the areola cross. The SEM-image is showing the areola cross as seen from above when the foramen layer is removed.

Indentation in the Foramen Pores

By indenting inside the foramen pores, the deflection of the free-standing foramen layer will be detected as seen in the initial testing in this study. If the indent is well positioned, high forces were needed to fracture the foramen layer. At low loading, the foramen layer would act as fixed to the areola walls. With higher loading, the force will be distributed through the foramen-areola connection and down the areola walls.
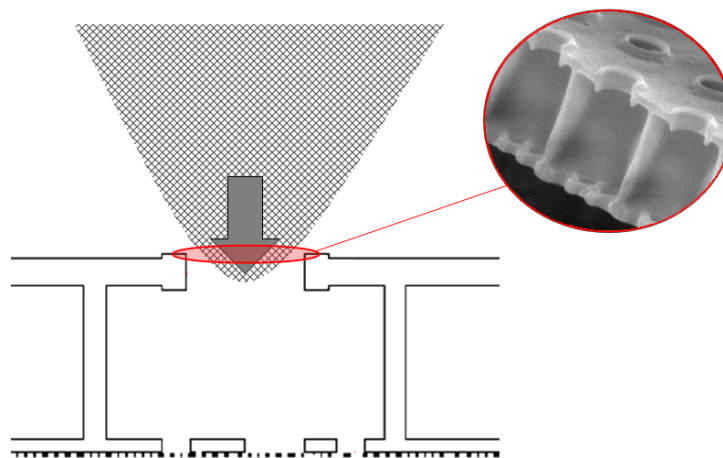
FIGURE 5.31: Schematic illustration of the planned location of the indentation between the foramen pores. The SEM image is a cross-section from a broken frustule, showing the connection between the areola and the foramen layer.

A conical tip should be chosen, small enough to partly enter the pore. Also this set-up is suitable for comparison with FEM-simulations. Also this experiment should be done together with a finite element analysis. Good models could be obtained by

using principles of symmetry and by adjusting the parameters, material properties, e.g. the elastic modulus could be extracted.

5.8 Cantilever Bending Test

The cantilever bending test is in theory suitable to investigate the properties of pure diatom biosilica. The method almost eliminates geometric variation from the layers as well as the porous structure. The CBT could also detect organic materials that might be dissolved inside the biosilica, both by visual inspections as might be seen in Fig. 5.18. When the cultivation of diatom frustules is more stable, the mechanical effects of e.g. titanium doping could also potentially be revealed. This will be highly valued when decisions shall be made based on a possible inverse relationship between mechanical properties and optical functionalities.

The first step towards a successfull CBT, would be to enhance the adherence between frustules and the substrate. This must be done without effecting the reproducibility of the test. Some experiments were done in this study with silver glue. The silver glue made the frustules gather in large clusters and was therefore useless. Polylysine is another alternative, and has previously been reported in literature on sample holders of glass [20]. When the sample holder in the CBT is made from aluminium, a chemical adherence study should be performed to find a optimal recipe which can enhance the adherence and avoid clusters of frustules as seen in Fig. 5.26. Secondly, suitable parameters for regulation systems in both equipments must be found. When the test scheme is functional, CBT from bulk silica could be performed for comparison to the diatom beams of biosilica.

As initially planned, an analysis of the CBT should be performed when the test scheme is fully developed. The suggested analysis seen in Appendix C is good in theory, but should be adopted to the small scales of the diatom cantilever beam. When the sizes are this small, van der Waals forces and other atomic forces starts to dominate. Normal methods of fracture mechanics might not be applied. In addition the biosilica has been reported to contain silica spheres. This makes the matrix it self a composite material and even harder to analyse. A numerical analysis in finite elements could be the only solution.

Bibliography

[1] C.A. Lembi and J.R. Waaland. *Algea and Human Affairs*. Cambridge University Press, 1988.

[2] B.-C. Yoseph. Biomimetics – using nature to inspire human innovation. *Bioinspiration and Biomimetics*, 1.1:1–12, 2006.

[3] A.P. Garcia and M.J. Buehler. Bioinspired nanoporous silicon provides great toughness at great deformability. *Computational Materials Science*, 48(2):303–309, Dec 2010.

[4] M.L. Chiappino and B.E. Volcanic. Studies on the biochemistry and fine structure of silicia shell formation in diatoms. *Protoplasma*, 93:205–221, Jun 1977.

[5] S.H. Bjø rnøy. Nanomechanical testing of diatoms. Master thesis, NTNU, Jun 2012.

[6] M.J. Vebner. Nanocomposites from diatoms. Project thesis, NTNU, Dec 2012.

[7] D. Losic, K. Short, J.G. Mitchell, R. Lal, and N.H. Voelcker. Afm nanoindentations of diatom biosilica surfaces. *Langmuir*, 23(9):5014–5021, Apr 2007.

[8] F.E. Round, R.M. Crawford, and D.G. Mann. *The Diatoms: Biology and Morphology of the genera*. Cambridge University Press, 1990.

[9] J. Bradbury. Nature's nanotechnologists: unveiling the secrets of diatoms. *PLoS Biology*, 2(10):1512–1515, Oct 2004.

[10] D. Werner. *The Biology of Diatoms*. Blackwell Scientific Publications, 1977.

[11] P.J. Lopez, J. Desclés, A.E. Allen, and C. Bowler. Prospects in diatom research. *Current Opinion in Biotechnology*, 16(2):180–186, Apr 2005.

[12] C.B. Field, M.J. Behrenfeld, J.T. Randerson, and P. Falkowski. Primary production of the biosphere: integrating terrestrial and oceanic components. *Science*, 281(5374): 237–240, Jul 1998.

[13] D.G. Mann and S.J.M. Droop. 3. biodiversity, biogeography and conservation of diatoms. *Hydrobiologia*, 336:19–32, 1996.

[14] F. Hustedt. *Die Süsswasserflora Mitteleuropas - Heft 10: Bacillariophyta (Diatomeae)*. Verlag von Gustav Fischer, 2nd edition edition, 1930.

[15] N. Kröger and N. Poulsen. Diatoms-from cell wall biogenesis to nanotechnology. *Annual Review of Genetics*, 42:83–107, 2008.

[16] E. V. Armbrust. The life of diatoms in the worlds oceans. *Nature*, 459(7244): 185–192, May 2009.

[17] M. Sumper and E. Brunner. Learning from diatoms: Nature's tools for the production of nanostructured silica. *Advanced Functional Materials*, 16(1):17–26, 2006. ISSN 1616-3028.

[18] R. Gordon, D. Losic, M.A. Tiffany, S.S. Nagy, and F.A.S. Sterrenburg. The glass menagerie: diatoms for novel applications in nanotechnology. *Trends in Biotechnology*, 27(2):116–127, Feb 2009.

[19] A. Linder, J. Colchero, H.J. Apell, O. Marti, and J. Mlynek. Scanning force microscopy of diatom shells. *Ultramicroscopy*, 42–44, Part 1:329–332, 1992. ISSN 0304-3991.

[20] D. Losic, R.J. Pillar, T. Dilger, J.G. Mitchell, and N.H. Voelcker. Atomic force microscopy (afm) characterisation of the porous silica nanostructure of two centric diatoms. *Journal of Porous Materials*, 14:61–69, 2007. ISSN 1380-2224.

[21] A.K. Noren. Characterization of structure and optical properties of diatoms for improved solar cell efficiency. Master thesis, NTNU, Jun 2011.

[22] L. P. Kollár and G. S. Springer. *Mechanics of composite structures.* Cambridge University Press, 2003.

[23] L. de Stefano, P. Maddalenab, L. Moretti, I. Reaa, I. Rendina, E. De Tommasi, and V. Mocella M. De Stefano. Nano-biosilica from marine diatoms: A brand new material for photonic applications. *Superlattices and Microstructures*, 46:84–89, Nov 2008.

[24] N. Kröger, R. Deutzmann, C. Bergsdorf, and M. Sumper. Species-specific polyamines from diatoms control silica morphology. *Proceedings of the National Academy of Sciences of the USA*, 97(26):14133–14138, Dec 2000.

[25] D.H. Robinson and C.W. Sullivan. How do diatoms make silicon biominerals? *Trends in Biochemical Sciences*, 12:151–154, 1987. ISSN 0968-0004.

[26] E.G. Vrieling, W. W. C. Gieskes, and T.P.M. Beelen. Silicon deposition in diatoms: control by the ph inside the silicon deposition vesicle. *Journal of Phycology*, 35(3): 548–559, 1999. ISSN 1529-8817.

[27] M. Sumper. A phase separation model for the nanopatterning of diatom biosilica. *Science*, 295(5564):2430–2433, Mar 2002.

[28] J. Parkinson, Y. Brechet, and R. Gordon. Centric diatom morphogenesis: a model based on a dla algorithm investigating the potential role of microtubules. *Biochimica et Biophysica Acta*, 1452(1):89–102, Oct 1999.

[29] E.G. Vrieling, T.P.M. Beelen, R.A. van Santen, and W.W.C. Gieskes. Mesophases of (bio)polymer-silica particles inspire a model for silica biomineralization in diatoms. *Angewandte Chemie International Edition*, 41(9):1543–1546, 2002. ISSN 1521-3773.

[30] T. Fuhrmann, S. Landwehr, M. El Rharbi-Kucki, and M. Sumper. Diatoms as living photonic crystals. *Applied Physics B*, 78:257–260, Feb 2004. ISSN 0946-2171.

[31] N. Hall and G. Ozin. The photonic opal - the jewel in the crown of optical information processing. *Chemical Communications*, 21:2639–2643, 2003.

[32] C. Jeffryes, Campbell J., H. Li, J. Jiao, and G. Rorrer. The potential of diatom nanobiotechnology for applications in solar cells, batteries, and electroluminescent devices. *Energy, Environment and Science*, 4:3930–3941, 2011.

[33] Alicona. *Alicona InfiniteFocus IFM Manual*, Nov 2008.

[34] P. J. Goodhew, J. Humphreys, and R. Beanland. *Electron microscopy and analysis*. London : Taylor & Francis, 2001.

[35] C.A. Volkert and A.M. Minor. Focused ion beam microscopy and micromachining. *MRS Bulletin*, 32:389–399, 2007.

[36] W.C. Oliver and G.M. Pharr. An improved technique for determining hardness and elastic modulus using load and displacement sensing indentation experiments. *Journal of Materials Research*, 7:1564–1583, 1992.

[37] H. Chandler. *Hardness testing*. ASM International, 1999.

[38] A.C. Fischer-Cripps. *Nanoindentation*. Springer Science and Buisness Media, 2011.

[39] Hysitron. *TI 950 Triboindenter User Manual*, 2011. Revision 9.3.0313.

[40] Hysitron. *PI 85 SEM PicoIndenter User Manual*, 2011. Revision 9.2.1211.

[41] D. Losic, J.G. Mitchell, and N.H. Voelcker. Diatomaceous lessons in nanotechnology and advanced materials. *Advanced Materials*, 21(29):2947–2958, 2009. ISSN 1521-4095.

[42] N. Almqvist, Y. Delamo, B.L. Smith, N.H. Thomson, A. Bartholdson, R. Lal, M. Brzezinski, and P.K. Hansma. Micromechanical and structural properties of a pennate diatom investigated by atomic force microscopy. *Journal of Microscopy*, 202(3):518–532, Jun 2001.

[43] C.E. Hamm, R. Merkel, O. Springer, P. Jurkojc, C. Maier, K. Prechtel, and V. Smetacek. Architecture and material properties of diatom shells provide effective mechanical protection. *Nature*, 421(6925):841–843, Feb 2003.

[44] C. Jeffryes, T. Gutu, J. Jiao, and G.L. Rorrer. Metabolic insertion of nanostructured tio2 into the patterned biosilica of the diatom pinnularia sp. by a two-stage bioreactor cultivation process. *ACS Nano*, 2(10):2103–2112, Oct 2008.

[45] K. Matoy, H. Schönherr, T. Detzel, T. Schöberl, R. Pippan, C. Motz, and G. Dehm. A comparative micro-cantilever study of the mechanical behavior of silicon based passivation films. *Thin Solid Films*, 518(1):247–256, 2009. ISSN 0040-6090.

[46] C. et al. Bowler. The phaeodactylum genome reveals the evolutionary history of diatom genomes. *Nature*, 456(456):239–244, October 2008. doi: 10.1038/nature07410.

Appendix A

Recipe for Chemical Treatments of Diatoms

SDS/EDTA-CLEANING

Approximate dry-weight of cells: 2 mg (after step 2)

Samples should be checked in light microscope after step 3 and 4, to follow the degree of frustule disruption

NB! Cells are harvested by centrifugation, depending on the available volume this may take some time (before Step 1 can be initiated).

| STEP 1: | Wash with MQ-water, 15 mL, Centrifugation between each washing, 4500 rpm/10 min/room temp | **x 3** |

| STEP 2: | Dry in heating chamber overnight at 60°C, weigh the sample and adjust the protocol if necessary | |

| STEP 3: | Wash with 4 mL SDS/EDTA and mix/vortex 1 min Reaction time 20 min Centrifugation between each washing, 4500 rpm/10 min/room temp

After last washing the frustules were left to stand overnight in SDS/EDTA in the freezer. | **x 6** |

| STEP 4: | Wash with MQ-water, 4 mL Centrifugation between each washing, 4500 rpm/10 min/room temp | **x 3** |

| STEP 5: | Dry in heating chamber overnight at 60°C | |

| STEP 6: | Wash with 96% ethanol Centrifugation between each washing, 4500 rpm/10 min/room temp | **x 3** |

| STEP 7: | Storage in the freezer for further use | |

H_2O_2–CLEANING

Approximate dry-weight of cells: 2 mg (after step 2)

Samples should be checked in light microscope after step 3 and 4, to follow the degree of frustule disruption

NB! Cells are harvested by centrifugation, depending on the available volume this may take some time (before Step 1 can be initiated).

STEP 1:	Wash with MQ-water, 15 mL, Centrifugation between each washing, 4500 rpm/10 min/room temp	**x 3**
STEP 2:	Dry the sample overnight at 60°C, weigh the sample and adjust the protocol if necessary	
STEP 3:	Add 3 mL H_2O_2 (30%) and place in a warm bath 90°C for 6 hours. Check pH at the start and end. Add 1 mL HCl (37%) Centrifugation, 4500 rpm/10 min/room temp After the addition of the sulphuric acid the mixture was left standing overnight.	
STEP 4:	Wash with MQ-water, 4 mL Centrifugation between each washing, 4500 rpm/10 min/room temp	**x 3**
STEP 5:	Dry in heating chamber overnight at 60°C.	
STEP 6:	Wash with 96% ethanol Centrifugation between each washing, 4500 rpm/10 min/room temp	**x 3**
STEP 7:	Storage in the freezer for further use	

Appendix B

Extensive Results

A name convention was introduced and was maintained throughout the practical part of this project thesis. A general name from the nanoindentation would have the following structure:

AB-CCC(CC)-D _ E, where:

A indicates if the diatom sample is collected from sea, S or culture, C.

B indicates the batch number, first batch 1 or the second batch2. The different batches were both collected and treated chemically at different times.

CCC(CC) indicates the chemical treatment applied, SDS, H_2SO_4 or H_2O_2

D indicates different diatom frustules, A-X.

E indicates the number of the indent.

For the cantilever beams, the chemical treatment and the batch numbers are irrelevant. The beams are therefore titled with N for nanoindenter or P for picoindenter, depending on the instrument used in the loading. This letter is followed by the beam number for in the respective instrument.

B.1   Characterisation

TABLE B.1: Extensive results from the characterisation in the nanoindenter.

Sample	Height of dome		Length of dome	Tilt
	Not levelled	Levelled		
S1-H2O2-G	330 nm	658 nm	33,5 μm	0,5°
S1-H2O2-K	354 nm	703 nm	31,9 μm	0,6°
S1-H2O2-L	414 nm	615 nm	26,3 μm	0,8°
S1-H2SO4-C	977 nm	942 nm	22,6 μm	2,2°
S1-H2SO4-D	599 nm	751 nm	31,8 μm	1,5°
S1-SDS-E	883 nm	826 nm	28,8 μm	1,8°
S1-SDS-F	695 nm	797 nm	29,1 μm	1,3°
S1-SDS-G	479 nm	631 nm	34,0 μm	0,6°
S1-SDS-H	834 nm	732 nm	28,5 μm	2,3°
S1-SDS-I	358 nm	687 nm	26,2 μm	0,5°
Mean	**592 nm**	**734 nm**	**29,3 μm**	**1,2°**
SD	**242 nm**	**100 nm**	**3,6 μm**	**0,7°**

TABLE B.2: Extensive results from the characterisation in the confocal microscope

Sample	Frustule diameter	Total internal height	Tilt
S1H-A	179 µm		
S1H-B	179 µm		
S1H-C	181 µm	26,8 µm	2,4°
S1H-D	155 µm	19,6 µm	-1,3°
S1H-E	214 µm	32,9 µm	5,1°
S1H-F	161 µm	21,7 µm	-2,6°
S1H-M	170 µm	21,6 µm	0,7°
S1H-G	202 µm		
S1H-H	166 µm		
S1H-I	200 µm		
S1H-J	191 µm		
S1H-K	155 µm		
S1H-N	151 µm	21,0 µm	-2,3°
S1H-O	231 µm	32,4 µm	-1,1°
S1H-P	215 µm	36,3 µm	-5,5°
S1H-Q	144 µm	21,0 µm	-3,4°
S1H-R	150 µm		
S1H-S	191 µm		
S1H-T	190 µm	26,3 µm	-1,5°
S1H-U	194 µm	23,1 µm	-1,2°
S1H-V	190 µm		
S1H-W	141 µm		
S2H-A	161 µm	25,7 µm	6,9°
S2H-B	159 µm	26,0 µm	-5,4°
S2H-C	163 µm		
S2H-C	148 µm		
S2H-D	161 µm	20,1 µm	-0,9°
S2H-E	141 µm	17,4 µm	-1,4°
S2H-F	180 µm	26,3 µm	-4,5°
S2H-G	177 µm	32,0 µm	4,3°
S2H-H	179 µm	21,9 µm	-0,6°
S2H-I	155 µm	27,4 µm	4,0°
S2H-J	189 µm	22,9 µm	0,4°
Average	**175 µm**	**25,1 µm**	**2,8°**
SD	**23 µm**	**5,1 µm**	**2,0°**

B.2   Nanoindentation

FIGURE B.1: Load-displacement curves from the representative indent-series A from sample C1-H_2O_2. This is a sample from culture of species *C. wailesii*, indented with a conical tip.
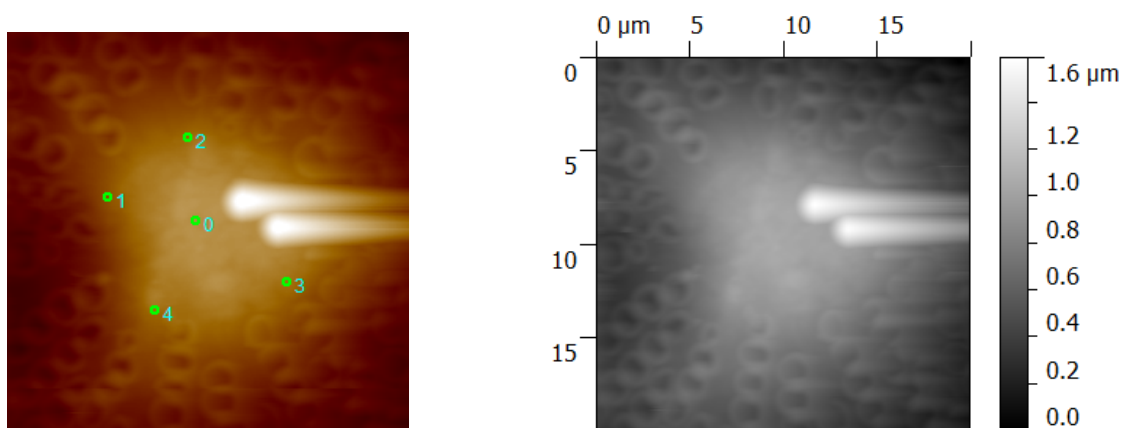
FIGURE B.2: Images showing defined location of indents prior to testing (left) and a topographic image after indentation (right) from indent-series C1-H_2O_2-A
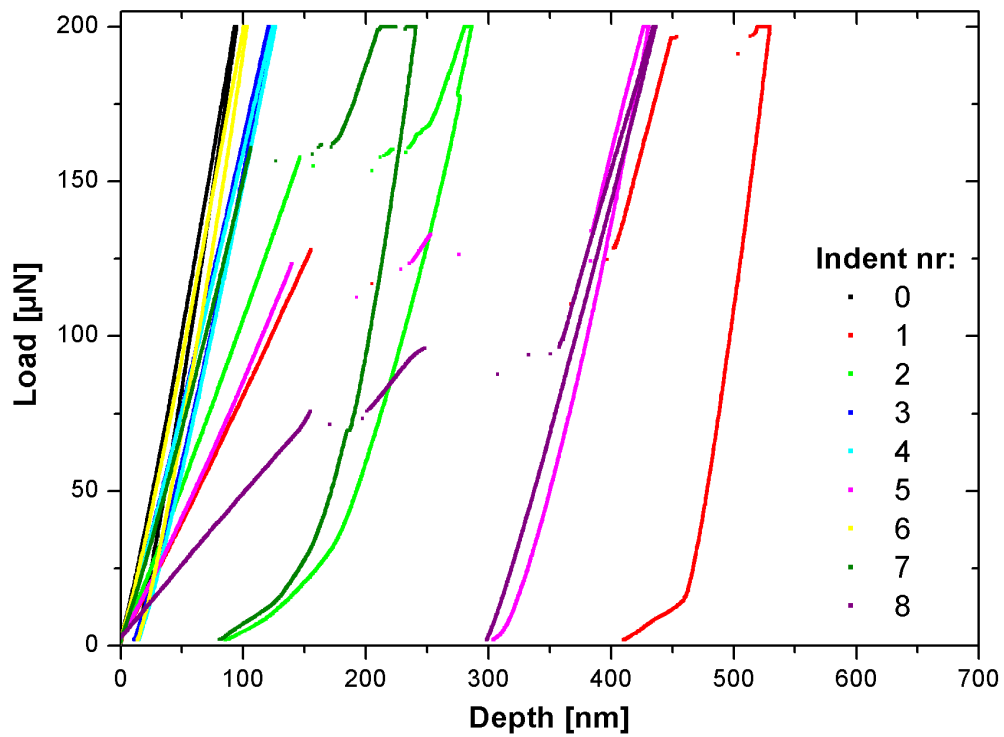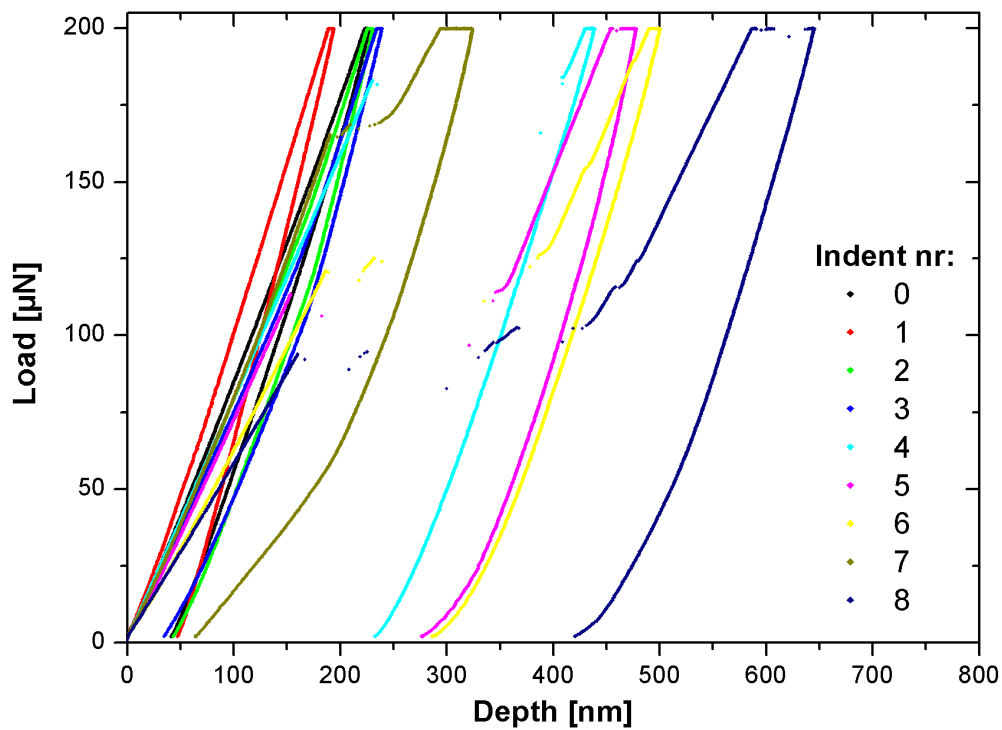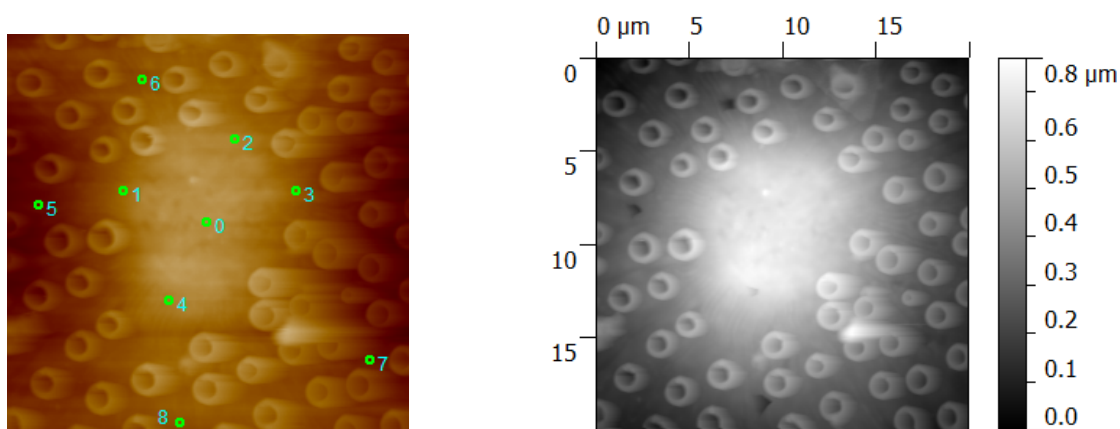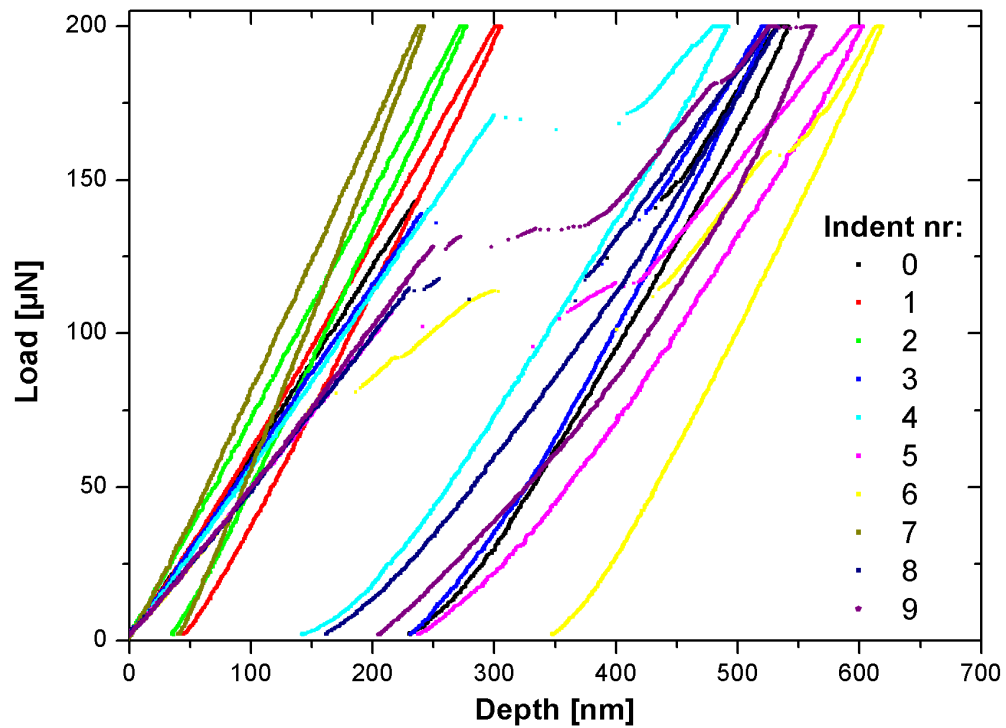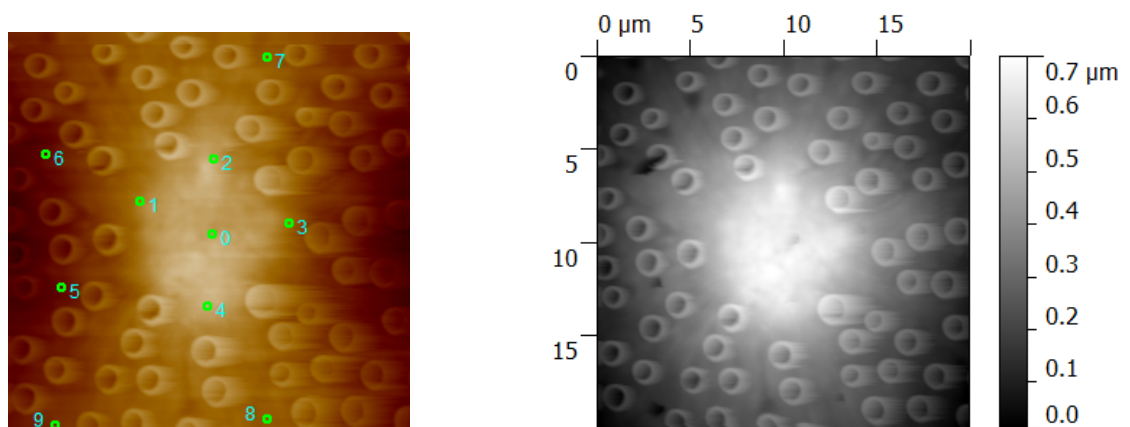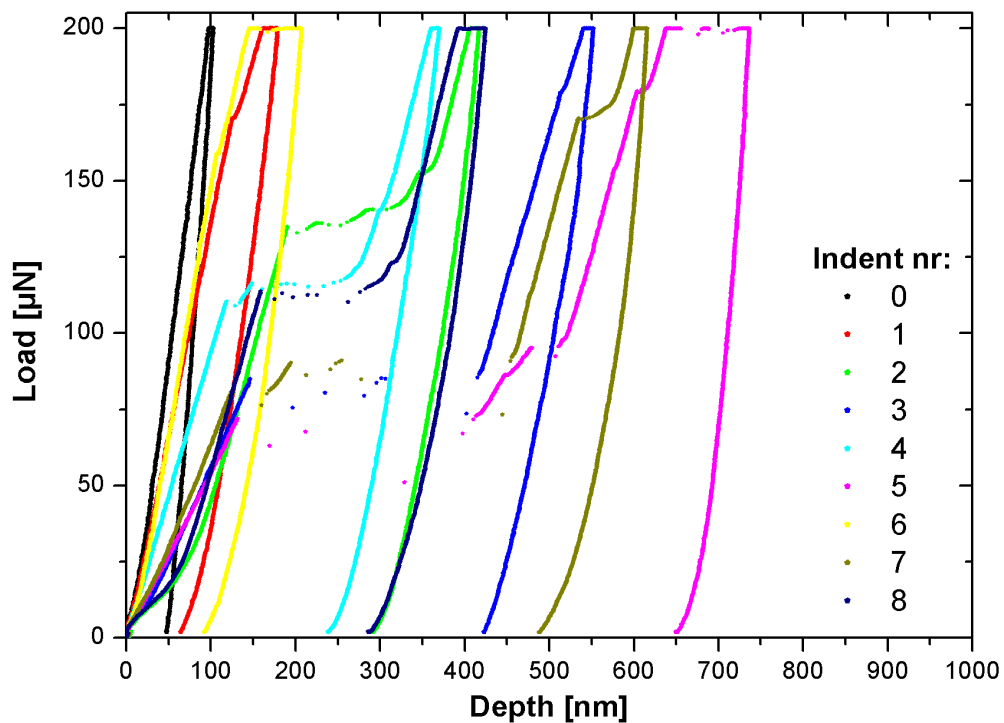
FIGURE B.3: Load-displacement curves from the representative indent-series C from sample S1-H_2O_2. This is a "net-haul"-sample of species *C. centralis* from batch 1, indented with a conical tip.
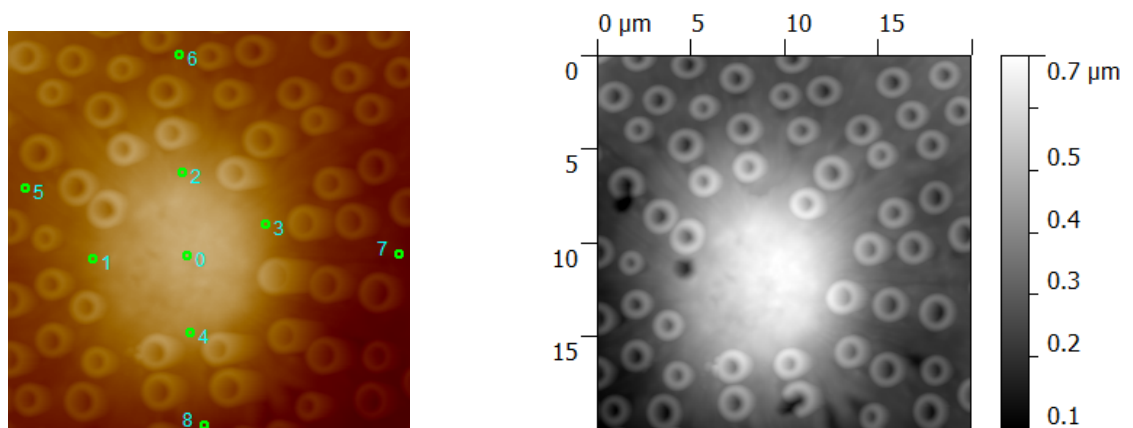
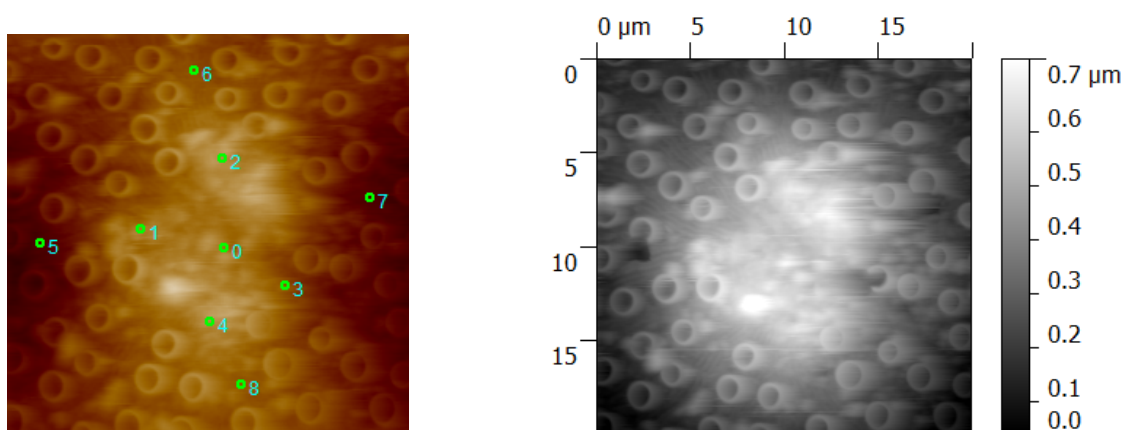
FIGURE B.4: Images showing defined location of indents prior to testing (left) and a topographic image after indentation (right) from indent-series S1-H_2O_2-C.
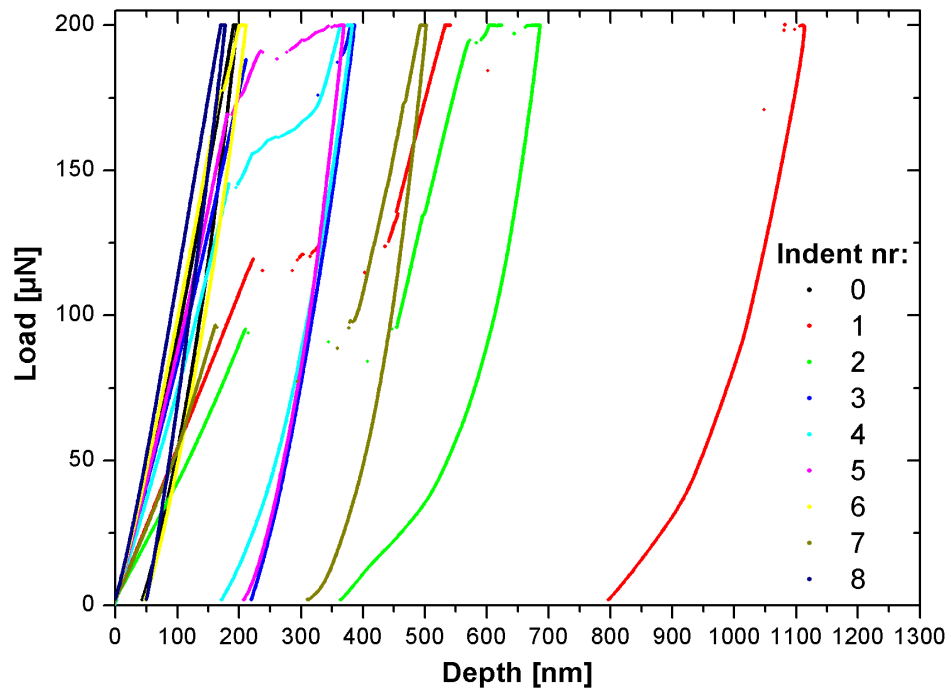
FIGURE B.5: Load-displacement curves from the representative indent-series F from sample S1-H_2O_2. This is a "net-haul"-sample of species *C. centralis* from batch 1, indented with a cube-cornered tip.
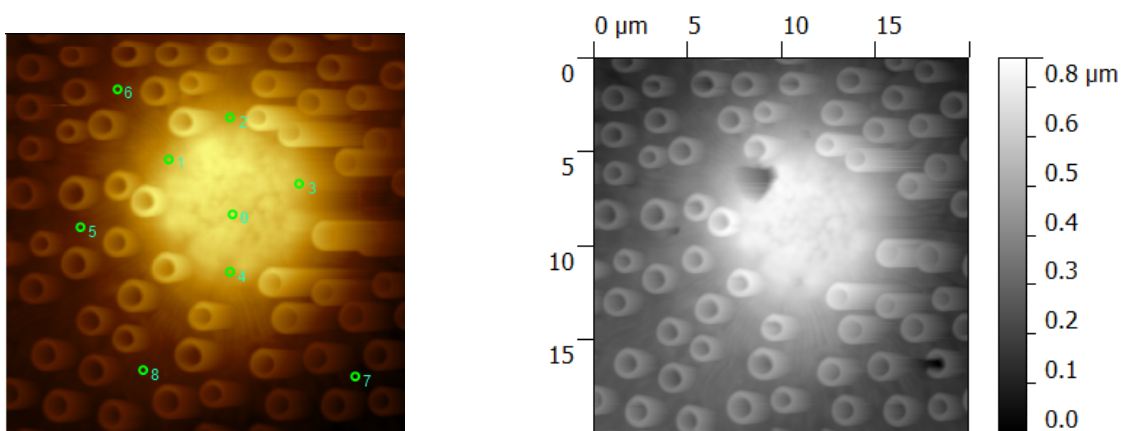
FIGURE B.6: Images showing defined location of indents prior to testing (left) and a topographic image after indentation (right) from indent-series S1-H_2O_2-F.
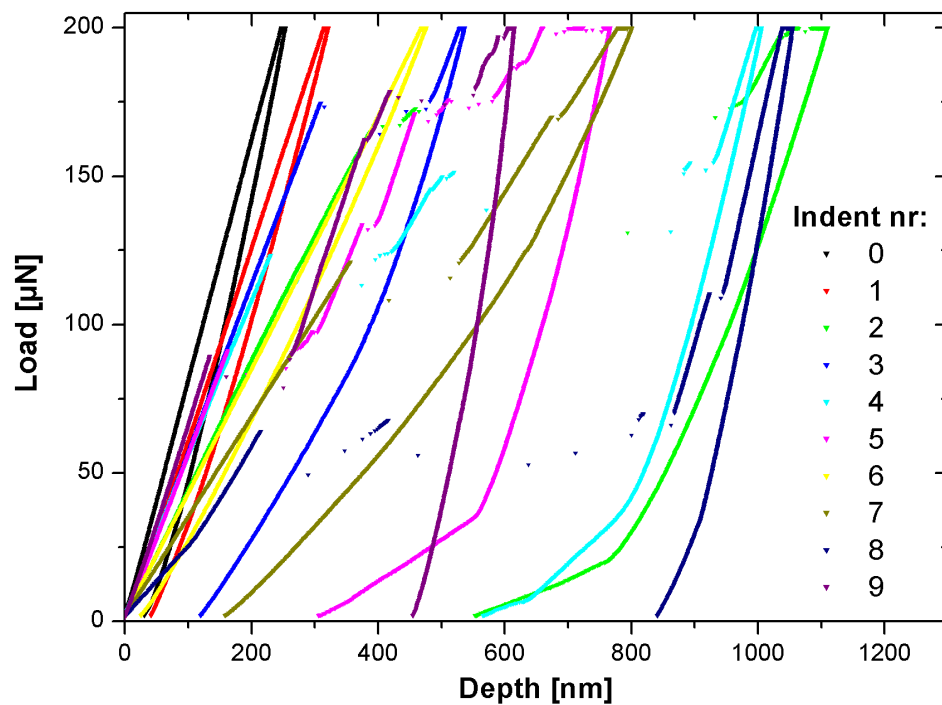
FIGURE B.7: Load-displacement curves from the representative indent-series C from sample S1-H$_2$SO$_4$. This is a "net-haul"-sample of species *C. centralis* from batch 1, indented with a cube-cornered tip.
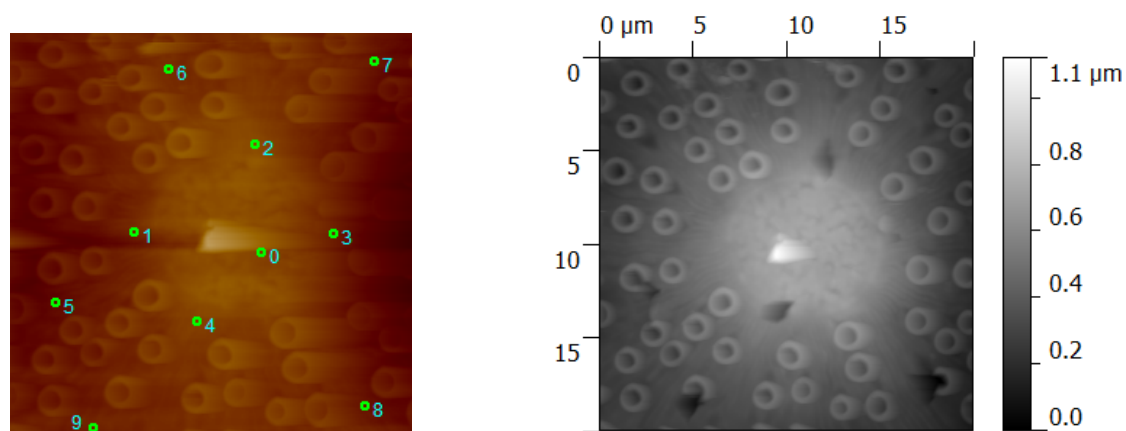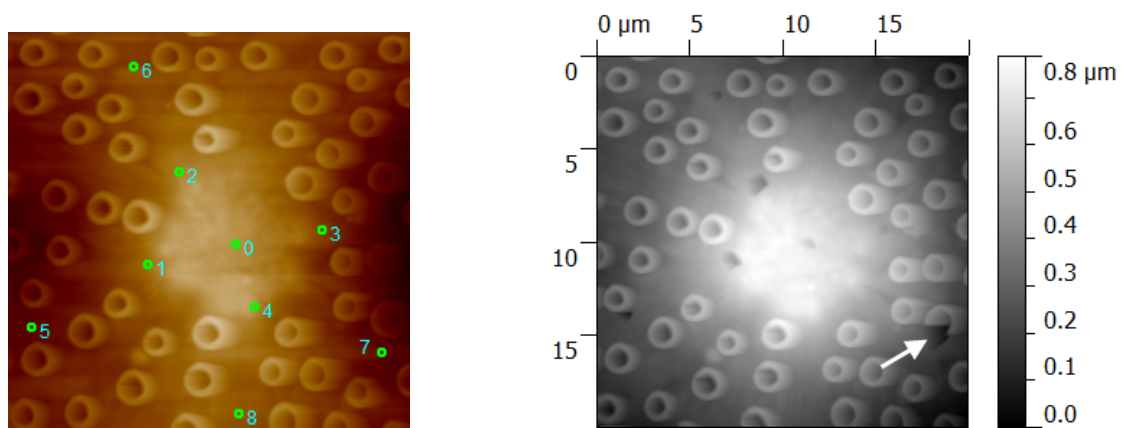

FIGURE B.8: Images showing defined location of indents prior to testing (left) and a topographic image after indentation (right) from indent-series S1-H$_2$SO$_4$-C

FIGURE B.9: Load-displacement curves from the representative indent-series G from sample S1-SDS. This is a "net-haul"-sample of species *C. centralis* from batch 1, indented with a cube-cornered tip.

FIGURE B.10: Images showing defined location of indents prior to testing (left) and a topographic image after indentation (right) from indent-series S1-SDS-G.

FIGURE B.11: Load-displacement curves from the representative indent-series G from sample S2-H$_2$O$_2$. This is a "net-haul"-sample of species *C. centralis* from batch 2, indented with a cube-cornered tip.
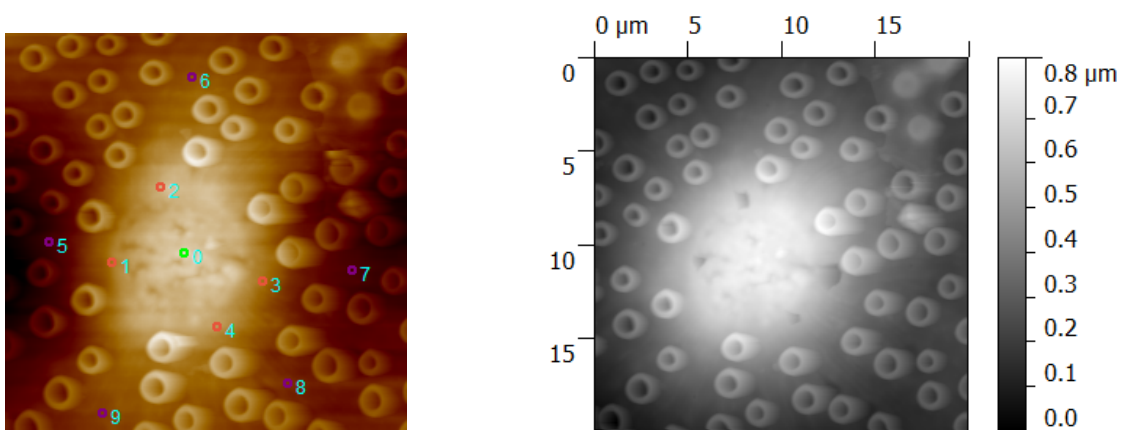

FIGURE B.12: Images showing defined location of indents prior to testing (left) and a topographic image after indentation (right) from indent-series S2-H$_2$O$_2$-G.

FIGURE B.13: Load-displacement curves from the representative indent-series B from sample S2-SDS. This is a "net-haul"-sample of species *C. centralis* from batch 2, indented with a cube-cornered tip.

FIGURE B.14: Images showing defined location of indents prior to testing (left) and a topographic image after indentation (right) from indent-series S2-SDS-B.

Rapid fracture with pop-in
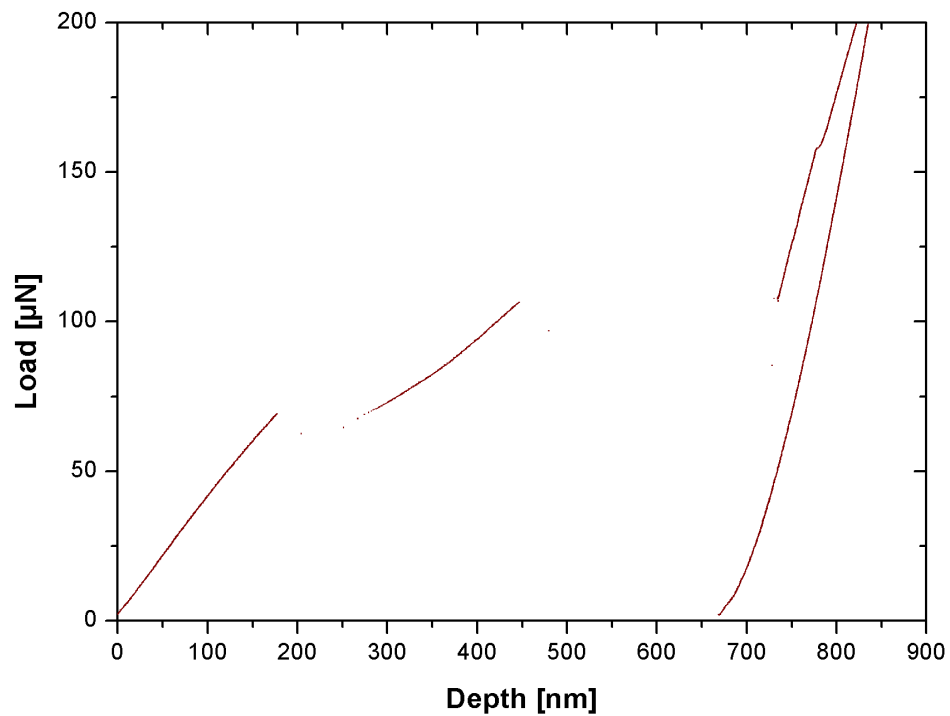
FIGURE B.15: Scatter plot of indent S1-H2O2-K-007. The second pop-in got a depth of 280 nm. With 2700 datapoints registered during the 12 second of the indentation, a velocity of 15820 nms^{-1} was reached.

FIGURE B.16: Images showing defined location of indents prior to testing (left) and a topographic image after indentation (right) from indent-series S1-H2O2-K. The arrow marks indentnr 007.

S1-SDS-I, distance from center vs. response
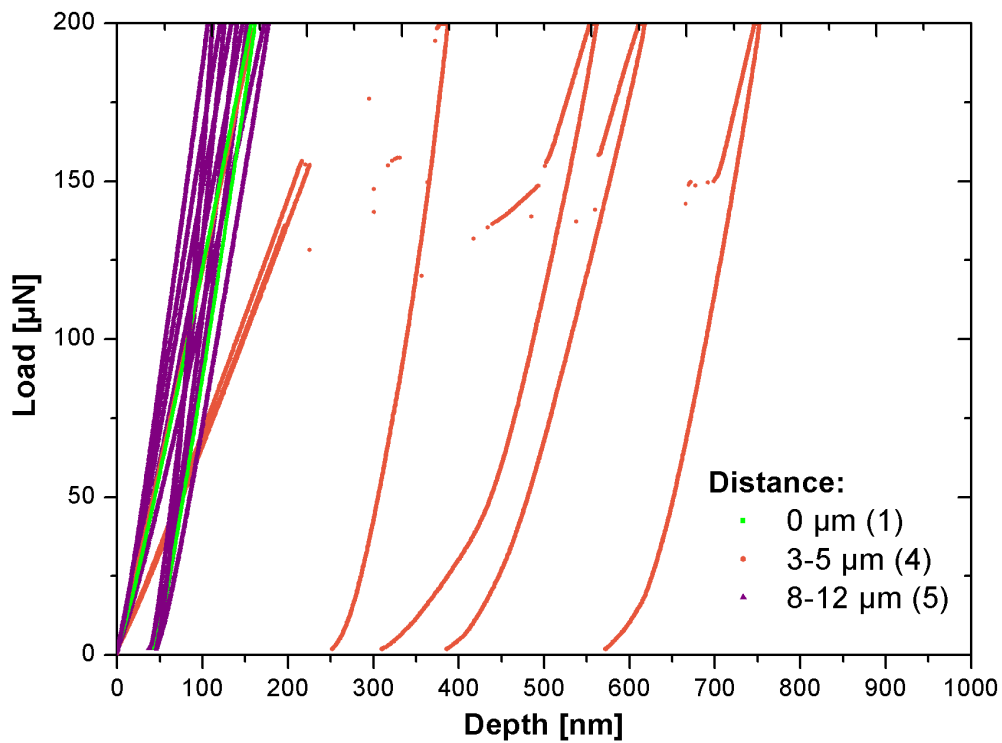
FIGURE B.17: S1-SDS-I, arranged after distance from the frustule center. All the five indents closest to the center did fracture the foramen.

FIGURE B.18: Images showing defined location of indents prior to testing (left) and a topographic image after indentation (right) from indent-series S1-SDS-I.

S1-H2O2-L, distance from center vs. response
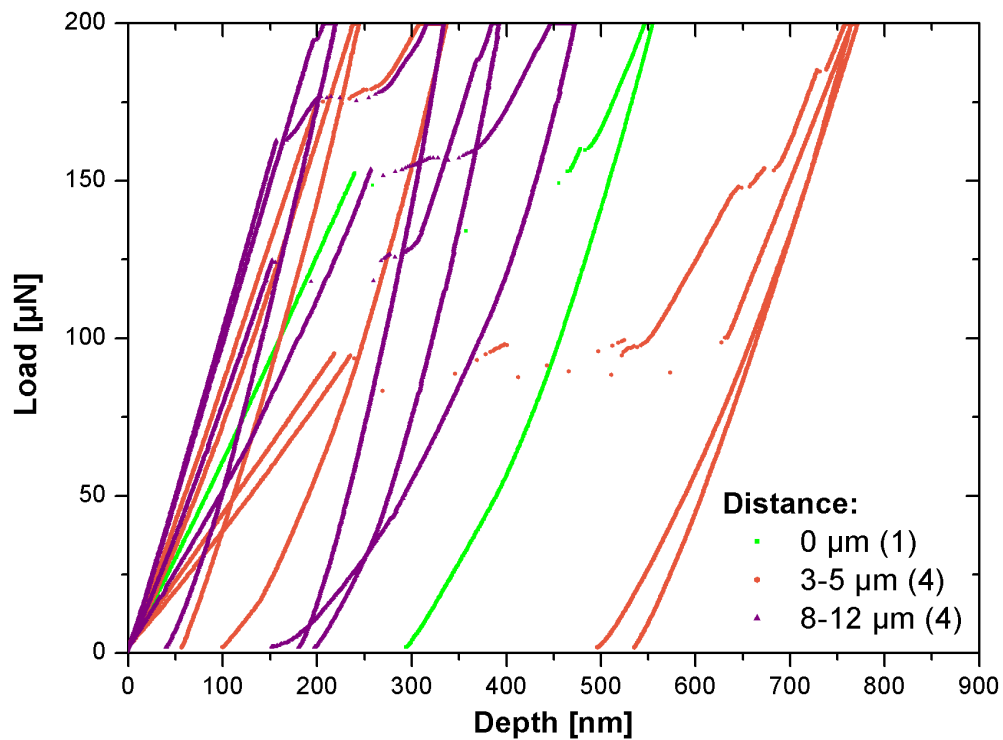
FIGURE B.19: S1-H2O2-L, arranged after distance from the frustule center. In this indent-series,the indents fractured the foramen with no relation to the distance from the center.
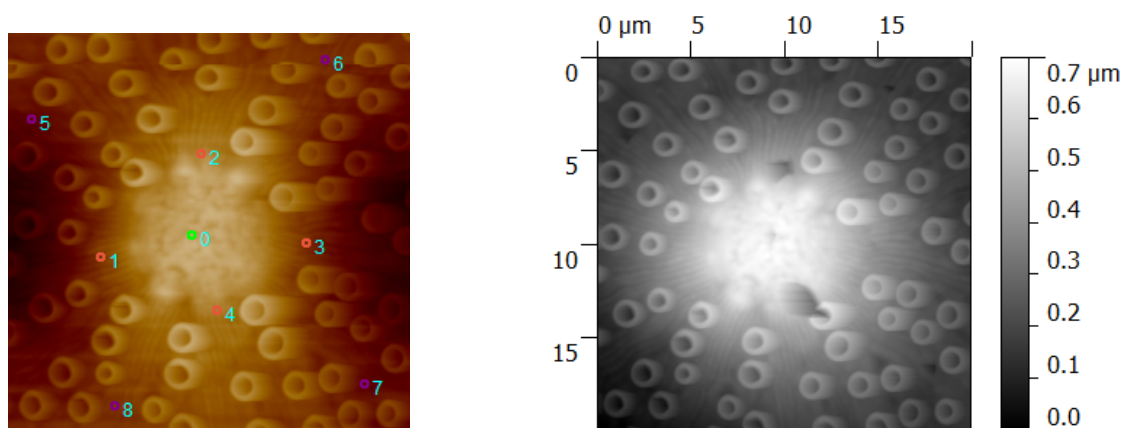
FIGURE B.20: Images showing defined location of indents prior to testing (left) and a topographic image after indentation (right) from indent-series S1-SDS-I.

Appendix C

Cantilever Test Analysis

When the cantilever beams are tested and loaded until fracture, the results should be analysed. With simple beam theory, load- and deformation data could in theory be converted into material properties with basic fracture mechanics. The same equations could also be used in calculations when estimating the expected force needed to break the beam based on previously reported values.

The following analysis is based on previous micro-cantilever tests reported in the work of Matoy et al. in 2009 [45].
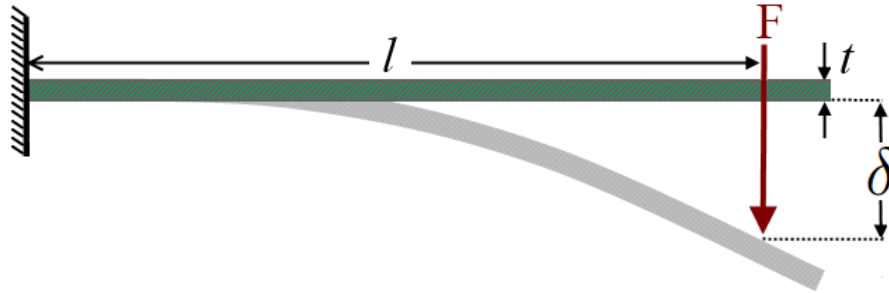
FIGURE C.1: Model of a diatom cantilever test.

First, Young modulus can be determined by using:

$$E = \frac{4F}{\delta w} \times \left(\frac{l}{t}\right)^3 \qquad (C.1)$$

where F is applied load, δ is the deflection at load F, l is the bending length, w is the cantilever beam width and t is the cantilever beam thickness. With linear-elastic bending theory the bending stress on the beam top surface can be determined:

$$\sigma = 6\frac{Fl}{wt^2} \tag{C.2}$$

If possible on the thin foramen beams, notches could be made to calculate the fracture toughness of the material. Fracture stress can be calculated by inserting the maximum load to Eq. C.2 at fracture and this value can again be used to calculate the fracture toughness with beams with notches:

$$K_{IC} = \sigma_F\sqrt{\pi a}f\left(\frac{a}{t}\right) \tag{C.3}$$

where σ_F is the fracture stress and $\frac{a}{t}$ is a function of the test geometry with crack-depth, a, and beam thickness t.

The equations above, are all for beams with a rectangular cross-section. When the diatom cantilevers are milled out, the stage can be tilted to -7°, creating a tilt of 59° between the sample surface and the ion beam. It is therefore not possible to isolate the foramen-beam completely. Some parts of the areola walls will be left at some points along the beams. The maximum cross-section will be triangular as illustrated in Fig. C.2.
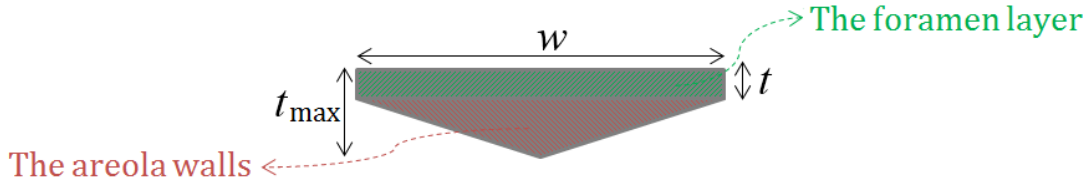

FIGURE C.2: Illustration of the maximum cross-section when the foramen-beam is partly isolated from of the areola structure. The obtainable geometry is limited, but an optimal geometry would be a rectangular cross-section.

The value of t_{max} is found with simple trigonometry:

$$t_{max} = t + \frac{w}{2}\tan 59 \tag{C.4}$$

Even though the areola is partly supporting the foramen beam, the cross-section used in these initial analysis was thought to be a square. The beams can be cut out so the cross-section of the fractured surface is rectangular. This makes the calculations more valid. In addition, the areola walls are only 135 nm thick as described in section 2.1.1. Still, they will give some mechanical support, but for the initial calculations the effect of the areola walls were neglected even though this will make the results slightly conservative. Fig. C.3 shows the remaining areola structure after one of the beams made from S. H. Bjørnøy, tested in a three point bending test.
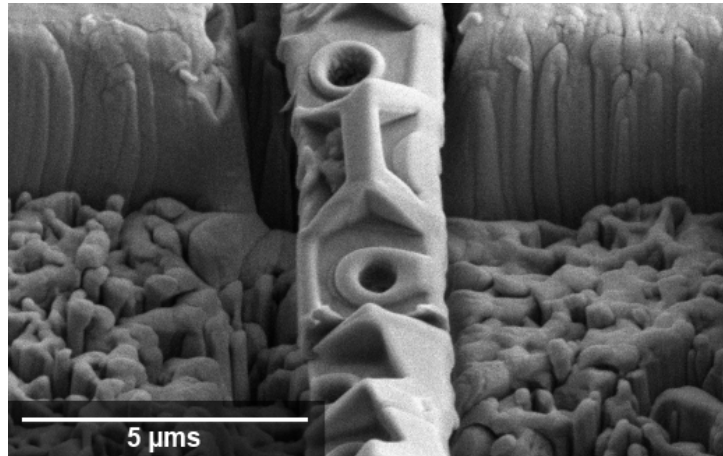
FIGURE C.3: Adapted SEM-image of "H_2O_2-beam 7" from S. H. Bjørnøy's master thesis [5] showing the areola left from a 4 μm wide foramen beam after a mill at 52°. This beam is also containing foramen pores. Since the beams in this study will be isolated from areas without pores, the analysis will be easier due to a more consistent cross-section.
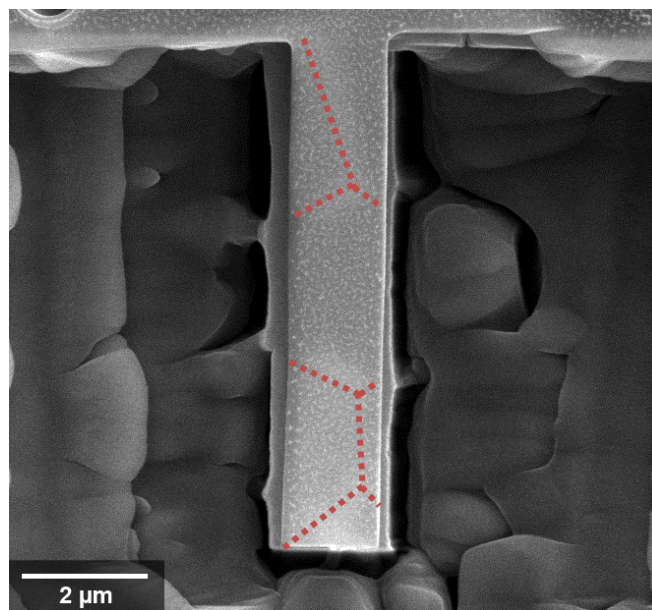

FIGURE C.4: Highlight of the areola walls under the foramen-beam. The dotted lines are drawn to mark the areola structure underneath.

Appendix D

Images and observations

D.1   DualBeam FIB

When working with the different equipment, some observations have been made that could ease the further work on diatoms. The different images are briefly explained in the figure texts. In Fig. D.1 the areola structure can be observed through a compact foramen layer only by increasing the acceleration voltage.
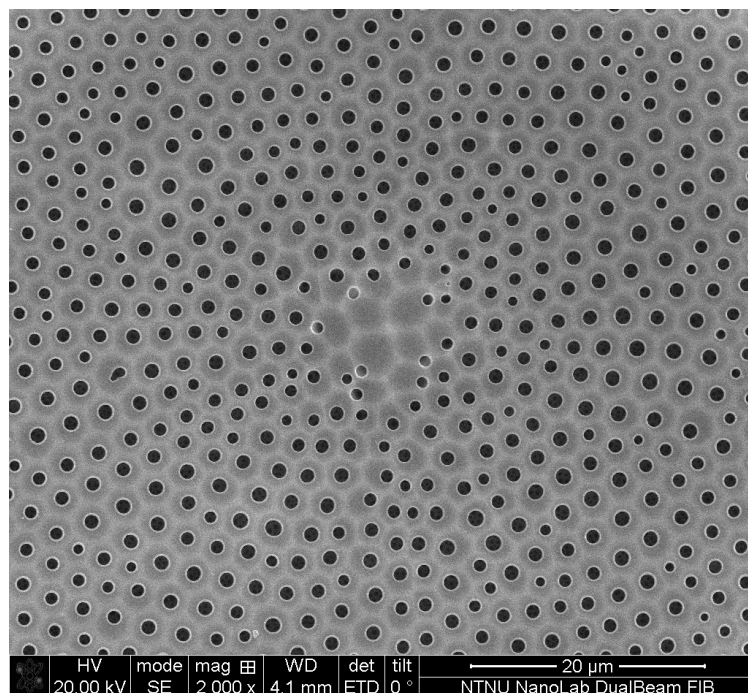

HV	mode	mag ⊞	WD	det	tilt	— 20 µm —
20.00 kV	SE	2 000 x	4.1 mm	ETD	0 °	NTNU NanoLab DualBeam FIB

FIGURE D.1: The areola structure is clearly visible. Here imaged at 20 keV with the SEM.
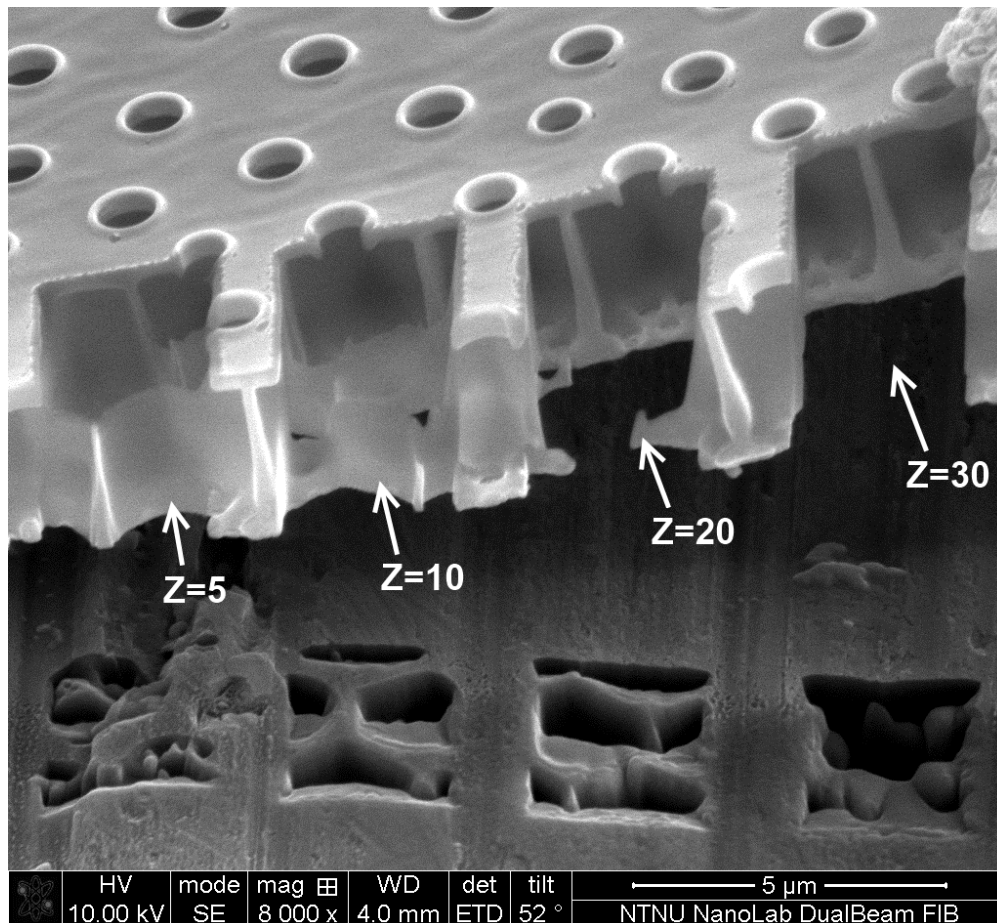
FIGURE D.2: Experiment of different milling depths, i.e. z-values, necessary to mill through the whole structure with a voltage of 93 pA, current of 30 keV. The cleaning cross-section tool was used and the material was sat at Si (silicium) in the software.
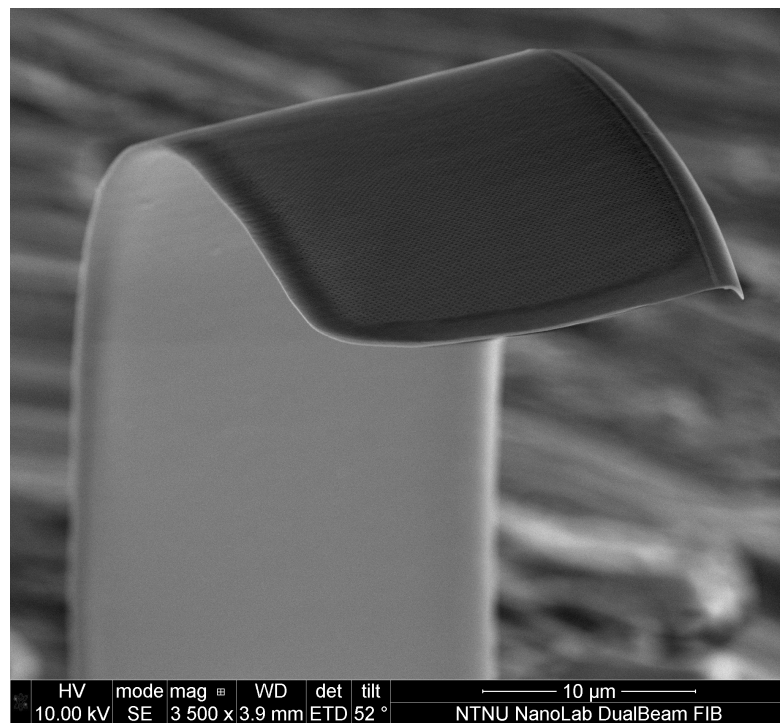
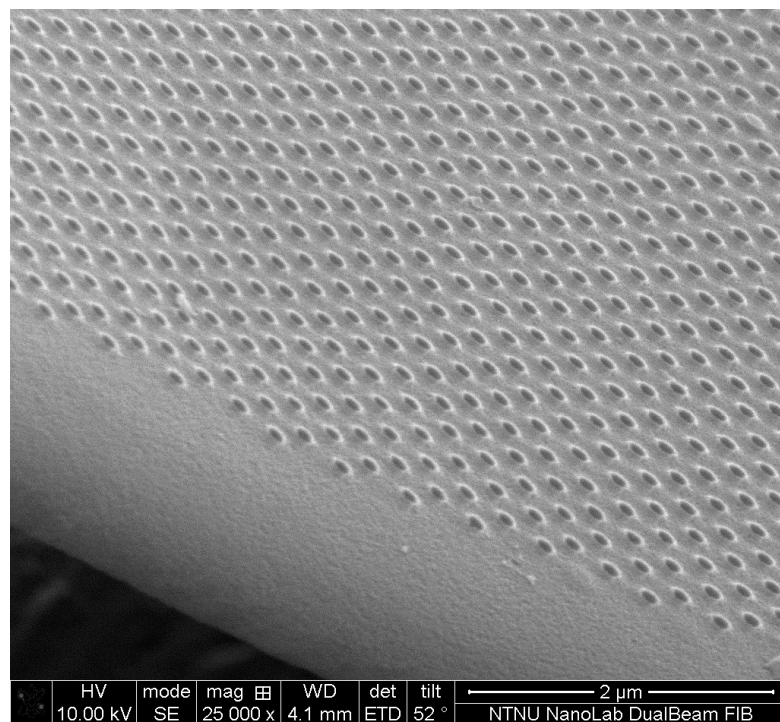| HV	mode	mag ⊞	WD	det	tilt	10 μm
10.00 kV	SE	3 500 x	3.9 mm	ETD	52 °	NTNU NanoLab DualBeam FIB

FIGURE D.3: SEM-image of a girdle band.

HV	mode	mag ⊞	WD	det	tilt	2 μm
10.00 kV	SE	25 000 x	4.1 mm	ETD	52 °	NTNU NanoLab DualBeam FIB

FIGURE D.4: SEM-image of the pores in a girdle band.

D.2 The Picondenter/SEM Supra

The biggest obstacle in the development of nanomechanical test methods is obviously the size. As a car-driver will become speed-blind when driving at a high velocities over a longer time, the same effect will be encountered in the world of nanomechanical testing. Fig. D.7 below gives a perspective of the size-range of the samples in this study. The tip is enormous compared to the small diatom, and the beams got a size even 100 times smaller.
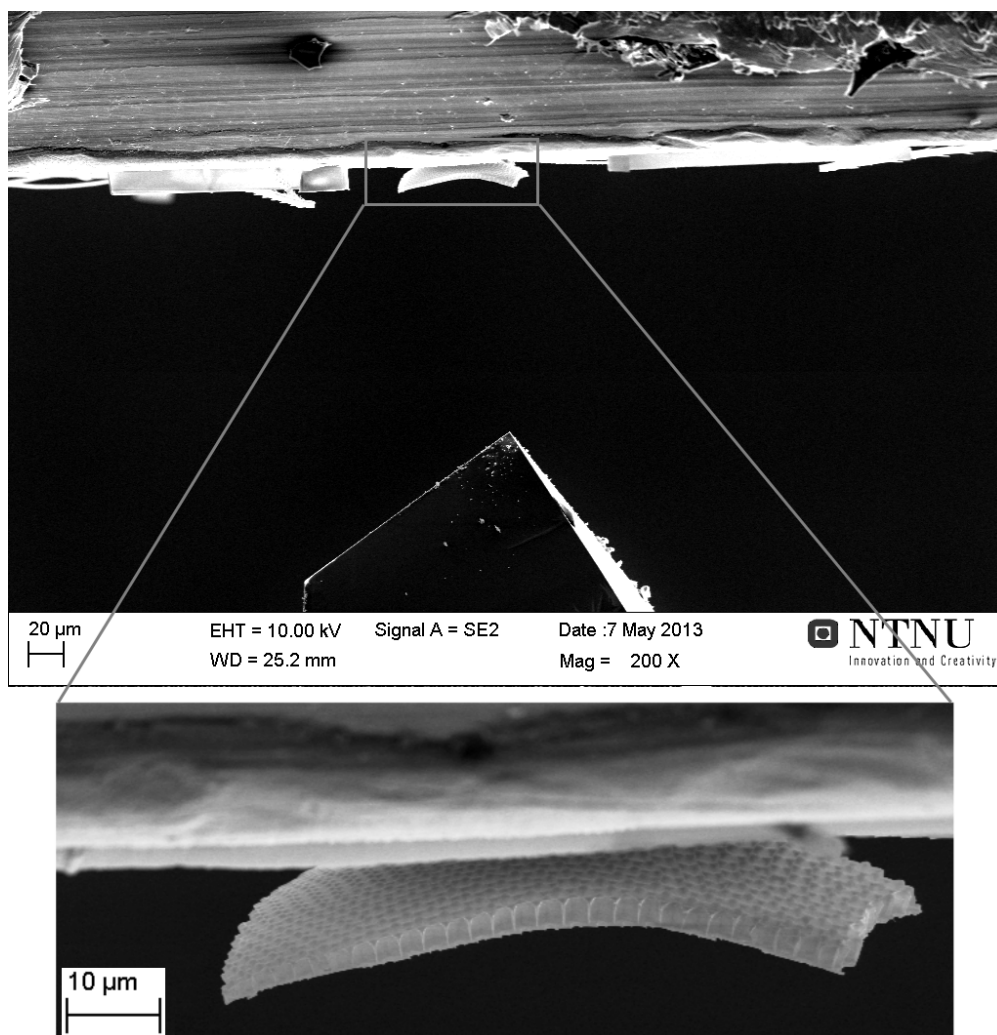

FIGURE D.5: SEM images of a broken frustule on a aluminium stub. Taken from the first meeting between the picoindenter tip and a diatom frustules.

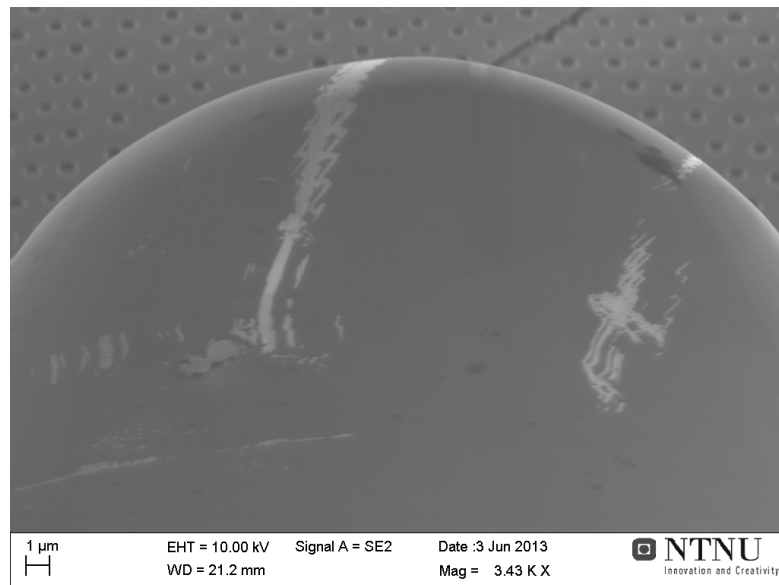| 1 µm | EHT = 10.00 kV | Signal A = SE2 | Date :3 Jun 2013 | ◉ NTNU |
| | WD = 21.2 mm | | Mag = 3.43 K X | Innovation and Creativity |

FIGURE D.6: The second tip available was also tried in the picoindenter, but was to big for any suitable indentations. The radius of the tip-end was measured to be 14 µm.

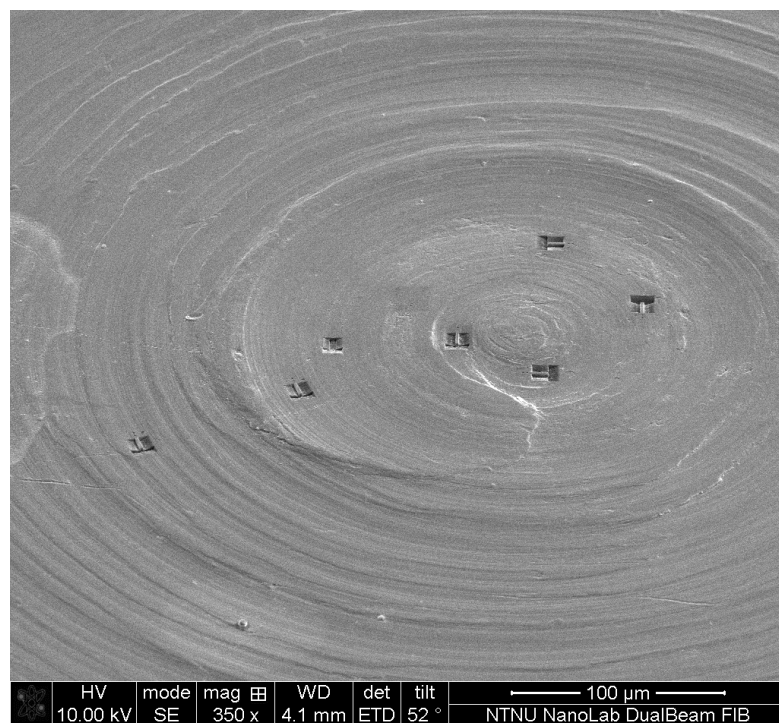| HV | mode | mag ⊞ | WD | det | tilt | ⊢ 100 µm ⊣ |
| 10.00 kV | SE | 350 x | 4.1 mm | ETD | 52 ° | NTNU NanoLab DualBeam FIB |

FIGURE D.7: Image of the aluminium mock-ups, cut out in different directions to practice positioning of the indenter tip, both with a scan in the nanoindenter and by the *in situ* navigation in the picoindenter.
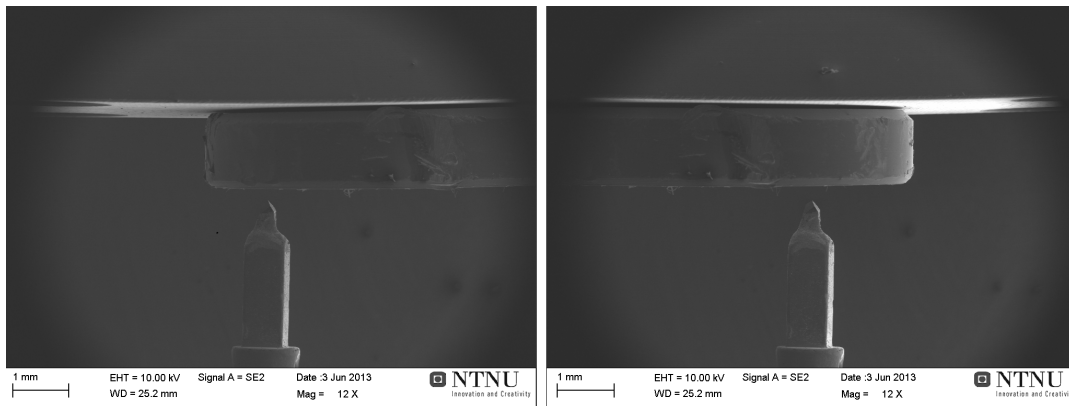
FIGURE D.8: Two SEM-images merged to illustrate the stage-limits in the picoindenter. The tip is located in the extreme positions. Vertical limitations was not examined.
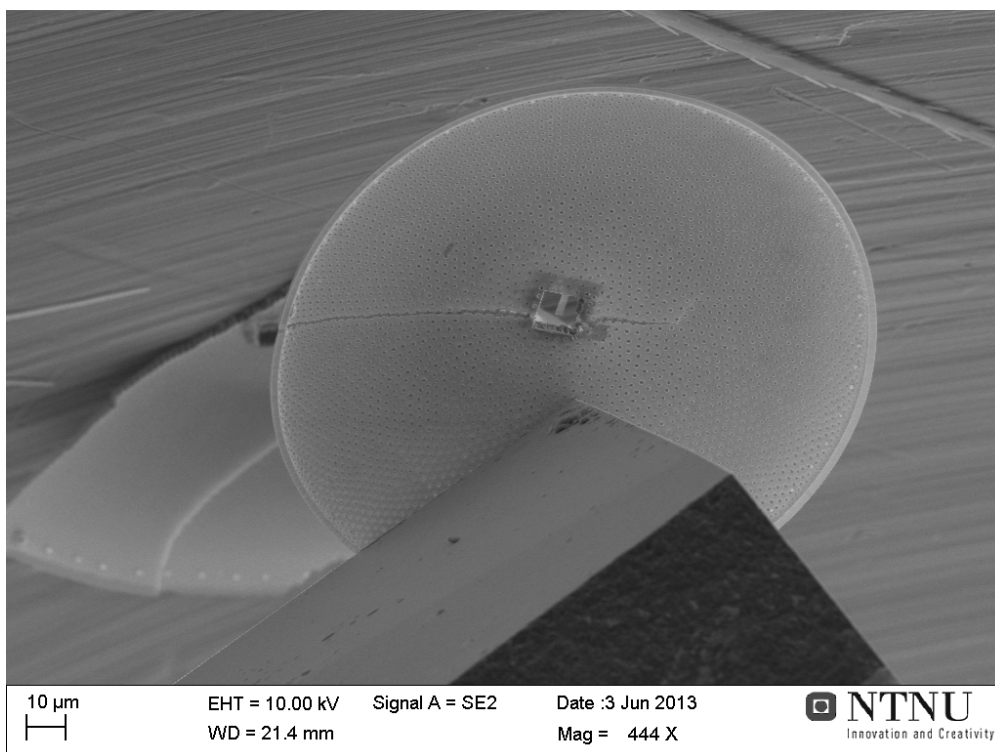

FIGURE D.9: SEM-image from a diatom frustule which was stuck at the tip.

D.3   Confocal microscope

"In 1703 an English country gentleman looked with his simple microscope at roots of the pond-weed *Lemna* and *...saw adhering to them, and sometimes separate in the water, many pretty branches, compos'd of rectangular oblongs and exact squares*" [8]. This is a description of what Round et al. almost 300 years later classified as the *Tabellaria Floccusa*, the first certain records of a diatom.

The images from the confocal microscope clearly illustrates where this scientist got his fascination from.
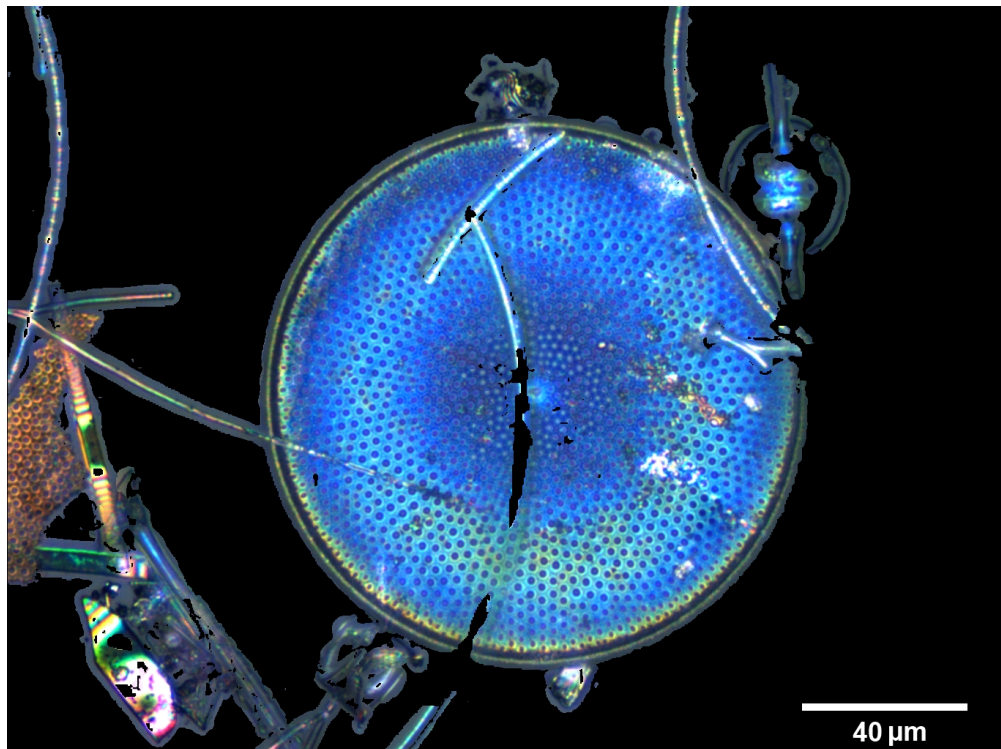

40 µm

FIGURE D.10: The light from the confocal microscope is refracted and reflected by the different frustule parts. This diatom valve is not lying alone, but is imaged together with broken pieces of other diatom valves and girdle bands.